Improving the Foundation Layers for Concrete Pavements

TECHNICAL REPORT:

Pavement Foundation Layer Reconstruction – Iowa I-29 Field Study

December 2015

Sponsored by
Federal Highway Administration (DTFH 61-06-H-00011 (Work Plan #18))
FHWA TPF-5(183): California, Iowa (lead state), Michigan, Pennsylvania, Wisconsin

National Concrete Pavement Technology Center
Tech Center

CENTER FOR CEER EARTHWORKS ENGINEERING RESEARCH
IOWA STATE UNIVERSITY
Institute for Transportation

About the National CP Tech Center

The mission of the National Concrete Pavement Technology (CP Tech) Center is to unite key transportation stakeholders around the central goal of advancing concrete pavement technology through research, tech transfer, and technology implementation.

About CEER

The mission of the Center for Earthworks Engineering Research (CEER) at Iowa State University is to be the nation's premier institution for developing fundamental knowledge of earth mechanics, and creating innovative technologies, sensors, and systems to enable rapid, high quality, environmentally friendly, and economical construction of roadways, aviation runways, railroad embankments, dams, structural foundations, fortifications constructed from earth materials, and related geotechnical applications.

Disclaimer Notice

The contents of this report reflect the views of the authors, who are responsible for the facts and the accuracy of the information presented herein. The opinions, findings and conclusions expressed in this publication are those of the authors and not necessarily those of the sponsors.

The sponsors assume no liability for the contents or use of the information contained in this document. This report does not constitute a standard, specification, or regulation.

The sponsors do not endorse products or manufacturers. Trademarks or manufacturers' names appear in this report only because they are considered essential to the objective of the document.

Iowa State University Non-Discrimination Statement

Iowa State University does not discriminate on the basis of race, color, age, ethnicity, religion, national origin, pregnancy, sexual orientation, gender identity, genetic information, sex, marital status, disability, or status as a U.S. veteran. Inquiries regarding non-discrimination policies may be directed to Office of Equal Opportunity, Title IX/ADA Coordinator, and Affirmative Action Officer, 3350 Beardshear Hall, Ames, Iowa 50011, 515-294-7612, email eooffice@iastate.edu.

Iowa Department of Transportation Statements

Federal and state laws prohibit employment and/or public accommodation discrimination on the basis of age, color, creed, disability, gender identity, national origin, pregnancy, race, religion, sex, sexual orientation or veteran's status. If you believe you have been discriminated against, please contact the Iowa Civil Rights Commission at 800-457-4416 or the Iowa Department of Transportation affirmative action officer. If you need accommodations because of a disability to access the Iowa Department of Transportation's services, contact the agency's affirmative action officer at 800-262-0003.

The preparation of this report was financed in part through funds provided by the Iowa Department of Transportation through its "Second Revised Agreement for the Management of Research Conducted by Iowa State University for the Iowa Department of Transportation" and its amendments.

The opinions, findings, and conclusions expressed in this publication are those of the authors and not necessarily those of the Iowa Department of Transportation or the U.S. Department of Transportation Federal Highway Administration.

Technical Report Documentation Page

1. Report No.	2. Government Accession No.	3. Recipient's Catalog No.
DTFH 61-06-H-00011 Work Plan 18		

4. Title and Subtitle	5. Report Date
Improving the Foundation Layers for Concrete Pavements: Pavement Foundation Layer Reconstruction – Iowa I-29 Field Study	December 2015
	6. Performing Organization Code

7. Author(s)	8. Performing Organization Report No.
David J. White, Pavana Vennapusa, Heath H. Gieselman, Alexander J. Wolfe, Alex Johnson, and Samuel Douglas	InTrans Project 09-352

9. Performing Organization Name and Address	10. Work Unit No. (TRAIS)
National Concrete Pavement Technology Center and Center for Earthworks Engineering Research Iowa State University 2711 South Loop Drive, Suite 4700 Ames, IA 50010-8664	**11. Contract or Grant No.**

12. Sponsoring Organization Name and Address	13. Type of Report and Period Covered
Federal Highway Administration U.S. Department of Transportation 1200 New Jersey Avenue SE Washington, DC 20590	Technical Report
	14. Sponsoring Agency Code TPF-5(183)

15. Supplementary Notes

Visit www.cptechcenter.org or www.ceer.iastate.edu for color PDF files of this and other research reports.

16. Abstract

This technical project report is one of the field project reports developed as part of the TPF-5(183) and FHWA DTFH 61-06-H-00011:WO18 studies.

This report presents results and analysis of field and laboratory tests from a field study conducted on the I-29 interstate highway reconstruction project in Monona and Harrison Counties, Iowa. Falling weight deflectometer (FWD) and dynamic cone penetrometer (DCP) testing was conducted on the existing continuously reinforced concrete pavement (CRCP) and its foundation layers and on the newly placed jointed plain concrete pavement (JPCP) and its foundation layers. The results indicated that the modulus of subgrade reaction (*k*) values under the JPCP were on average about 1.3 to 1.7 times higher than the *k* values under the CRCP, which indicates improvement in the stiffness of the foundation layers under the new pavement. However, the *k* values determined from FWD and DCP test results were significantly different. The *k* values determined from FWD were about the same as the design target value, while the *k* values determined from correlations with DCP test results were significantly higher than the design target value if treated subgrade values were used and were slightly higher if results of weak subgrade within the top 450 mm were considered. The *k* value estimated from laboratory thawed California bearing ratio (CBR) values were about 0.4 times the design value and from unthawed CBR was about 2.2 times the design value. Roller integrated compaction monitoring (RICM) used on foundation layers identified "soft" and "stiff" measurements. Those measurements correlated well with light weight deflectometer (LWD) measurements and better than with DCP and nuclear gauge density measurements. Laboratory resilient modulus (M_r) tests conducted on layered composite samples (with both subbase and subgrade) indicated that the average M_r was either similar to the layer with a lower M_r value (i.e., subgrade) or about average of M_r values of the two layers. Frost heave tests on subgrade materials indicated that the material was susceptible to increasing heave with greater freeze-thaw cycles. The subgrade soil was classified to have high potential to frost-heave and very high potential to thaw-weakening.

17. Key Words	18. Distribution Statement
concrete pavement—pavement foundation—quality assurance—quality control—recycled base—subbase—subgrade	No restrictions.

19. Security Classification (of this report)	20. Security Classification (of this page)	21. No. of Pages	22. Price
Unclassified.	Unclassified.	104	NA

Form DOT F 1700.7 (8-72) **Reproduction of completed page authorized**

IMPROVING THE FOUNDATION LAYERS FOR CONCRETE PAVEMENTS: PAVEMENT FOUNDATION LAYER RECONSTRUCTION – IOWA I-29 FIELD STUDY

Technical Report
December 2015

Research Team Members
Tom Cackler, David J. White, Jeffrey R. Roesler, Barry Christopher, Andrew Dawson, Heath Gieselman, and Pavana Vennapusa

Report Authors
David J. White, Pavana K. R. Vennapusa,
Heath H. Gieselman, Alexander J. Wolfe, Alexander E. Johnson, and Samuel Douglas
Iowa State University

Sponsored by
the Federal Highway Administration (FHWA)
DTFH61-06-H-00011 Work Plan 18
FHWA Pooled Fund Study TPF-5(183): California, Iowa (lead state), Michigan, Pennsylvania, Wisconsin

Preparation of this report was financed in part
through funds provided by the Iowa Department of Transportation
through its Research Management Agreement with the
Institute for Transportation
(InTrans Project 09-352)

National Concrete Pavement Technology Center and
Center for Earthworks Engineering Research
Iowa State University
2711 South Loop Drive, Suite 4700
Ames, IA 50010-8664
Phone: 515-294-8103
www.cptechcenter.org and www.ceer.iastate.edu

TABLE OF CONTENTS

LIST OF FIGURES

LIST OF TABLES

ACKNOWLEDGMENTS

This research was conducted under Federal Highway Administration (FHWA) DTFH61-06-H-00011 Work Plan 18 and the FHWA Pooled Fund Study TPF-5(183), involving the following state departments of transportation:

- California
- Iowa (lead state)
- Michigan
- Pennsylvania
- Wisconsin

The authors would like to express their gratitude to the National Concrete Pavement Technology (CP Tech) Center, the FHWA, the Iowa Department of Transportation (DOT), and the other pooled fund state partners for their financial support and technical assistance.

Chris Brakee, Melissa Serio, and several others with the Iowa DOT provided assistance in identifying the project, providing access to the project site, and obtaining project design information and specifications. We greatly appreciate their help.

Volvo Construction Equipment provided the smooth drum intelligent compaction (IC) roller used on the project, outfitted with a Trimble compaction measurement and documentation system. We also thank Yang Zhang and Cheng Li of Iowa State University for their help with laboratory testing and Christianna White for comments and editorial assistance.

LIST OF ACRONYMS AND SYMBOLS

A_{Ω}	Acceleration of the fundamental component of the vibration
$A_{2\Omega}$	Acceleration of the first harmonic component of the vibration
a	Vibration amplitude
C	Constant
CBR	California bearing ratio
CMV	Compaction meter value
COV	Coefficient of variation
$DCP\text{-}CBR_{Subgrade}$	CBR of subgrade determined from DCP test
$DCP\text{-}CBR_{Subbase}$	CBR of subbase determined from DCP test
DPI	Dynamic penetration index
D_0	Deflection measured under the plate
D_1 to D_7	Deflections measured away from the plate at various set distances
D_{10}	Grain size diameter corresponding to 10% passing by mass
D_{60}	Grain size diameter corresponding to 60% passing by mass
E	Elastic modulus
E_s or $E_{s(T\text{-}307)}$	Dynamic secant modulus
$E_{LWD\text{-}Z3}$	Elastic modulus determined from 300 mm diameter plate Zorn light weight deflectometer
$E_{FWD\text{-}K3}$	Surface modulus determined using 300 mm diameter plate KUAB falling weight deflectometer
F	Shape factor
f	Vibration frequency
G_s	Specific gravity
I	Intercept
k	Modulus of subgrade reaction
k_{AASHTO}	Modulus of subgrade reaction determined following AASHTO (1993) procedure
k_{comp}	Composite modulus of subgrade reaction
$k_{comp\text{-}PCA}$	Composite modulus of subgrade reaction determined following PCA (1984) procedure
k_{PCA}	Modulus of subgrade reaction estimated from CBR following PCA (1984) procedure
$k_{FWD\text{-}Dynamic}$	Dynamic modulus of subgrade reaction from FWD test
$k_{FWD\text{-}Static}$	Static modulus of subgrade reaction from FWD test
k_1, k_2, k_3	Regression coefficients in “universal” model
L	Lane distribution factor
LL	Liquid limit
M_r	Resilient modulus
n	Number of measurements
p	Number of parameters
PI	Plasticity index
PL	Plastic limit
P_a	Atmospheric pressure
RMV	Resonant meter value

R^2	Coefficient of determination
r	Plate radius
s_u	Undrained shear strength
w	Moisture content
w_{opt}	Optimum moisture content
ε	Axial strain
ε_p	Permanent strain
ε_r	Resilient strain
γ_d	Dry unit weight
γ_{dmin}	Minimum dry unit weight
γ_{dmax}	Maximum dry unit weight
μ	Statistical mean or average
η	Poisson's ratio
σ	Statistical standard deviation
σ_B	Bulk stress
σ_d	Deviator stress
σ_0	Applied axial stress
$\sigma_1, \sigma_2, \sigma_3$	Principal stresses
τ_{oct}	Octahedral shear stress

EXECUTIVE SUMMARY

Quality foundation layers (the natural subgrade, subbase, and embankment) are essential to achieving excellent pavement performance. Unfortunately, many pavements in the United States still fail due to inadequate foundation layers. To address this problem, a research project, Improving the Foundation Layers for Pavements (FHWA DTFH 61-06-H-00011 WO #18; FHWA TPF-5(183)), was undertaken by Iowa State University (ISU) to identify, and provide guidance for implementing, best practices regarding foundation layer construction methods, material selection, in situ testing and evaluation, and performance-related designs and specifications. As part of the project, field studies were conducted in several in-service concrete pavements across the country that represented either premature failures or successful long-term pavements. A key aspect of each field study was to tie performance of the foundation layers to key engineering properties and pavement performance. In situ foundation layer performance data, as well as original construction data and maintenance/rehabilitation history data, were collected and geospatially and statistically analyzed to determine the effects of site-specific foundation layer construction methods, site evaluation, materials selection, design, treatments, and maintenance procedures on the performance of the foundation layers and of the related pavements. A technical report was prepared for each field study.

This report presents results and analysis of field and laboratory tests from a field study conducted on the I-29 interstate highway reconstruction project in Monona and Harrison Counties, Iowa. The project involved removal of the existing continuously reinforced concrete pavement (CRCP), reconstruction of the pavement foundation layers (base, subbase, and subgrade), and placement of a new jointed plain cement pavement (JPCP). The existing CRCP was about 200 mm thick and was supported on a leveling sand subbase and subgrade. The reconstruction involved removing the leveling sand subbase and the subgrade layers to about 300 to 600 mm below the existing grade, and placing a nominal 300 to 450 mm thick recycled asphalt subbase/select sand subbase layer, and a nominal 150 mm thick recycled portland cement concrete (PCC) base layer. The new JPCP was about 279 mm thick and was designed using the PCA (1984) design procedure.

The ISU research team was present on the project site during the reconstruction process. In situ FWD tests and DCP tests were conducted on the existing CRCP and the exposed foundation layers shortly after removal of the old pavement and on the new JPCP shortly after it was placed. The FWD and DCP tests were conducted to compare the foundation layer strength/stiffness profile between the old and new foundation layers, and to obtain mechanistic properties of the new foundation layers (i.e., modulus of subgrade reaction, k) and compare with the design k values. Some key findings from this testing and data analysis are as follows:

- On average, the plate deflection under a 40 kN applied load on the new JPCP was about 0.4 times the deflection on the existing CRCP.
- The FWD intercept values on the existing CRCP and new JPCP were low (< 0.04 mm) which do not indicate voids beneath the pavement.

- The average static *k* value determined from the FWD on the new JPCP was on average about 1.6 times higher than on the existing CRCP. This indicates that there was improvement in the foundation layer stiffness values under the new pavement compared to the old pavement.
- The *k* values determined from both DCP-CBR measurements and FWD measurements indicated higher values on the new JPCP than on the existing CRCP.
- Based on tests conducted on the new JPCP sections, the *k* values determined using FWD were similar to the values determined using CBR of the weak layer within the top 450 mm of the subgrade but were about 17 times lower than the values determined using CBR of the treated subgrade. This indicates that a weak layer within the top 450 mm of the subgrade contributes to low values observed in the FWD testing and that the use of high CBR values in the treated subgrade layers can result in unreasonably high *k* values.
- The subgrade *k* values estimated from laboratory CBR measurements in thawed state were about 2.8 times lower than the design value. The average treated subgrade *k* value estimated from DCP-CBR measurements was about 23 times higher than the design value, while the untreated weak subgrade *k* value estimated from DCP-CBR was about 1.4 times higher than the design value. The average *k* value determined from FWD test, however, was about the same as the design value.

A few foundation layer production areas on the project were mapped during construction using a Volvo vibratory smooth drum roller equipped with Trimble's roller integrated compaction monitoring (RICM) system, in conjunction with nuclear gauge density, moisture content, light weight deflectometer (LWD), and DCP tests. The RICM system used on this project measured compaction meter value (CMV). The in situ tests were conducted to correlate with CMV measurements. Some key findings from this testing are as follows:

- CMV maps with virtually 100% coverage of the compacted foundation layers identified "soft" and "stiff" areas as verified using in situ DCP and LWD measurements.
- CMV measurements were influenced by amplitude settings. CMV measurements were on average about 1.1 to 1.5 times greater in high amplitude setting than in low amplitude setting. This is likely due to potential differences in the magnitude of stresses applied on the materials by the roller drum under different amplitude settings.
- Results obtained from White et al. (2010) were combined with the results obtained from this project to obtain correlations over a wide measurement range between LWD modulus, DCP-CBR, and nuclear gauge dry unit weight measurements and CMV. Results showed non-linear exponential relationships for CMV vs. LWD modulus with $R^2 = 0.66$ to 0.86. Relatively weak regression relationships with $R^2 = 0.12$ to 0.18 were observed for CMV vs. CBR and no statistically significant relationships were found for CMV vs. dry unit weight. CMV provides a measure of composite layer ground stiffness and not necessarily the dry unit weight of a single layer.

Laboratory testing was conducted on foundation layer materials obtained from field to determine index properties, moisture-dry unit weight relationships from compaction tests, resilient modulus

(M_r), and frost-heave and thaw-weakening susceptibility rating. M_r tests were conducted on homogenous samples as well as well as layered composite samples (i.e., RPCC base over subbase, subbase over subgrade). Frost-heave tests were conducted on subgrade samples by exposing the samples to two freeze-thaw cycles according to ASTM D5918. Thaw-weakening susceptibility rating was determined by conducting California bearing ratio (CBR) tests on compacted samples before and after freeze thaw cycles. Some key findings from laboratory M_r and frost-heave/thaw-weakening susceptibility rating tests are as follows:

- Comparison of homogenous sample versus composite sample M_r values indicated that the average M_r of the composite sample was either similar to the layer with a lower M_r value, or about average of the two layer's M_r values.
- Frost-heave test results on subgrade samples indicated that the heave rate was greater for the second freezing cycle than for the first freezing cycle, which indicates that the material is susceptible to increased heave with greater freeze-thaw cycles. Based on the frost-heave rate measurements, the subgrade soil is classified to have *high* potential to frost-heave.
- Post freeze/thaw moisture content profiles of the samples were obtained by taking samples at different depths. Results showed that the moisture content was higher at all depths in the samples compared to the initial moisture content. The moisture content at the top of the sample was higher than at the middle or bottom of the sample, which indicates that water was drawn to the top cold plate through capillary action caused in part by the temperature gradient in the samples during testing.
- The CBR test on the thawed samples decreased to an average CBR < 1.0 on the four samples from about CBR = 22 on a sample tested before freezing-thawing. Based on the thawed CBR values, the soil is classified to have *very high* potential to thaw-weakening.

CHAPTER 1: INTRODUCTION

This report presents results and analysis of field and laboratory tests from a field study conducted on the I-29 interstate highway reconstruction project in Monona and Harrison Counties in Iowa. The project involved removal of the existing continuously reinforced concrete pavement (CRCP), reconstruction of the pavement foundation layers (base, subbase, and subgrade), and placement of a new jointed plain cement pavement (JPCP) on the north and south bound lanes of I-29, between just south of County Road F-20 to just north of I-75. The existing CRCP was about 200 mm thick and was supported on a leveling sand subbase and subgrade. The reconstruction involved removing the leveling sand subbase and the subgrade layers to about 300 to 600 mm below the existing grade. The exposed subgrade in the excavation was reworked and a 300 to 450 mm thick recycled asphalt subbase/select sand subbase layer (referred to as "special backfill subgrade treatment" in Iowa DOT specifications), and a 150 mm thick recycled portland cement concrete (PCC) base layer were placed. The new JPCP was about 279 mm thick. The new pavement was designed by the Iowa DOT in accordance with the PCA (1984) design procedure.

The Iowa State University (ISU) research team was present on the project site during the reconstruction process from August 31 to September 3, 2009 and on September 10, 2010. In situ falling weight deflectometer (FWD) tests and dynamic cone penetrometer (DCP) tests were conducted on the old CRCP and the exposed foundation layers shortly after removal of the old pavement and on the new JPCP shortly after it was placed. The FWD and DCP tests were conducted to compare the old and new foundation layer strength/stiffness profiles and to obtain mechanistic properties of the new foundation layers (i.e., modulus of subgrade reaction *k*) for comparison with the design *k* values.

A few foundation layer production areas on the project were mapped during construction using a Volvo vibratory smooth drum roller equipped with Trimble's roller integrated compaction monitoring (RICM) system, in conjunction with nuclear gauge density, moisture content, light weight deflectometer (LWD), and DCP tests. The RICM system used on this project measured compaction meter value (CMV). The in situ tests were conducted to correlate with CMV measurements. RICM mapping and tests were conducted in concurrence with another research project funded by the Iowa DOT at that time (White et al. 2010). Some results from White et al. (2010) are combined with the results from this study to illustrate correlations over a wide range of measurements.

Disturbed bag samples of subgrade, subbase, and base materials were obtained for laboratory testing that involved characterizing their index properties, moisture-dry unit weight relationships from compaction tests, resilient modulus (M_r) tests, and frost-heave and thaw-weakening susceptibility tests. M_r tests were conducted on homogenous samples and on layered composite samples (i.e., RPCC base over subbase, subbase over subgrade). Frost-heave tests were conducted on subgrade material using a setup fabricated at ISU for this research project to assess the foundation materials susceptibility to frost-heave by exposing the samples to two freeze-thaw cycles. Thaw-weakening susceptibility ratings of the foundation materials were determined by conducting California bearing ratio (CBR) tests on compacted samples before and after two

thawing cycles. The unthawed and thawed CBR values were also used to estimate *k* values for comparison with design values.

This report contains six chapters. Chapter 2 provides project background information, pavement foundation layer construction details, and the pavement design input parameters. Chapter 3 presents an overview of the laboratory and in situ testing methods used in this project. Chapter 4 presents results from laboratory testing. Chapter 5 presents results from in situ testing and analysis and compares the laboratory and in situ measured values with the design assumed values. Chapter 6 presents key findings and conclusions from this study.

The findings from this report should be of significant interest to researchers, practitioners, and agencies who deal with design, construction, and maintenance aspects of PCC pavements. Results from this project provide one of several field project reports developed as part of the TPF-5(183) and FHWA DTFH 61-06-H-00011:WO18 studies.

CHAPTER 2: PROJECT INFORMATION

This chapter presents brief background information on the project, photos taken during pavement foundation layer construction, and pavement thickness design parameter selection and assumptions during the design phase of the project.

Project Background

This project was located on I-29 in Monona and Harrison Counties in Iowa and involved reconstruction of pavement foundation layers (base, subbase, and subgrade) of the interstate highway on I-29 north and south bound lanes between just south of county road F-20 to just north of I-75 (Sta. 2097 to 781+70 on north bound (about 11.7 miles) and Sta. 2097+59 to 2675+93 on south bound (about 4.7 miles); Iowa DOT project number ESIMX-029-5(100)95--1S-43). The project location map is shown in Figure 1. The existing CRCP was removed and the underlying base and subgrade layers were undercut to about 300 to 600 mm below the existing grade. The exposed subgrade in the excavation was scarified and re-compacted. The excavation was then replaced with a 300 to 450 mm thick special backfill subgrade treated with recycled asphalt material and a 150 mm thick recycled PCC (RPCC) subbase layer. Select sand material was also used subgrade treatment in some areas. Photographs of the existing CRCP, its removal process, and the pavement foundation layers construction process are shown in Figure 2 to Figure 10.

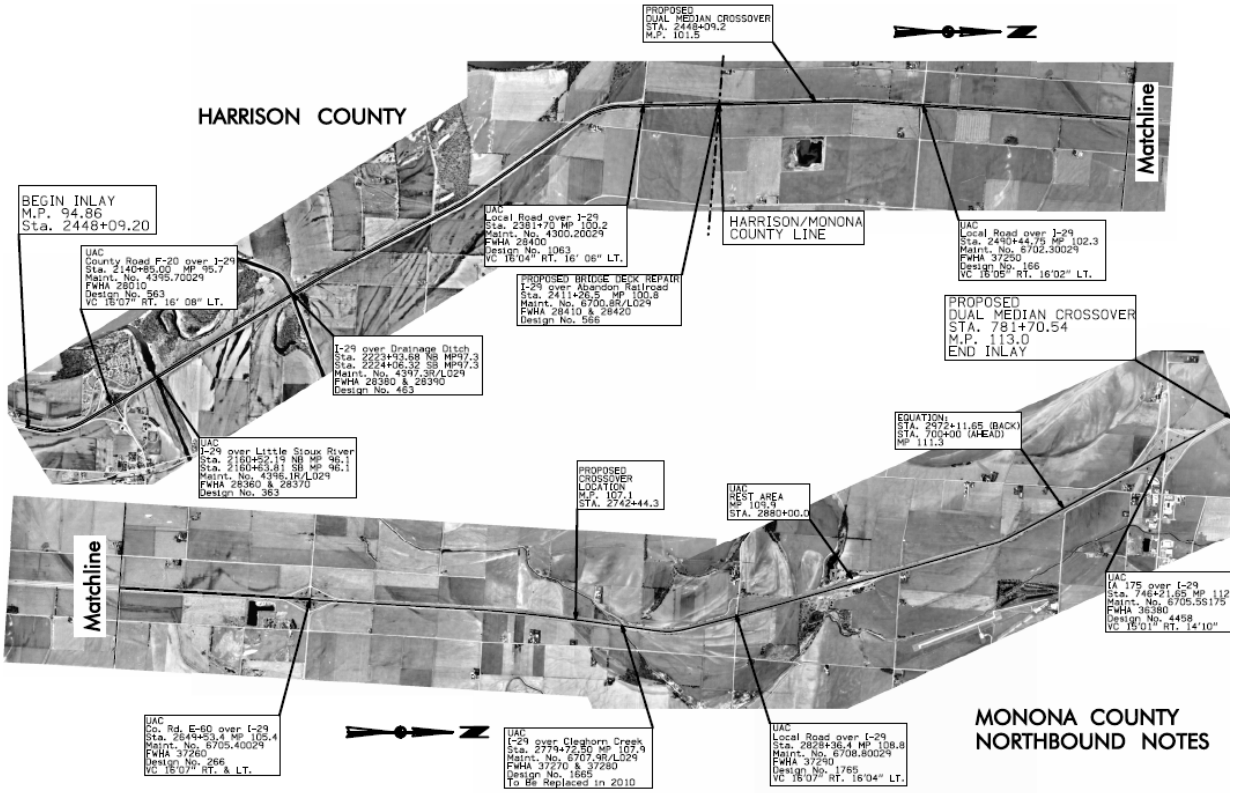

Figure 1. I-29 demonstration project location map constructed from aerial photographs

Figure 2. Existing CRCP

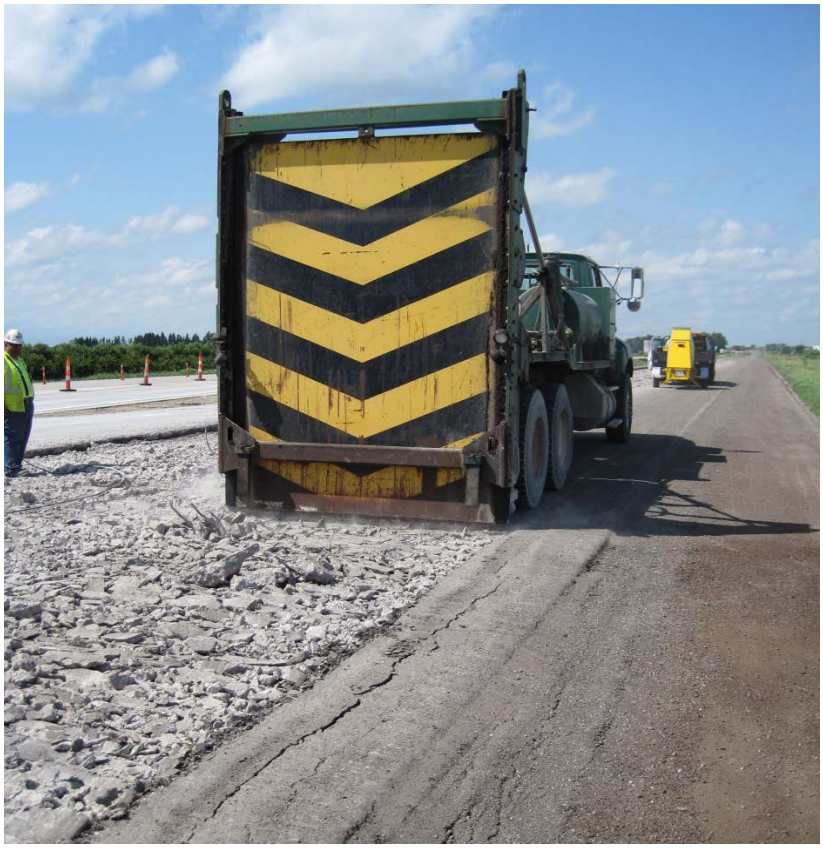

Figure 3. Breaking existing CRCP

Figure 4. Removing existing CRCP

Figure 5. Blading existing subbase material down to subgrade

Figure 6. Spreading special backfill material over compacted subgrade

Figure 7. Compacted special backfill layer

Figure 8. RPCC subbase layer trimming process

Figure 9. RPCC subbase layer before trimming

Figure 10. RPCC subbase layer after trimming

Pavement Design Input Parameter Selection and Assumptions

Table 1 summarizes the pavement thickness design input parameters. A composite modulus of subgrade reaction, k_{comp} = 43 kPa/mm (160 pci), was determined by the Iowa DOT engineer following PCA (1984) design guide. A 279 mm (11 in.) thick JPCP was designed for the new pavement.

Table 1. Summary of pavement thickness design input parameters and assumptions (PCA 1984 method)

Parameter	Value
Surface Layer Design Assumptions	
Design period	40
Average daily traffic (ADT) volume	14,385 (in 2009), 46,400 (in 2049)
Average daily truck traffic (ADTT) volume	9,915 (in 2049)
ADT annual growth	~ 3%
Doweled joints (yes/no)	Yes
Concrete shoulder (yes/no)	No
Concrete modulus of rupture	3965 kPa (575 psi)
Load safety factor	1.2
Equivalent stresses (for single and tandem axles)	Single: 1110 kPa (161 psi) Tandem: 1061 kPa (154 psi)
Stress ratio factors (for single and tandem axles)	Single: 0.280 Tandem: 0.268
Erosion factors (for single and tandem axles)	Single: 2.40 Tandem: 2.62
Allowable load repetitions	Variable for each axle category
Lane distribution factor, *L*	1.0
Foundation Layer Design Assumptions	
Modulus of subgrade reaction, *k*	34 kPa/mm (125 pci)
Type of subbase (treated/untreated)	untreated
Subbase layer thickness	Variable (150 mm minimum and 200 mm average)
Composite modulus of subgrade reaction, k_{comp}	43 kPa/mm (160 pci)
Pavement Thickness Design	
Calculated design thickness	279 mm (11 in.)

CHAPTER 3: EXPERIMENTAL TEST METHODS

This chapter summarizes the laboratory and in situ testing methods used in this research and describes the procedures used to determine *k* values.

Laboratory Testing Methods and Data Analysis

Particle Size Analysis and Index Properties

Samples from existing subbase layers, subgrade layers, and the new special backfill subbase and base layers were collected from the field and were carefully sealed and transported to the laboratory for testing. Particle-size analysis tests were performed in accordance with ASTM C136-06 *Standard test method for sieve analysis of fine and coarse aggregates.* Particle-size analysis tests on the sand subbase and subgrade materials were conducted in accordance with ASTM D422-63 *Standard test method for particle-size analysis of soils.*

Atterberg limit tests (i.e., liquid limit—LL; plastic limit—PL and plasticity index—PI) were performed in accordance with ASTM D4318-10 *Standard test methods for liquid limit, plastic limit, and plasticity index of soils* using the dry preparation method. The results from particle-size analysis and Atterberg limits tests were used to classify the materials on the unified soil classification system (USCS) in accordance with ASTM D2487-10 *Standard practice for classification of soils for engineering purposes (Unified Soil Classification System)* and AASHTO classification system in accordance with ASTM D3282-09 *Standard practice for classification of soils and soil-aggregate mixtures for highway construction purposes.*

Specific gravity tests were performed on the samples in accordance with ASTM D854-10 *Standard test methods for specific gravity of soil solids by water pycnometer*.

Two laboratory compaction tests were used to determine the relationship between dry density and moisture content for the soils obtained from the field. Subgrade soil compaction characteristics were determined using standard and modified Proctor compaction methods in accordance with ASTM D698-07 *Standard test methods for laboratory compaction characteristics of soil using standard effort* and ASTM D1557-07 *Standard test methods for laboratory compaction characteristics of soil using modified effort*, respectively. Maximum and minimum index density tests were performed using a vibratory table on subbase materials in accordance with ASTM D4253-00 *Standard test methods for maximum index density and unit weight of soil using a vibratory table* and ASTM D4254-00 *Standard test methods for minimum index density and unit weight of soils and calculation of relative density.* Moisture-unit weight relationships of subbase materials were determined by performing maximum index density tests by incrementally increasing the moisture content by approximately 1.5% for each test.

Sample Preparation for Resilient Modulus and Shear Strength Testing

Homogenous samples of granular base/subbase and cohesive subgrade materials were tested for resilient modulus (M_r) and unconsolidated undrained (UU) shear strength generally following the AASHTO T-307 procedure. Layered composite soil samples (i.e., those with both subbase and subgrade) were also tested. The following sections describe the methods used to prepare the samples for testing.

Granular Materials:

Granular materials were prepared using the vibratory compaction method as described in AASHTO T-307 for preparation of granular base/subbase materials. Prior to compaction, materials were moisture-conditioned and allowed to mellow for at least 3 to 6 hours. A 101.6 mm (4 in.) diameter split mold was used to compact the sample (Figure 11) in five lifts of equal mass and thickness using an electric rotary hammer drill and a circular steel platen placed against the material (Figure 12). Calipers were used to verify consistent compaction layer thicknesses (Figure 12). The AASHTO T-307 procedure requires that the maximum particle size of the material should be 1/5th of the sample diameter, which is approximately 20.3 mm (0.8 in.) for a 101.6 mm (4 in.) diameter sample. The RPCC base material and special backfill subbase material tested in this study contained a maximum particle size larger than 19.1 mm (0.75 in.). To meet the AASHTO T-307 specifications, the particle size distribution of the untrimmed base material was modified by scalping off particles retained on the 19.1 mm (0.75 in.) sieve and replacing them with the same percentage by weight of the material that was retained on the No. 4 sieve and passing the 19.1 mm (¾ in.) sieve.

Figure 11. Split mold, steel platen (4 in. diameter), and vibratory hammer for compaction of granular materials

Figure 12. Compaction of granular materials in split mold (left) and verification of thickness of each lift using calipers (right)

Cohesive Materials:

Disturbed bag samples obtained from field were used to prepare samples for testing using static compaction method as described in AASHTO T-307. Before compaction, the materials were moisture-conditioned and allowed to mellow for at least 16 hours. Static compaction involved a hydraulic press, steel mold, and six steel spacers (Figure 13) to form the soil into a 101.6 mm diameter by 203.2 mm tall (4 in. diameter by 8 in. tall) cylinder. It must be noted that AASHTO T-307 describes compaction procedure to prepare a 71 mm diameter by 142 mm tall (2.8 in. diameter by 5.6 in. tall) samples. The larger size samples were used in this study to compare with the layered composite samples. The static compaction process is shown in Figure 14. When making the samples, the soil was compacted in five lifts of equal mass and thickness. Each lift of soil was pressed between the steel spacers to a uniform thickness. After compaction, the soil samples were extruded (Figure 14).

Layered Composite Samples:

AASHTO T-307 does not describe a procedure for fabricating layered composite samples. Two kinds of layered composite samples were prepared for this study, base over subgrade and base over subbase. The base over subgrade layered composite samples consisted of a 101.6 mm (4 in.) thick base over a 101.6 mm (4 in.) thick subgrade. The bottom subgrade layer was compacted first using the static compaction technique described in AASHTO T-307 in three lifts. The first two lifts were about 40.6 mm (1.6 in.) thick, and the third lift was about 20.3 mm (0.8 in.) thick. A pre-determined amount of material was placed in each lift to keep the unit weight constant in

each lift. After compaction of the subgrade, the sample was extruded and placed on the triaxial chamber base. The split mold used for granular materials was then placed around the sample, and the top, base layer was compacted in three equal lifts of 33.9 mm (1.3 in.) using the vibratory compaction procedure described in AASHTO T-307.

For the base over subbase layered composite sample, the compaction process for granular materials was followed. The bottom, subgrade layer was compacted in three lifts. The first two lifts were about 40.6 mm (1.6 in.) thick, and the third lift was about 20.3 mm (0.8 in.) thick. The top, base layer was compacted in three lifts as well with the first lift about 20.3 mm (0.8 in.) thick, and the remaining two lifts about 40.6 mm (1.6 in.) thick.

Figure 13. Aluminum spacers (4 in. diameter) used during static compaction

Figure 14. Photos showing static compaction procedure (left) and sample extrusion procedure (right) of a compacted cohesive soil sample

Resilient Modulus and Shear Strength Testing

M_r and UU tests were performed using the Geocomp automated M_r test setup (Figure 6) in accordance with AASHTO T-307. The setup consists of a Load Trac-II load frame, an electrically controlled servo valve, an external signal conditioning unit, and a computer with a network card for data acquisition. The system uses a real-time adjustment of proportional-integral-derivative (PID) controller to adjust the system control parameters as the stiffness of the sample changes to apply the target loads during the test. Figure 6 shows the triaxial test chamber used in this study. The chamber is set up for both 71 mm (2.8 in.) and 101.6 mm (4 in.) diameter samples. Two linear voltage displacement transducers (LVDTs) are mounted to the piston rod to measure resilient strains in the sample during the test.

M_r tests were performed following the AASHTO T-307 conditioning and loading sequences suggested for base and subgrade materials (Table 2). Each load cycle consisted of a 0.1 second haversine-shaped load pulse followed by a 0.9 second rest period. M_r is calculated as the ratio of the applied cyclic deviator stress (σ_d) and resilient strain (ε_r). The σ_d and ε_r values from a typical stress-strain cycle during the test are shown in Table 2. The average σ_d and ε_r of the last five cycles of a loading sequence are used in M_r calculations. After M_r testing, UU shear strength testing was performed on each sample by applying a confining pressure of 34.5 kPa (5 psi) to the base and subbase samples and 27.6 kPa (4 psi) to the subgrade samples.

Figure 15. Triaxial chamber, load frame, and computer equipment for M_r testing

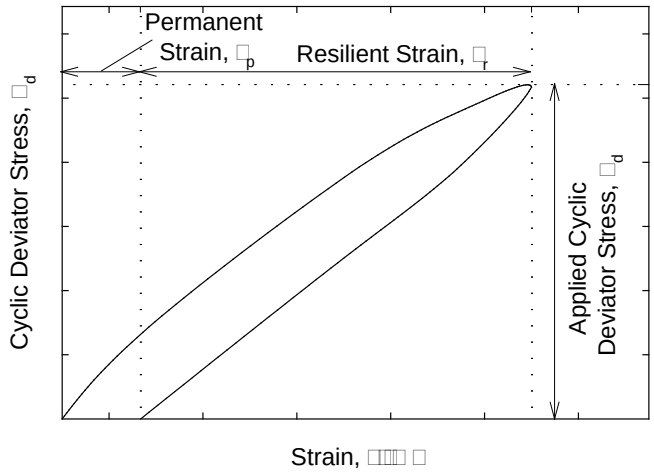

Figure 16. Graphical representation of one load cycle in M_r testing

Table 2. Resilient modulus test sequences and stress values for base/subbase and subgrade materials (AASHTO T-307)

Base/Subbase Materials						Subgrade Materials					
	Confining Pressure		Max. Axial Stress				Confining Pressure		Max. Axial Stress		
Sequence No.	kPa	psi	kPa	psi	No. of cycles	Sequence No.	kPa	psi	kPa	psi	No. of cycles
0	103.4	15	103.4	15	500-1000	0	41.4	6	27.6	4	500-1000
1	20.7	3	20.7	3	100	1	41.4	6	13.8	2	100
2	20.7	3	41.4	6	100	2	41.4	6	27.6	4	100
3	20.7	3	62.1	9	100	3	41.4	6	41.4	6	100
4	34.5	5	34.5	5	100	4	41.4	6	55.2	8	100
5	34.5	5	68.9	10	100	5	41.4	6	68.9	10	100
6	34.5	5	103.4	15	100	6	27.6	4	13.8	2	100
7	68.9	10	68.9	10	100	7	27.6	4	27.6	4	100
8	68.9	10	137.9	20	100	8	27.6	4	41.4	6	100
9	68.9	10	206.8	30	100	9	27.6	4	55.2	8	100
10	103.4	15	68.9	10	100	10	27.6	4	68.9	10	100
11	103.4	15	103.4	15	100	11	13.8	2	13.8	2	100
12	103.4	15	206.8	30	100	12	13.8	2	27.6	4	100
13	137.9	20	103.4	15	100	13	13.8	2	41.4	6	100
14	137.9	20	137.9	20	100	14	13.8	2	55.2	8	100
15	137.9	20	275.8	40	100	15	13.8	2	68.9	10	100

Resilient Modulus Data Analysis

M_r values are used in pavement design as a measure of stiffness of unbound materials in the pavement structure. The M_r parameter is a highly stress-dependent parameter. Many non-linear constitutive models have been proposed that incorporate the effects of stress levels and predict M_r values. Most soils exhibit the effects of increasing stiffness with increasing bulk stress and decreasing stiffness with increasing shear stress (Andrei et al. 2004). A non-linear constitutive model (also called the "universal" model) proposed by Witczak and Uzan (1988) (Equation 1) was used in this study

$$M_r = k_1 P_a \left(\frac{\sigma_B}{P_a} \right)^{k_2} \left(\frac{\tau_{oct}}{P_a} + 1 \right)^{k_3} \quad (1)$$

where P_a = atmospheric pressure (MPa); σ_B = bulk stress (MPa) = $\sigma_1 + \sigma_2 + \sigma_3$; τ_{oct} = octahedral shear stress (MPa) = $\{[(\sigma_1-\sigma_2)^2+(\sigma_2-\sigma_3)^2+(\sigma_3-\sigma_1)^2]^{1/2}\} / 3$; σ_1, σ_2, σ_3 = principal stresses; and k_1, k_2, k_3 = regression coefficients. The k_1 coefficient is proportional to M_r and therefore is always > 0. The k_2 coefficient explains the behavior of the material with changes in the volumetric stresses. Increasing volumetric stresses increases the M_r value and therefore the k_2 coefficient should be ≥ 0. The k_3 coefficient explains the behavior of the material with changes in shear stresses. Increasing shear stress softens the material and yields a lower M_r value; therefore, the k_3 coefficient should be ≤ 0.

The R^2 values determined for this model were adjusted for the number of regression parameters using Equation 2

$$R^2(\text{Adjusted}) = 1 - \left[\frac{(1 - R^2)(n-1)}{n-p-1} \right] \quad (2)$$

where *n* = the number of data points and *p* = the number of regression parameters.

Determination of Dynamic Secant Modulus from Cyclic Stress-Strain Data

The cyclic stress-strain data obtained from resilient modulus tests were used to estimate dynamic secant modulus (E_s) to compare with dynamic elastic modulus measurements obtained from field tests. Secant modulus was determined from the slope of the line connecting the origin to a selected point on the stress-strain curve of a material, as illustrated in Figure 17. The difference between secant moduli and resilient moduli is the use of permanent strain instead of resilient strain in the calculations.

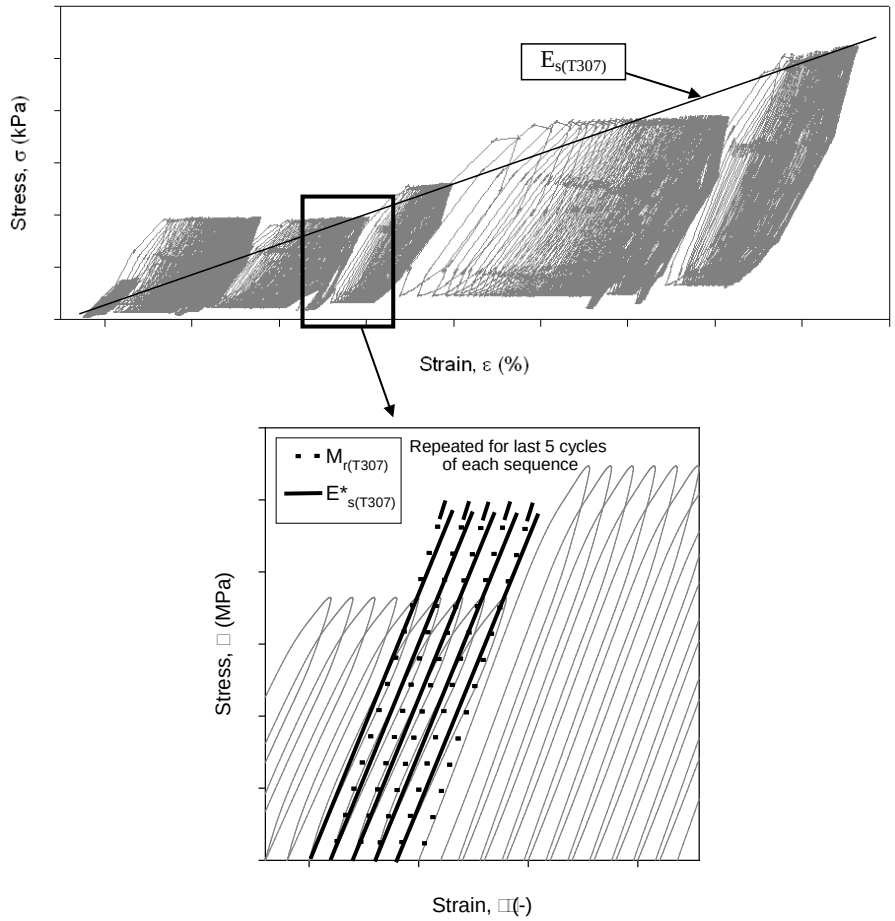

Figure 17. Comparison of resilient ($M_{r(T-307)}$), cyclic secant ($E^*_{s(T-307)}$), and dynamic secant ($E_{s(T-307)}$) modulus values

Frost Heave and Thaw Weakening Test

Frost heave and thaw weakening tests were performed in general accordance with ASTM D5918-06 *Standard test methods for frost heave and thaw weakening susceptibility of soils*. The test is used to classify the frost heave and thaw weakening susceptibility of soils based on the heave rate and the thawed CBR values. The heave rate and thawed CBR values are compared with a classification system provided in the standard to determine the susceptibility ratings (Table 3). It must be noted that the test results can only be used to compare the relative frost heave and thaw weakening susceptibility between material types and cannot be used to directly determine the amount of frost heave or thaw weakening in a pavement system.

A cross-sectional view and a three-dimensional view of the custom freeze/thaw (F/T) test setup fabricated at Iowa State University are shown in Figure 18 and Figure 19, respectively. The samples were 146 mm (5.75 in.) in diameter and 152 mm (6 in.) in height and were compacted inside six rings with a rubber membrane between the soil and the rings. The compaction mold setup is shown in Figure 20 and Figure 21. A water supply was made available at a level of 13 mm (0.5 in.) above the bottom of the sample using a Mariotte tube (Figure 18) to saturate the

sample. A surcharge weight was applied to the sample to simulate the loading of a typical pavement section. During F/T testing, laser transducers installed on a ring stand and a bracket above the sample obtained measurements of the samples' heave and consolidation, and thermocouples installed in the sample obtained the temperature profile (Figure 18). The laser transducers used in this study had a measurement range of 50 mm and a resolution of 0.75 μm. The lasers and thermocouples were connected to a data acquisition system that recorded the temperature in one-minute intervals.

Table 3. Frost susceptibility classifications (ASTM D5918-06)

Frost Susceptibility Classification	Heave Rate (mm/day)	Thawed CBR (%)
Negligible	<1	>20
Very low	1 to 2	20 to 15
Low	2 to 4	15 to 10
Medium	4 to 8	10 to 5
High	8 to 16	5 to 2
Very High	>16	<2

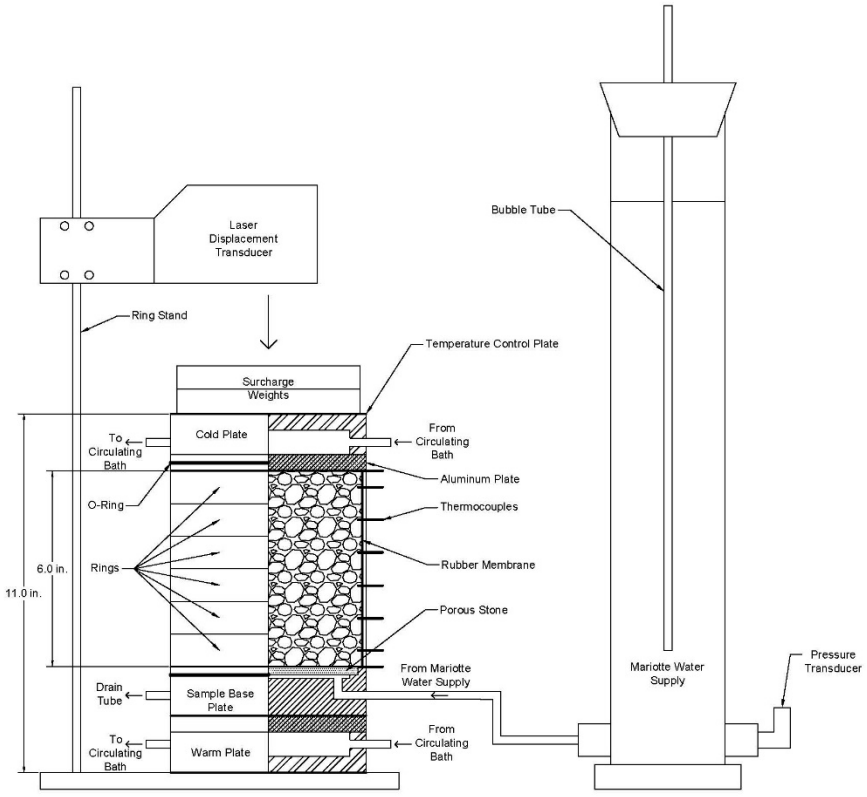

Figure 18. Illustration of frost-heave and thaw-weakening test assembly

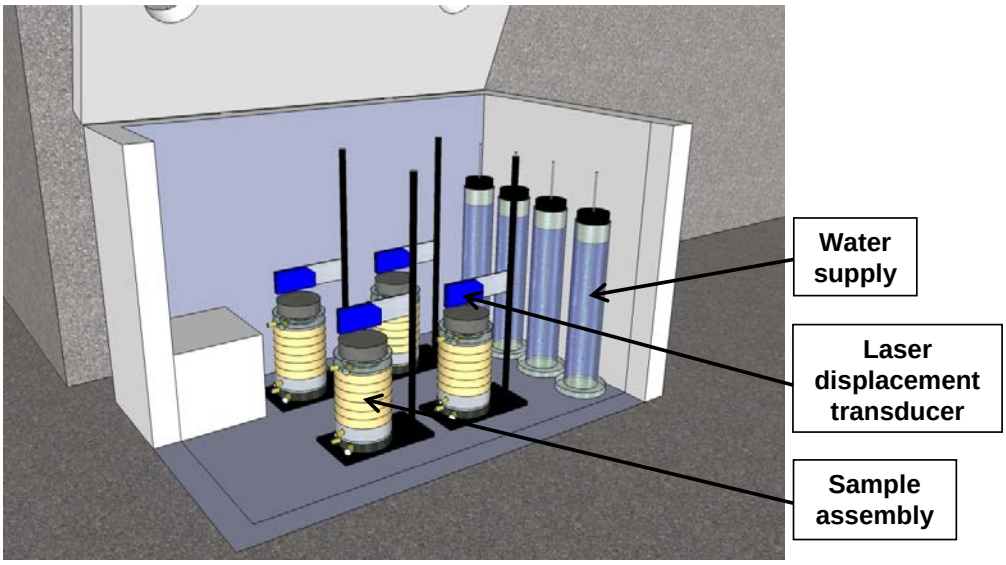

Figure 19. Three dimensional illustration of frost-heave and thaw-weakening test assembly

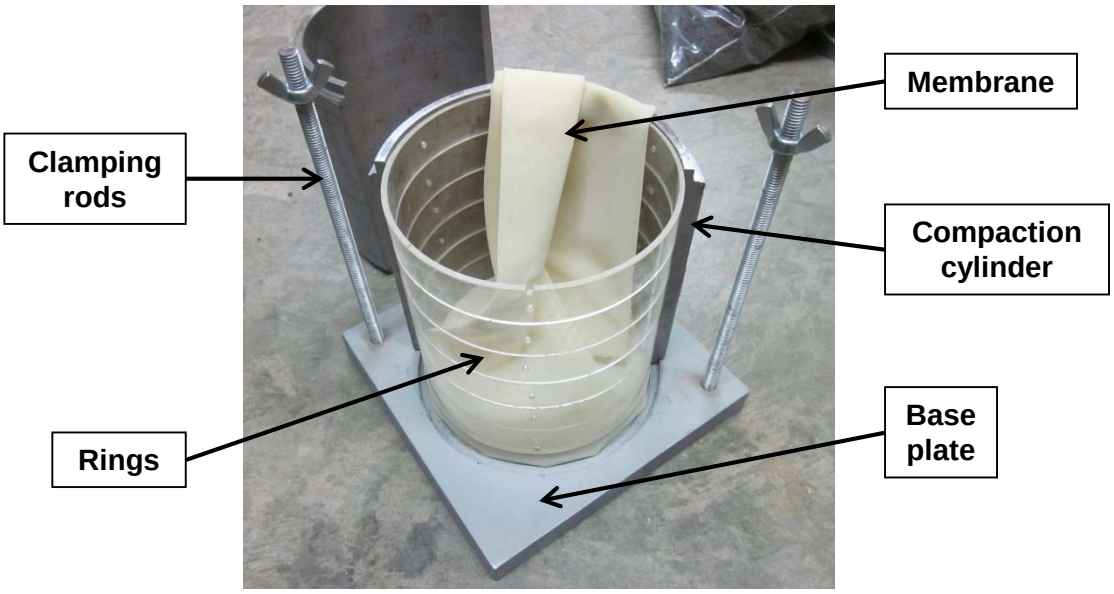

Figure 20. View of frost-heave and thaw-weakening test compaction mold with six rings

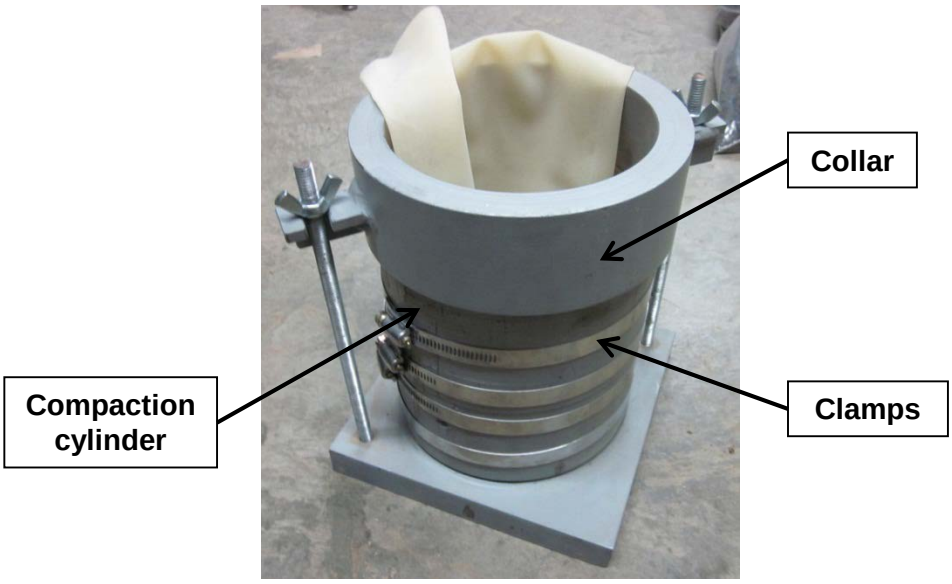

Figure 21. Frost-heave and thaw-weakening test compaction mold setup with collar

The F/T test was carried out by exposing four soil samples to two freeze-thaw cycles over a five day period. The samples were placed in a temperature controlled chest freezer (Figure 19) and then frozen and thawed by changing the temperature at the top and bottom of the samples using temperature controlled water baths (Figure 22). The programmable water baths used in this study had an operating range of -30°C to +200°C and adjustable to ±0.01°C, and were filled with 50% ethylene glycol-water solution. Insulating tape was wrapped around the flexible tubing between the water baths and the temperature control end plates, to help reduce temperature variations in the solution. The target top and bottom of the sample temperatures (Figure 23) were programmed into the water baths and the actual temperatures were measured during the test. An example of the measured temperatures at the top and bottom of the sample is shown in Figure 24. Results indicated that the measured temperatures were higher during freezing and lower during thawing than the target values. This discrepancy likely occurred because of temperature losses in the glycol solution when transported from the temperature control baths to the temperature control end plates (although care was taken to reduce these variations as indicated above). After the F/T test was completed, a CBR test was performed on the thawed samples in accordance with ASTM D1883-07 and a moisture content profile of the sample was determined by carefully trimming the thawed sample to desired depths.

The heave rate of the sample was determined from the slope of the heave versus time plot as illustrated in Figure 24 for a period of about 24 hours for both the 1st and 2nd freezing cycles. The ASTM D5918 specifies determining heave rate during the first eight hours of each freezing cycle. However, a few samples that were obtained from other research project sites did not heave during the first eight hours, and the samples that did heave during the first eight hours showed similar heave rates over the 8 hour and the 24 hour periods. To be consistent in comparing measurements from different project sites, the research team decided to present the heave rate over the 24 hour period.

Figure 22. Temperature control water baths used to freeze and thaw samples

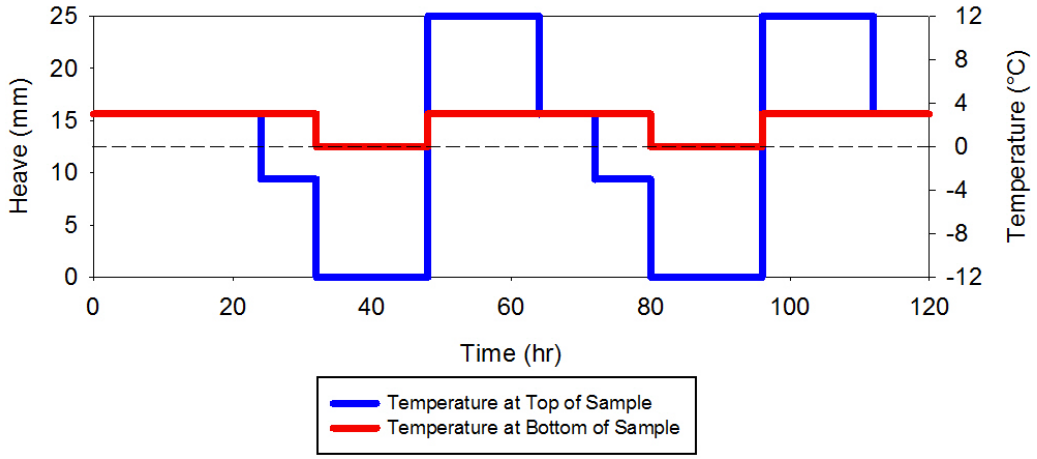

Figure 23. Target top and bottom temperatures with time per ASTM standard during F/T cycles

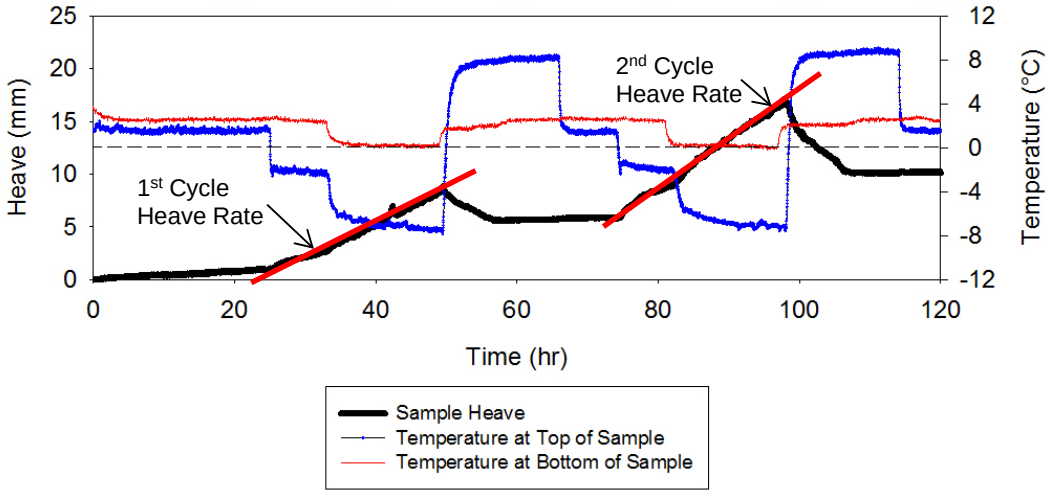

Figure 24. Example of measured top and bottom temperatures during freeze-thaw cycles and determination of heave rate for 1st and 2nd freezing cycles

In Situ Testing Methods and Data Analysis

The following in situ testing methods and devices were used in this study: a real-time kinematic (RTK) global positioning system (GPS); a Zorn lightweight deflectometer (LWD) setup with a 300 mm diameter plate; a Kuab falling weight deflectometer (FWD) setup with a 300 mm diameter plate; a dynamic cone penetrometer (DCP); and a calibrated Humboldt nuclear gauge (NG). Roller-integrated compaction measurements were taken with a Volvo vibratory smooth drum roller equipped with Trimble's roller integrated compaction monitoring (RICM) system. Pictures of these test devices are shown in Figure 25.

Real-Time Kinematic Global Positioning System

An RTK-GPS system was used to obtain spatial coordinates (x, y, and z) of in situ test locations and tested pavement slabs. A Trimble SPS 881 receiver was used with base station correction provided from a Trimble SPS851 established on site. According to the manufacturer, this survey system is capable of horizontal accuracies of < 10 mm and vertical accuracies of < 20 mm.

Zorn Light Weight Deflectometer

Zorn LWD tests were performed on base and subbase layers to determine elastic modulus. The LWD was setup with 300 mm diameter plate and 71 cm drop height. The tests were performed following manufacturer recommendations (Zorn 2003) and the elastic modulus values were determined using Equation 3, where E = elastic modulus (MPa), D_0 = measured deflection under the plate (mm), η = Poisson's ratio (0.4), σ_0 = applied stress (MPa), r = radius of the plate (mm), F = shape factor depending on stress distribution (assumed as 8/3) (see Vennapusa and White 2009). The results are reported as $E_{LWD\text{-}Z3}$ (Z represents Zorn LWD and 3 represents 300 mm diameter plate).

$$E = \frac{(1-\eta^2)\sigma_0 r}{D_0} \times F \quad (3)$$

Figure 25. In situ test equipment: Trimble SPS-881 hand-held receiver, Kuab FWD, and Zorn LWD (top row left to right); DCP, NG, and Volvo smooth drum vibratory roller equipped with CMV measurement system (bottom row left to right)

Kuab Falling Weight Deflectometer

Falling weight deflectometer (FWD) tests were conducted using a Kuab FWD setup with a 300 mm (11.81 in) diameter loading plate by applying one seating drop and three loading drops. The applied loads varied from about 27 kN (6,000 lb) to 54 kN (12,000 lb) in the three loading drops. The actual applied loads were recorded using a load cell, and deflections were recorded using seismometers mounted on the device, per ASTM D4694-09 *Standard Test Method for Deflections with a Falling-Weight-Type Impulse Load Device.* The FWD plate and deflection

sensor setup and a typical deflection basin are shown in Figure 26. To compare deflection values from different test locations at the same applied contact stress, the values at each test location were normalized to a 40 kN (9,000 lb) applied force.

FWD tests were conducted at the center of the PCC slab panels and at the joints. Tests conducted at the joints were used to determine joint load transfer efficiency (LTE) and voids beneath the pavement based on "zero" load intercept values. Tests conducted at the center of the slab panels were used to determine modulus of subgrade reaction (*k*) values and the intercept values. The procedure used to calculate these parameters are described below.

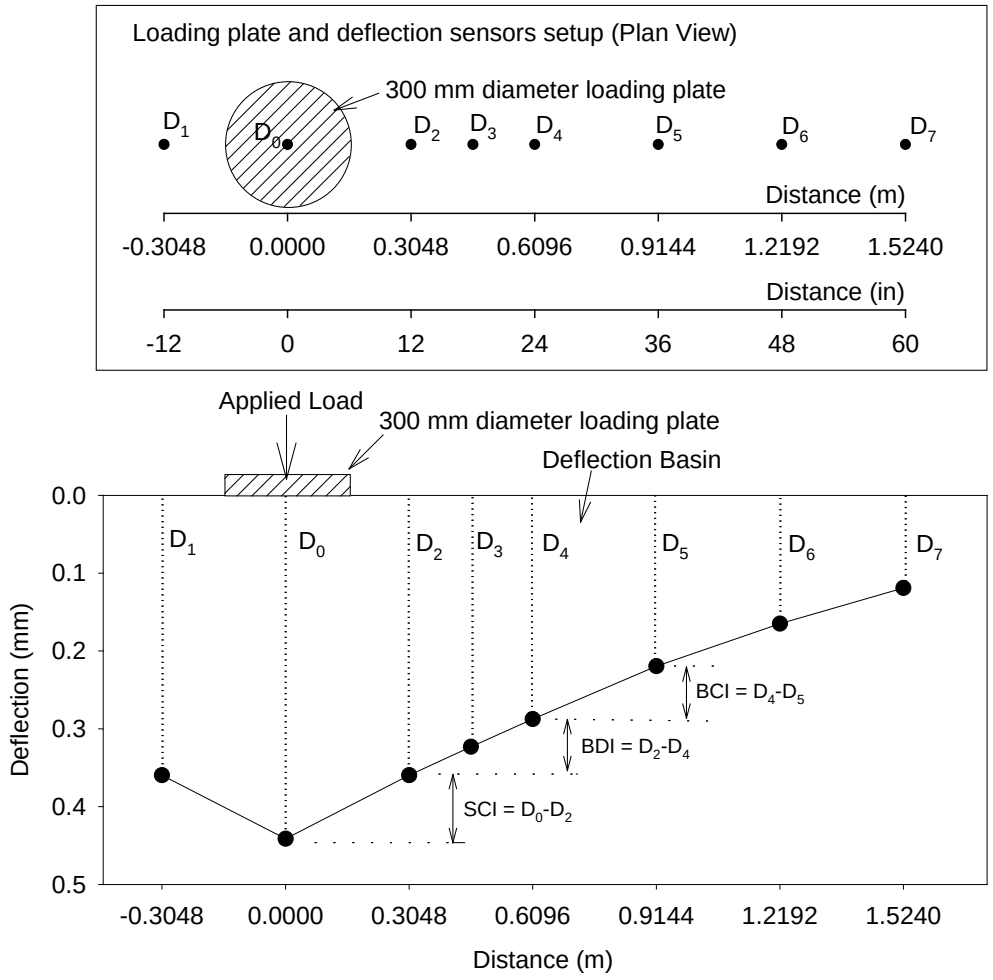

Figure 26. FWD deflection sensor setup used for this study and an example deflection basin

LTE was determined by obtaining deflections under the plate on the loaded slab (D_0) and deflections of the unloaded slab (D_1) using a sensor positioned about 305 mm (12 in.) away from the center of the plate (Figure 26). The LTE was calculated using Equation 4.

$$LTE(\%) = \frac{D_1}{D_0} \times 100 \quad (4)$$

Voids underneath pavements can be detected by plotting the applied load measurements on the X-axis and the corresponding deflection measurements on the y-axis and plotting a best fit linear regression line, as illustrated in Figure 27, to determine the "zero" load intercept (I) values. AASHTO (1993) suggests I = 0.05 mm (2 mils) as a critical value for void detection. According to Quintus and Simpson (2002), if I = -0.01 and +0.01 mm, then the response would be considered elastic. If I > 0.01 then the response would be considered deflection hardening, and if I < -0.01 then the response would be considered deflection softening.

Pavement layer temperatures at different depths were obtained during FWD testing, in accordance with the guidelines from Schmalzer (2006). The temperature measurements were used to determine equivalent linear temperature gradients (T_L) following the temperature-moment concept suggested by Jannsen and Snyder (2000). According to Vandenbossche (2005), I-values are sensitive to temperature induced curling and warping affects. Large positive temperature gradients (i.e., when the surface is warmer than the bottom) that cause the panel corners to curl down result in false negative I-values. Conversely, large negative gradients (i.e., when the surface is cooler than the bottom) that cause the panel corners to curl upward result in false positive I-values. Interpretation of I-values therefore should consider the temperature gradient. Concerning LTE measurements for doweled joints, the temperature gradient is reportedly not a critical factor (Vandenbossche 2005).

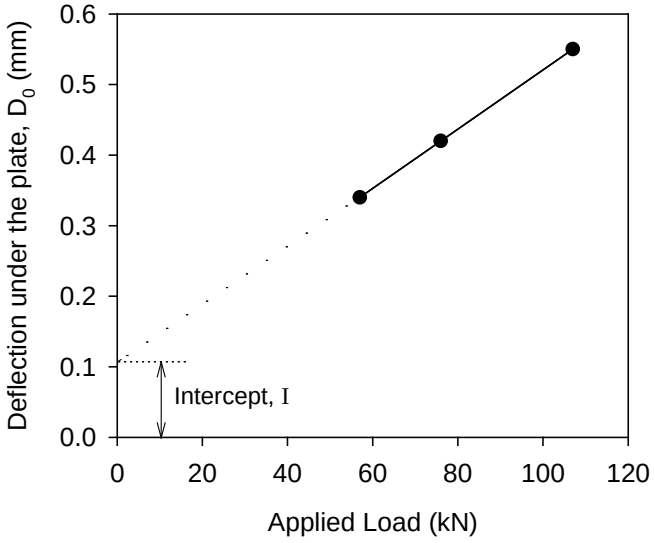

Figure 27. Void detection using load-deflection data from FWD test

The *k* values were determined using the $AREA_4$ method described in AASHTO (1993). Since the *k* value determined from FWD test represents a dynamic value, it is referred to here as $k_{FWD\text{-}Dynamic}$. Deflections obtained from four sensors (D_0, D_2, D_4, and D_5 shown in Figure 26)

were used in the $AREA_4$ calculation. The AREA method was first proposed by Hoffman and Thompson (1981) for flexible pavements and has since been applied extensively for concrete pavements (Darter et al. 1995). $AREA_4$ is calculated using Equation 5 and has dimensions of length (in inches), as it is normalized with deflections under the center of the plate (D_0):

$$AREA_4 = 6 + 12 \times \left(\frac{D_2}{D_0} \right) + 12 \times \left(\frac{D_4}{D_0} \right) + 6 \times \left(\frac{D_5}{D_0} \right) \quad (5)$$

where D_0 = deflections measured directly under the plate (in.); D_2 = deflections measured at 305 mm (12 in.) away from the plate center (in.); D_4 = deflections measured at 610 mm (24 in.) away from the plate center (in.); and D_5 = deflections measured at 914 mm (36 in.) away from the plate center (in.). The $AREA_4$ method can also be calculated using different sensor configurations and setups, (i.e., using deflection data from 3, 5, or 7 sensors), and those methods are described in detail in the literature (Substad et al. 2006, Smith et al. 2007)

In early research conducted using the AREA method, the ILLI-SLAB finite element program was used to compute a matrix of maximum deflections at the plate center and the AREA values by varying the subgrade *k*, the modulus of the PCC layer, and the thickness of the slab (ERES Consultants, Inc. 1982). Measurements obtained from FWD tests were then compared with the ILLI-SLAB program results to determine the *k* values through back calculation. Barenberg and Petros (1991) and Ioannides (1990) proposed a forward solution procedure based on Westergaard's solution for loading on an infinite plate to replace the back calculation procedure. This forward solution presented a unique relationship between AREA value (for a given load and sensor arrangement) and the dense liquid radius of relative stiffness (L) in which subgrade is characterized by the *k* value. The radius of relative stiffness (L) is estimated using Equation 6:

$$L = \left[\frac{\ln\left(\frac{x_1 - AREA_4}{x_2} \right)}{x_3} \right]^{x_4} \quad (6)$$

where x_1 = 36, x_2 = 1812.279, x_3 = -2.559, x_4 = 4.387. It must be noted that the x_1 to x_4 values vary with the sensor arrangement and these values are only valid for the $AREA_4$ sensor setup. Once, the L value is known, the $k_{FWD\text{-}Dynamic}$ value can be estimated using Equation 7:

$$k_{FWD-Dynamic} \ (pci) = \frac{PD_0^*}{D_0 L^2} \quad (7)$$

where P = applied load (lbs), D_0 = deflection measured at plate center (inches), and D_0^* = non-dimensional deflection coefficient calculated using Equation 8:

$$D_0^* = a \cdot e^{-be^{-cL}} \quad (8)$$

where a = 0.12450, b = 0.14707, c = 0.07565. It must be noted that these equations and coefficients are valid for an FWD setup with an 11.81 in. diameter plate.

The advantages of the $AREA_4$ method are the ease of use without back calculations and the use of multiple sensor data. The disadvantages are that the process assumes that the slab and the subgrade are horizontally infinite. This assumption leads to underestimating the k values of jointed pavements. Crovetti (1993) developed the following slab size corrections for a square slab that is based on finite element analysis conducted using the ILLI-SLAB program and is for use in the $k_{FWD\text{-}Dynamic}$:

$$Adjusted\ D_0 = D_0\left(1 - 1.15085e^{-0.71878\left(\frac{L'}{L}\right)^{0.80151}}\right) \quad (9)$$

$$Adjusted\ L = L\left(1 - 0.89434e^{-0.61662\left(\frac{L'}{L}\right)^{1.04831}}\right) \quad (10)$$

where L′ = slab size (smaller dimension of a rectangular slab, length or width). This procedure also has limitations: (1) it considers only a single slab with no load transfer to adjacent slabs, and (2) it assumes a square slab. The square slab assumption is considered to produce sufficiently accurate results when the smaller dimension of a rectangular slab is assumed as L′ (Darter et al. 1995). Darter et al. 1995 suggested using $L' = \sqrt{Length \times Width}$ to further refine slab size corrections. However, no established procedures for correcting for load transfer to adjacent slabs have been reported so accounting for load transfer remains as a limitation of this method.

AASHTO (1993) suggests dividing the $k_{FWD\text{-}Dynamic}$ value by a factor of 2 to determine the equivalent $k_{FWD\text{-}Static}$ value. The origin of this factor 2 dates back to Foxworthy's work in the 1980's. Foxworthy (1985) reported comparisons between the $k_{FWD\text{-}Dynamic}$ values obtained using Dynatest model 8000 FWD and the Static k values (Static k_{PLT}) obtained from 30 in. diameter plate load tests (the exact procedure followed to calculate the Static k_{PLT} is not reported in Foxworthy 1985). Foxworthy used the AREA based back calculation procedure using the ILLI-SLAB finite element program. Results obtained from Foxworthy's study (Figure 28) are based on 7 FWD tests conducted on PCC pavements with slab thicknesses varying from about 10 in. to 25.5 in. and plate load tests conducted on the foundation layer immediately beneath the pavement over a 4 ft x 5 ft test area. A few of these sections consisted of a 5 to 12 in. thick base course layer and some did not. The subgrade layer material consisted of CL soil from Sheppard Air Force Base in Texas, SM soil from Seymour-Johnson Air Force Base in North Carolina, and an unspecified soil type from McDill Air Force base in Florida. No slab size correction was performed on this dataset.

Data from Foxworthy (1985) yielded a logarithmic relationship between the dynamic and the static *k* values. On average, the $k_{FWD\text{-}Dynamic}$ values were about 2.4 times greater than the Static k_{PLT} values. Darter et al. (1995) indicated that the factor 2 is reasonable based on results from other test sites (Figure 28). Darter et al. (1995) also compared FWD test data from eight long-term pavement performance (LTPP) test sections with the Static k_{PLT} values and reported factors ranging from 1.78 to 2.16, with an average of about 1.91. The $k_{FWD\text{-}Dynamic}$ values used in that comparison were corrected for slab size. For the analysis conducted in this research project, the corrected $k_{FWD\text{-}Dynamic}$ values (for finite slab size) were divided by 2 and are reported as $k_{FWD\text{-}Static\text{-}Corr}$ values.

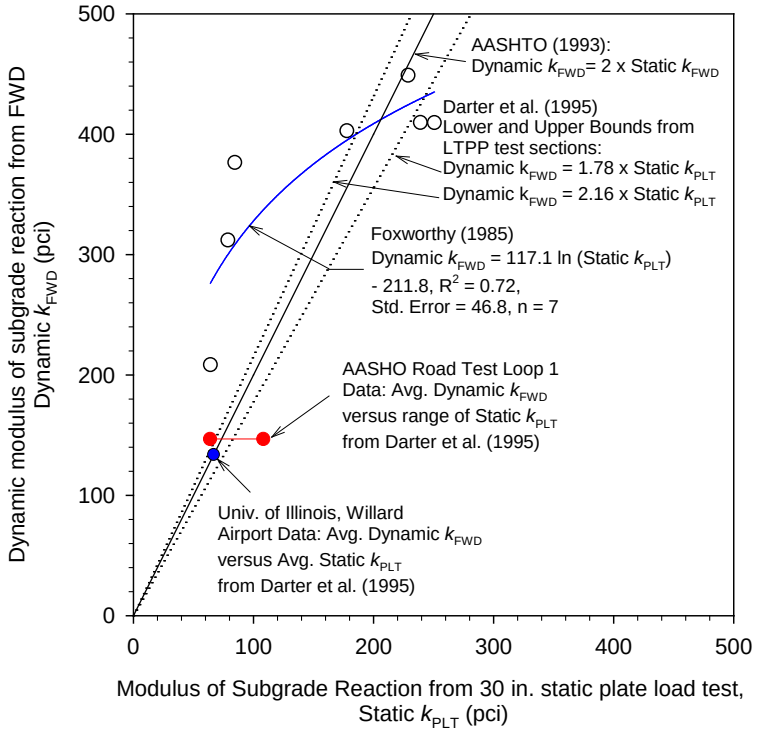

Figure 28. Static k_{PLT} values versus $k_{FWD\text{-}Dynamic}$ measurements reported in literature

Dynamic Cone Penetrometer

DCP tests were performed in accordance with ASTM D6951-03 *Standard Test Method for Use of the Dynamic Cone Penetrometer in Shallow Pavement Applications* to determine dynamic penetration index (DPI) and calculate California bearing ratio (CBR) using Equation 11.

$$CBR = \frac{292}{DPI^{1.12}} \tag{11}$$

The DCP test results are presented in this report as CBR with depth profiles at a test location and as point values of $DCP\text{-}CBR_{Subbase}$ representative of the subbase layer, $DCP\text{-}CBR_{Treated\ Subgrade}$ representative of the special backfill subgrade treatment layer, and DCP-CBRSubgrade

representative of the top 300 mm of the subgrade. The point data values represent the weighted average CBR within each layer. Because the subbase layer under the existing CRCP was very thin (25 to 50 mm) the DCP-$CBR_{Subbase}$ was not separately calculated. CBR of the weakest layer within the subgrade, within the top 450 mm of the subgrade was also calculated and reported as DCP-$CBR_{Subgrade\text{-}Weak}$ to assess its influence on the overall structural response.

Nuclear Gauge

A calibrated Humboldt nuclear moisture-density gauge (NG) device was used to provide rapid measurements of soil dry unit weight (γ_d) and moisture content (w) in the base materials. Tests were performed following ASTM D6938-10 *Standard Test Method for In-Place Density and Water Content of Soil and Soil-Aggregate by Nuclear Methods (Shallow Depth)*. Measurements of w and γ_d were obtained at each test location and the average values are reported.

Roller-Integrated Compaction Measurements

A Volvo SD116DX vibratory smooth drum roller equipped with compaction meter value (CMV) measurement system was used on this project. Features of the CMV are provided below, and some key features of the roller are summarized in Table 4.

Table 4. Volvo SD116DX vibratory smooth drum IC roller features

Feature	Description
Drum Geometry	Smooth drum
Frequency (f)	34 Hz (low amplitude setting) 30 Hz (high amplitude setting)
Amplitude (a) Settings	1.60 mm (low) 2.00 mm (high)
Compaction Measurement Values (MVs)	Compaction Meter Value (CMV)
Display Software	Trimble® CB430/ Sitevision ™ office
Output Documentation	Date/Time; Location (Northing/Easting/ Elevation of left and right ends of the roller drum); Speed; CMV; RMV; Frequency; Amplitude (theoretical); Direction (forward/ backward); Vibration (On/Off)

CMV is a dimensionless compaction parameter developed by Geodynamik that depends on roller dimensions, (i.e., drum diameter and weight) and roller operation parameters (e.g., frequency, amplitude, speed), and is determined using the dynamic roller response (Sandström 1994). CMV is calculated using Equation 12, where C is a constant (300), $A_{2\Omega}$ = the acceleration of the first harmonic component of the vibration, and A_{Ω} = the acceleration of the fundamental component of the vibration (Sandström and Pettersson 2004). Correlation studies relating CMV to soil dry unit weight, strength, and stiffness are documented in the literature (e.g., Floss et al. 1983,

Samaras et al. 1991, Brandl and Adam 1997, Thompson and White 2008, White and Thompson 2008).

$$CMV = C \cdot \frac{A_{2\Omega}}{A_{\Omega}} \tag{12}$$

Determination of *k* values

Subgrade *k* values were determined from field measurements using FWD testing, empirical relationships from DCP-CBR measurements, and empirical relationships from laboratory measurements. All of these values are compared with the assumed design *k* and k_{comp} values. The following list provides the notations for the *k* values and the procedures used to determine those *k* values.

- $k_{FWD\text{-}Static\text{-}Corr}$ determined from the FWD test and corrected for slab size.
- $k_{FWD\text{-}Static\text{-}Corr\text{-}comp\text{-}PCA}$ determined from $k_{FWD\text{-}Static\text{-}Corr}$ and Table 5 based on H_{SB} = 150 mm (thickness of the RPCC base layer).
- k_{PCA} determined from DCP-CBR using charts provided in PCA (1984) (see Appendix A). For values under the new JPCP, DCP-$CBR_{Treated\ Subgrade}$ was used and for values under the existing CRCP, DCP-$CBR_{Subgrade}$ was used.
- $k_{PCA\text{-}Weak\ Subgrade}$ determined from DCP-$CBR_{Subgrade\text{-}Weak}$ using charts provided in PCA (1984) (see Appendix A).
- $k_{comp\text{-}PCA}$ determined from k_{PCA} and Table based on H_{SB} = 150 mm.
- $k_{comp\text{-}PCA\text{-}Weak\ Subgrade}$ determined from $k_{PCA\text{-}Weak\ Subgrade}$ and Table 5 based on H_{SB} = 150 mm.

Table 5. Estimation of $k_{comp\text{-}PCA}$ based on subgrade k_{PCA} and subbase layer thickness

	$k_{comp\text{-}PCA}$ (kPa/mm) based on subbase layer thickness (H_{SB})			
k_{PCA} (kPa/mm)	H_{SB} = 100 mm	150 mm	230 mm	300 mm
13.7	17.8	20.5	23.2	30.1
27.3	35.5	38.3	43.7	51.9
54.6	60.1	62.8	73.8	87.4
82.0	87.4	90.2	101.1	117.5

CHAPTER 4: LABORATORY TEST RESULTS

Two samples from the existing foundation layers (subgrade and existing sand subbase) and three samples from the new foundation layers (i.e., recycled asphalt special backfill subgrade treatment with recycled asphalt and treatment with select sand and RPCC subbase) were collected from field and tested in the laboratory as part of this project. A summary of the material index properties (i.e., laboratory compaction test, grain-size analysis, Atterberg limits test, soil classification, and specific gravity results) is provided in Table 6.

Table 6. Summary of material index properties

Parameter	Subgrade	Existing Sand Subbase	Recycled Asphalt Special Backfill Subgrade Treatment	Select Sand Special Backfill Subgrade Treatment	RPCC Subbase
Standard Proctor γ_{dmax} (kN/m^3)	16.47				
Standard Proctor γ_{dmax} (pcf)	104.8				
Standard Proctor w_{opt} (%)	19.7				
Modified Proctor γ_{dmax} (kN/m^3)	18.01		—		
Modified Proctor γ_{dmax} (pcf)	114.7				
Modified Proctor w_{opt} (%)	14.1				
Relative Density Test* γ_{dmin} (kN/m^3)	—	14.20	14.82	16.39	14.76
Relative Density Test* γ_{dmin} (pcf)	—	90.4	94.3	104.3	94.0
Relative Density Test* γ_{dmax} (kN/m^3)	—	20.80	18.87	20.67	19.31
Relative Density Test* γ_{dmax} (pcf)	—	132.4	120.1	131.6	122.9
Gravel Content (%) (> 4.75mm)	3	25	51	36	59
Sand Content (%) (4.75mm – 75μm)	5	65	42	54	31
Silt Content (%) (75μm – 2μm)	65	7	7	10	10
Clay Content (%) (< 2μm)	27	3			
Liquid Limit, LL (%)	41				
Plastic Limit, PL (%)	21		Non-Plastic		
Plasticity Index, PI (%)	20				
AASHTO Classification	A-7-6 (19)	A-1-b	A-1-a	A-1-a	A-1-a
USCS Classification	CL	SW-SM	GW-GM	SP-SM	GP-GM
Specific Gravity, G_s	2.70	2.80	2.51	2.68	2.65

— Not measured
* at oven-dry moisture content

Particle Size Analysis Results

Grain-size distribution curves from particle-size analysis tests on RPCC, recycled asphalt, select sand, existing sand, and subgrade materials are provided in Figure 29. The gradation parameters (i.e., gravel content, sand content, silt content, and clay content) for each material are summarized in Table 6.

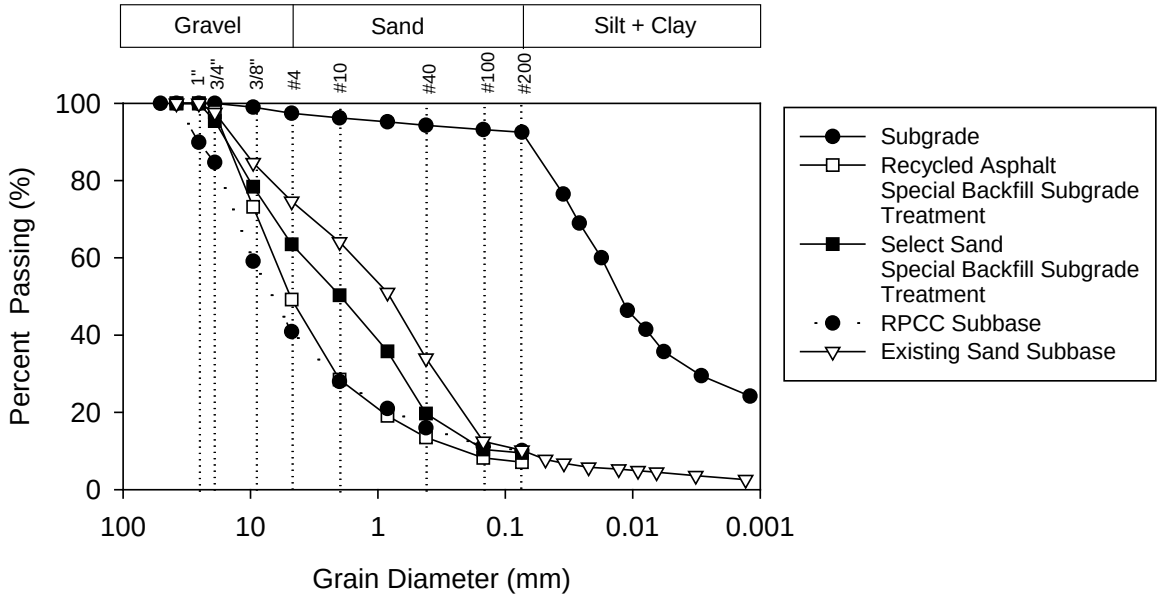

Figure 29. Particle size distribution curves of materials collected from the existing and new foundation layers

Moisture-Dry Unit Weight Results

Moisture-dry unit weight results from laboratory standard Proctor and modified Proctor tests are presented in Figure 30. The in situ moisture-dry unit weight measurements from NG testing and moisture-dry unit weight of a sample tested for resilient modulus are also shown in Figure 30. The average in situ moisture content of the subgrade material was about 20.3% (i.e., 0.6% of standard Proctor w_{opt}), and the average relative compaction of the material was about 94% standard Proctor γ_{dmax}. The relative compaction of the resilient modulus sample was about 109% of the maximum standard Proctor dry unit weight with moisture content about 2.9% dry of standard Proctor w_{opt}.

Moisture-dry unit weight results obtained from laboratory relative density compaction tests on existing sand subbase, recycled asphalt special backfill, select sand special backfill, and RPCC subbase material are presented in Figure 31, Figure 32, Figure 33, Figure 34, respectively. The in situ moisture-dry unit weight measurements from NG testing (where available) and moisture-dry unit weight of samples tested for resilient modulus are also shown in these figures. A summary of the maximum and minimum dry unit weights obtained from relative density tests for the

special backfill and subbase material samples, and maximum dry unit weights and optimum moisture contents obtained from Proctor tests for subgrade samples is provided in Table 6.

The relative density of the resilient modulus samples of the existing sand subbase material ranged from 64–107% with moisture content varying between 0 and 9.4%.

In situ relative densities for the recycled asphalt special backfill material ranged from about 76–106%. In situ moisture contents ranged from 6.9–9.3%. Relative densities of the resilient modulus test samples on this material ranged from about 68–122% with moisture contents varying between 0.5 and 9.8%.

In situ relative densities for the select sand special backfill material ranged from about 90–129%. In situ moisture contents ranged from 4.2–7.1%. Relative densities of the resilient modulus test samples on this material ranged from about 99–124% with moisture contents varying between 3.6 and 7.1%.

In situ relative densities for the RPCC subbase ranged from about 12–58%. In situ moisture contents ranged from 6.4–8.9%. Relative densities of the resilient modulus test samples on this material ranged from about 29–56% with moisture contents varying between 5.3 and 13.2%. One sample was back-saturated before testing as noted in Figure 34.

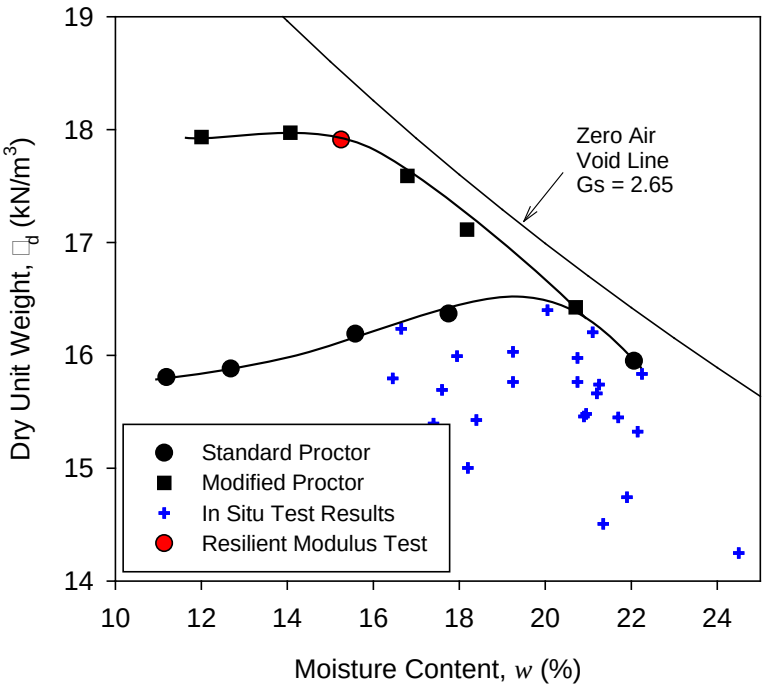

Figure 30. Laboratory standard and modified Proctor test results with resilient modulus test sample moisture-dry unit weight and in situ moisture-dry unit weight test results for subgrade material

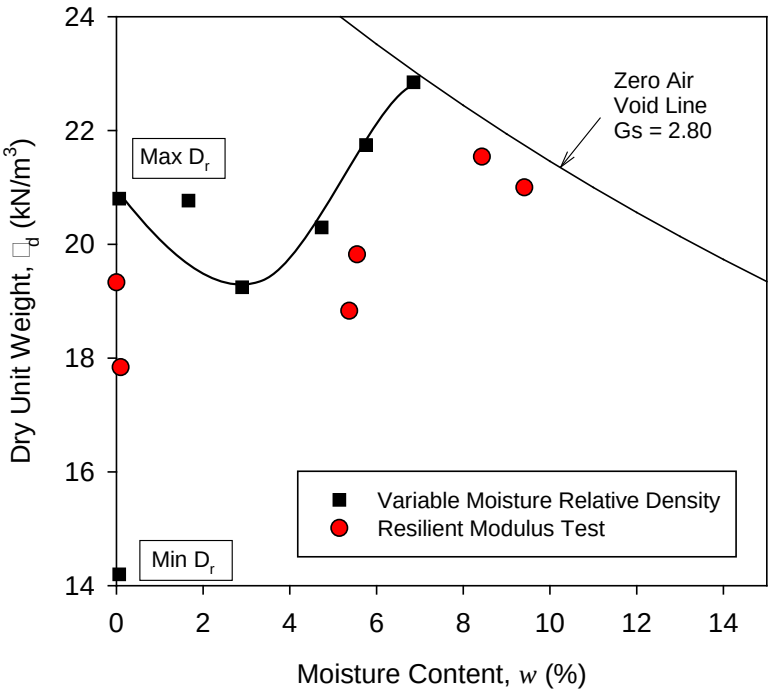

Figure 31. Laboratory relative density test results at variable moisture contents, resilient modulus test samples moisture-dry unit weights for existing sand subbase material

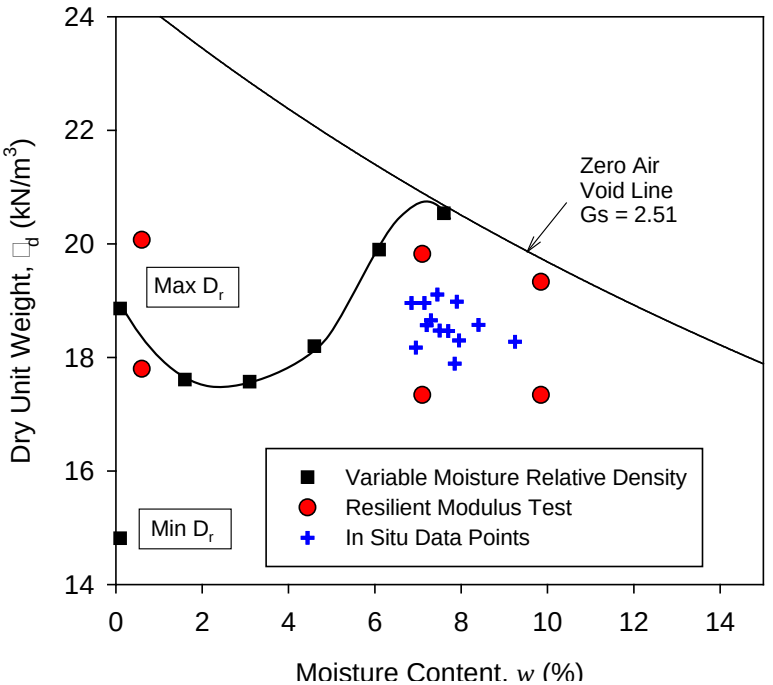

Figure 32. Laboratory relative density test results at variable moisture contents, resilient modulus test samples moisture-dry unit weights, and in situ moisture-dry unit weights for recycled asphalt special backfill material

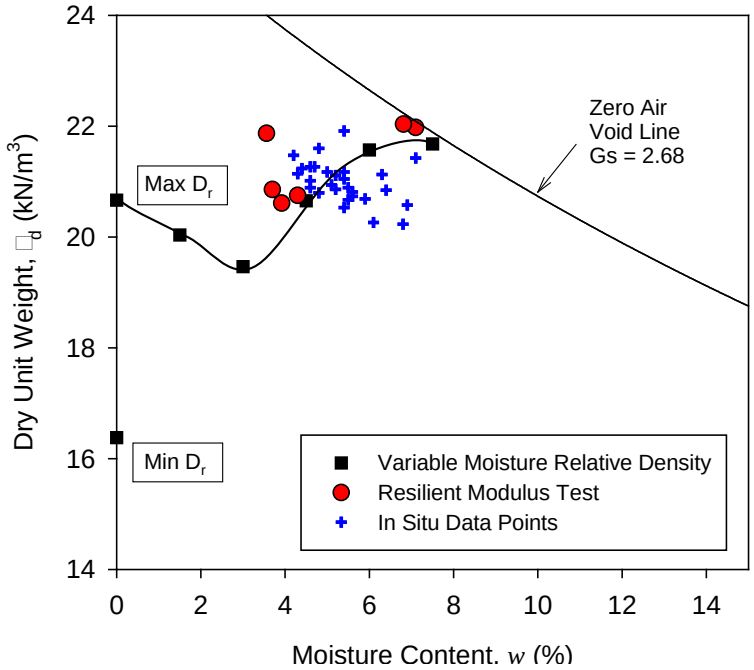

for

Figure 33. Laboratory relative density test results at variable moisture contents, resilient modulus test samples moisture-dry unit weights, and in situ moisture-dry unit weights for select sand special backfill material

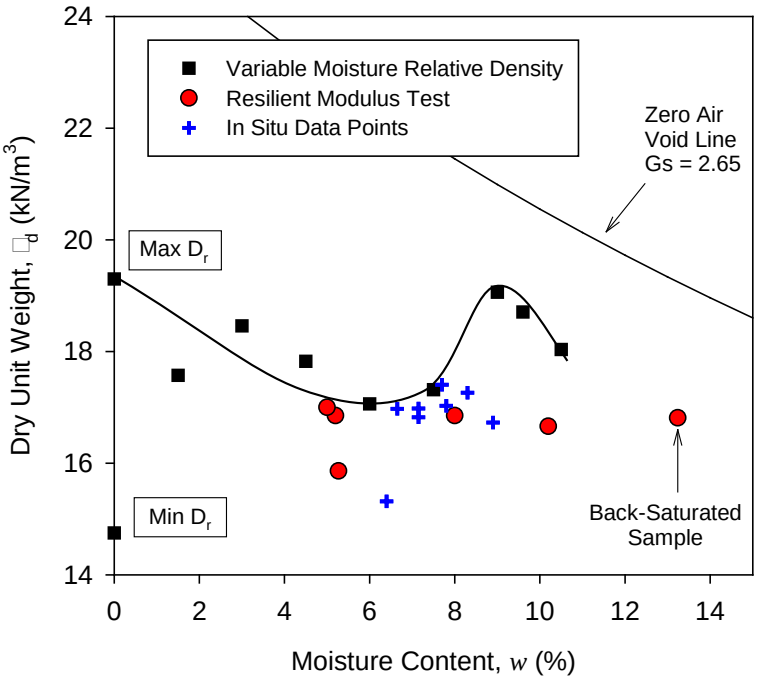

Figure 34. Laboratory relative density test results at variable moisture contents, resilient modulus test samples moisture-dry unit weights, and in situ moisture-dry unit weights for RPCC subbase material

M_r and UU Test Results

The M_r and UU test results for the existing and new foundation materials obtained from field are shown in Table 7. The summary results include γ_d; *w*%; average M_r of the 15 AASHTO T-307 loading sequences; M_r at selected stress states; dynamic secant modulus (E_s); permanent strain (ε_p) at the end of the M_r test; "universal model" regression coefficients; undrained shear strength (s_u) at failure or at 5% axial strain; and s_u at 1 strain. Selected stress states for granular and cohesive materials were as recommended in NCHRP 1-28A report (NCHRP 2004) as σ_3 = 35 kPa (5 psi) and σ_{cyclic} = 103 kPa (15 psi) for base or subbase materials. Equation 1 and the k_1, k_2, and k_3 regression coefficients were used to calculate the M_r at those stress states.

Bulk stress (σ_B) versus M_r for laboratory compacted RPCC subbase, recycled asphalt special backfill, and select sand special backfill samples along with the corresponding "universal model" prediction curves are presented in Figure 35 to Figure 37, respectively. As expected, results indicated that the M_r of these granular materials increased with increasing bulk stresses. Increasing moisture content generally decreased M_r and increasing dry unit weight generally increased M_r for these materials.

Figure 39 and Figure 41 show σ_B versus M_r along with corresponding "universal model" prediction curves for composite subbase and special backfill samples. σ_B versus M_r along with corresponding "universal model" prediction curves for composite special backfill and subgrade samples are shown in Figure 43, Figure 45, and Figure 46. Photographs of these layered composite samples after M_r and UU testing are shown in Figure 39, Figure 41, Figure 43, and Figure 45. A comparison of average M_r and ε_p between homogenous samples and layered composite samples with similar moisture and dry unit weight values is provided in Figure 47 and Figure 48. This comparison revealed that the average M_r of the layered composite sample was either similar to the layer with the lower average M_r value or about the average of the M_r values of the two layers. This is an important finding and must be further studied with adequate testing in various combinations of composite sample configurations. Efforts are underway in this research study to further investigate the influence of composite sample layer configurations on M_r properties.

Table 7. Summary of M_r and UU test results

			M_r Test								UU Test	
Sample	γ_d (kN/m^3)	w (%)	Ave. M_r (MPa)	M_r at Stress States (MPa)[#]	E_s (MPa)	ε_p (%)	k_1	k_2	k_3	R^2	s_u (kPa)[§]	s_u @ ε = 1% (kPa)
Select Sand	20.61	3.9	212.2	162.8	148.0	0.5	863.6	0.86	-0.25	0.85	161.5	159.8
	21.87	3.6	289.1	252.4	221.8	0.5	1612.6	0.60	-0.20	0.83	337.0	330.9
	20.75	4.3	206.8	171.4	182.0	0.4	947.2	0.80	-0.32	0.97	209.4	198.7
	20.86	3.7	243.6	183.7	152.7	0.5	1022.1	0.79	-0.08	0.87	232.9	214.1
	21.98	7.1	211.1	168.6	136.6	0.6	959.4	0.76	-0.16	0.84	209.3	206.2
	22.04	6.8	206.2	143.8	111.7	0.7	698.4	0.98	-0.16	0.95	216.3	215.1
RPCC Subbase	15.86	5.3	246.7	181.8	164.5	0.4	1148.6	0.61	0.09	0.92	236.3	175.0
	16.85	8.0	238.4	165.3	92.5	1.0	830.8	0.93	-0.10	0.95	292.7	229.4
	16.85	5.2	274.4	213.8	197.2	0.3	1090.3	0.91	-0.30	0.91	297.4	256.4
	17.00	5.0	251.1	140.4	257.3	0.3	913.0	0.57	0.83	0.88	303.3	305.3
	16.66	10.2	274.9	205.3	262.0	0.3	1044.6	0.92	-0.22	0.92	428.1	428.3
	16.81	13.2	234.8	222.5	169.9	0.4	1451.8	0.57	-0.36	0.63	159.0	159.6
Recycled Asphalt	17.80	0.5	281.9	231.0	57.4	0.8	1355.2	0.72	-0.16	0.85	152.5	112.6
	20.07	0.5	286.8	205.5	149.3	0.4	1325.6	0.58	0.28	0.85	248.8	217.5
	17.34	7.0	226.0	190.0	31.7	2.2	1218.9	0.59	-0.10	0.94	103.4	94.5
	19.82	7.0	327.4	243.4	201.9	0.3	1413.8	0.73	-0.03	0.97	260.3	248.2
	17.34	9.8	270.3	247.2	83.5	0.8	1472.3	0.70	-0.41	0.87	140.1	125.2
	19.33	9.8	363.4	309.2	106.9	1.1	1608.3	0.89	-0.48	0.83	185.1	160.8
Existing Sand Subbase	18.83	6.4	163.2	137.5	35.4	1.3	825.0	0.68	-0.26	0.97	91.9	91.0
	19.82	6.4	167.0	127.4	83.5	0.8	839.3	0.55	0.17	0.96	111.2	110.6
	17.84	0.0	192.6	159.8	87.2	0.8	1047.1	0.56	-0.04	0.85	136.5	129.0

			M_r Test								UU Test	
Sample	γ_d (kN/m^3)	w (%)	Ave. M_r (MPa)	M_r at Stress States (MPa)[#]	E_s (MPa)	ε_p (%)	k_1	k_2	k_3	R^2	s_u (kPa)[§]	s_u @ ε = 1% (kPa)
Existing Sand Subbase	19.33	0.0	205.4	155.5	145.6	0.6	936.4	0.68	0.03	0.99	191.5	187.7
	21.00	10.3	149.0	109.9	40.1	1.8	511.9	1.03	-0.35	0.94	133.7	134.1
	21.54	10.1	163.2	119.0	51.5	1.6	592.9	0.94	-0.21	0.95	140.5	141.5
RPCC Base + Select Sand Composite	16.90	5.8	239.0	166.6	228.4	0.3	1148.6	0.49	0.44	0.93	264.0	262.1
	20.41	4.9										
	15.67	5.7	223.6	139.4	140.4	0.4	947.7	0.51	0.66	0.98	196.3	180.1
	21.35	5.2										
	15.73	5.3	229.6	182.6	172.6	0.5	1088.0	0.69	-0.10	0.95	160.9	154.3
	20.41	5.0										
	16.92	5.7	202.7	118.1	233.4	0.3	840.2	0.44	0.90	0.94	245.7	214.4
	21.41	4.9										
RPCC Base + Recycled Asphalt Composite	16.93	4.9	292.9	227.5	226.6	0.3	1328.2	0.72	-0.07	0.91	244.3	214.4
	19.94	7.3										
	15.75	4.5	239.5	184.0	123.6	0.5	1083.0	0.71	-0.04	0.91	175.2	140.7
	19.86	7.7										
	15.67	5.0	219.9	189.5	83.7	0.8	1110.9	0.72	-0.31	0.88	143.3	122.3
	18.12	6.3										
	16.93	4.9	220.6	159.3	144.0	0.4	1057.7	0.54	0.30	0.95	171.3	158.3
	18.29	5.3										
Select Sand + Subgrade Composite	21.13	8.1	95.0	83.1	22.2	2.3	453.3	0.81	-0.45	0.97	106.6	100.5
	17.39	16.3										

			M_r Test								UU Test	
Sample	**γ_d (kN/m^3)**	***w* (%)**	**Ave. M_r (MPa)**	**M_r at Stress States (MPa)[#]**	**E_s (MPa)**	**ε_p (%)**	**k_1**	**k_2**	**k_3**	**R^2**	**s_u (kPa) [§]**	**s_u @ ε = 1% (kPa)**
Recycled Asphalt + Subgrade Composite	18.82	8.3	124.2	114.1	31.9	2.3	697.9	0.65	-0.38	0.94	114.0	111.0
	17.29	16.6										
Existing Sand + Subgrade Composite	20.46	6.6	106.2	95.1	46.5	1.1	571.4	0.68	-0.34	0.98	117.4	112.3
	16.95	16.5										
	21.85	4.2	64.8	51.2	5.4	8.4	267.8	0.86	-0.23	1.00	Not Performed	
	16.80	19.1										

[#] subgrade: σ_3 = 14 kPa (2 psi) and σ_{cyclic} = 41 kPa (6 psi), and for subbase σ_3 = 35 kPa (5 psi), σ_{cyclic} = 103 kPa (15 psi); [§]at axial strain ε = 5% or at failure, whichever occurs first.

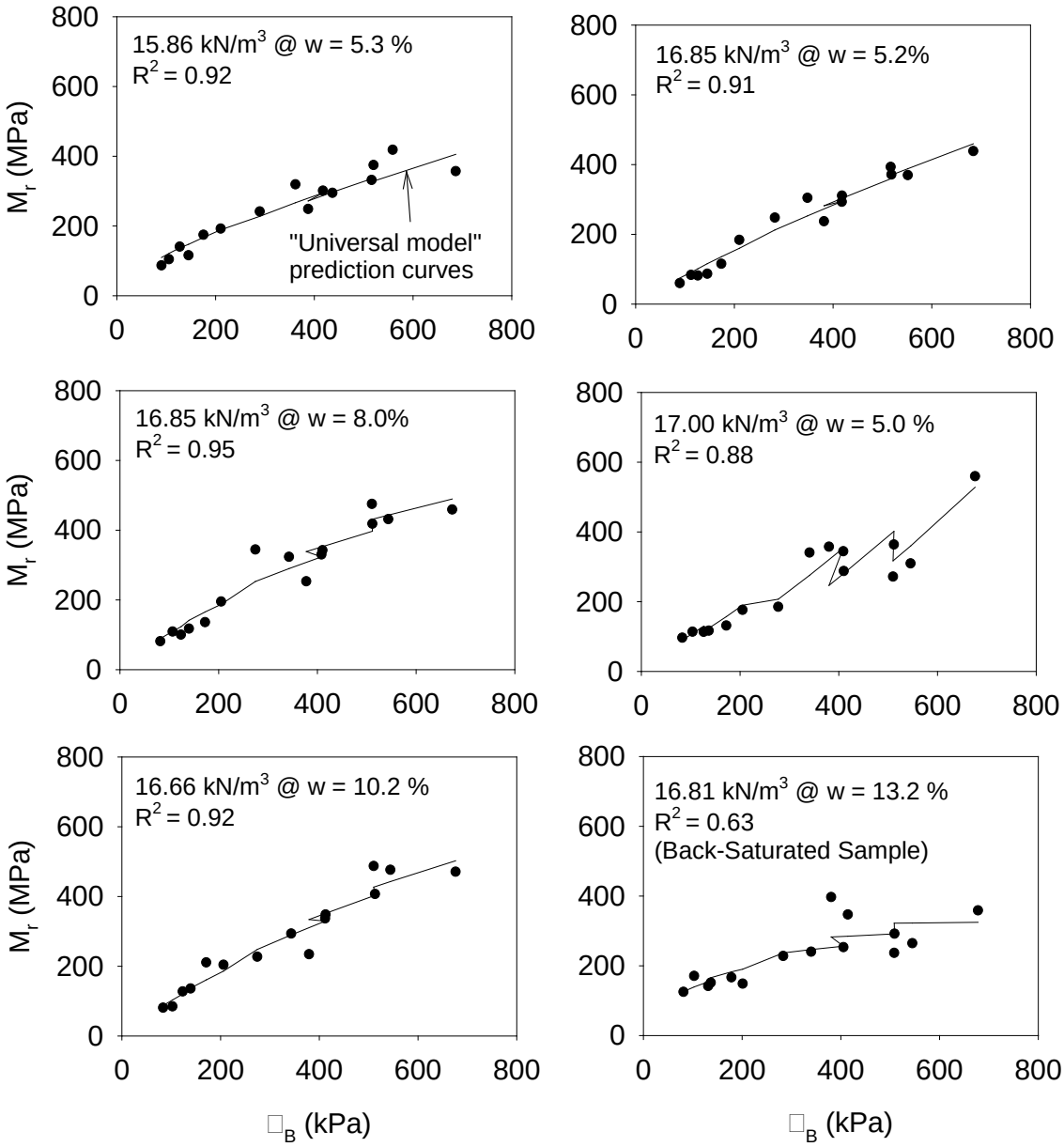

Figure 35. M_r test results for RPCC subbase samples

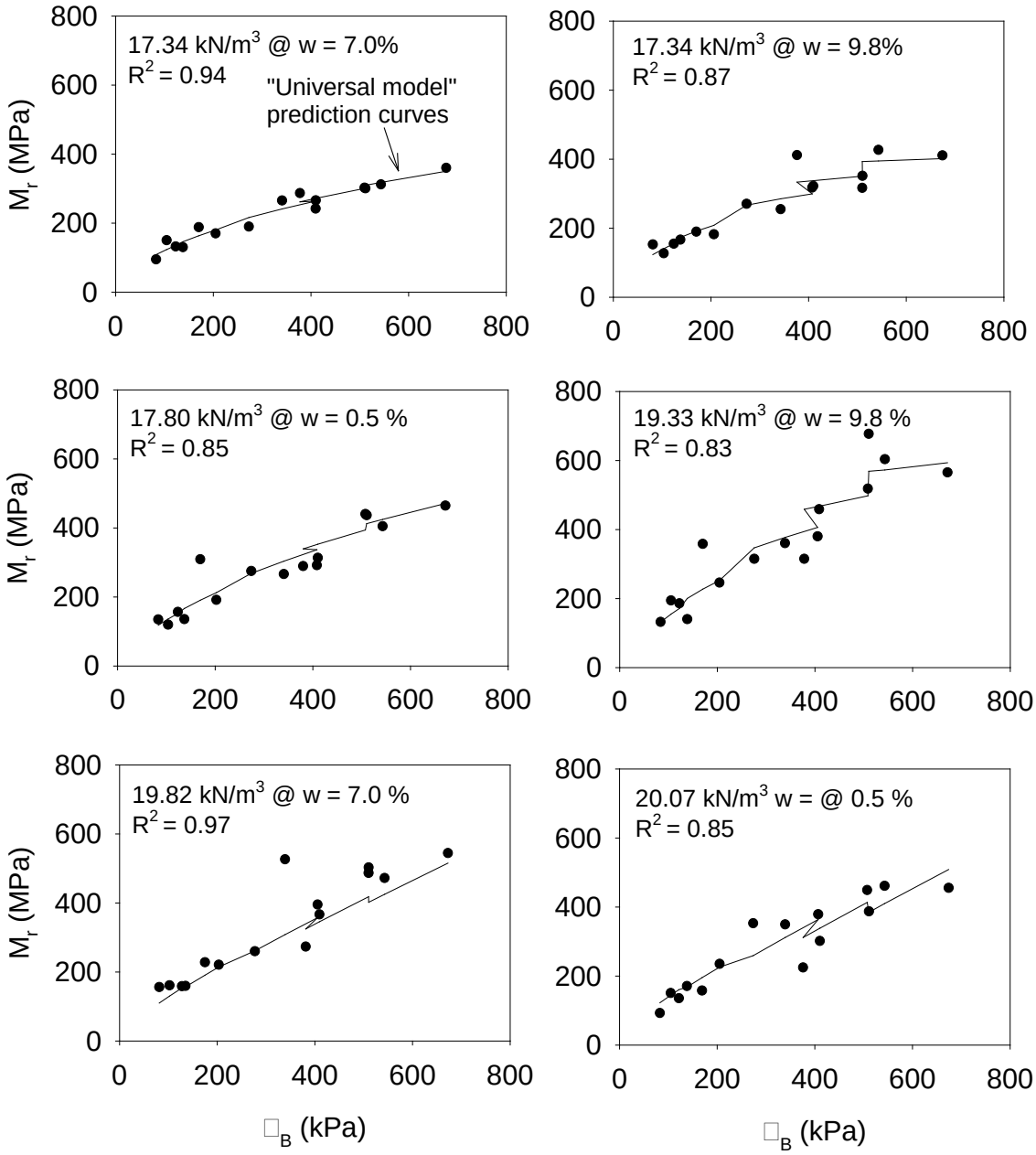

Figure 36. M_r test results for recycled asphalt special backfill samples

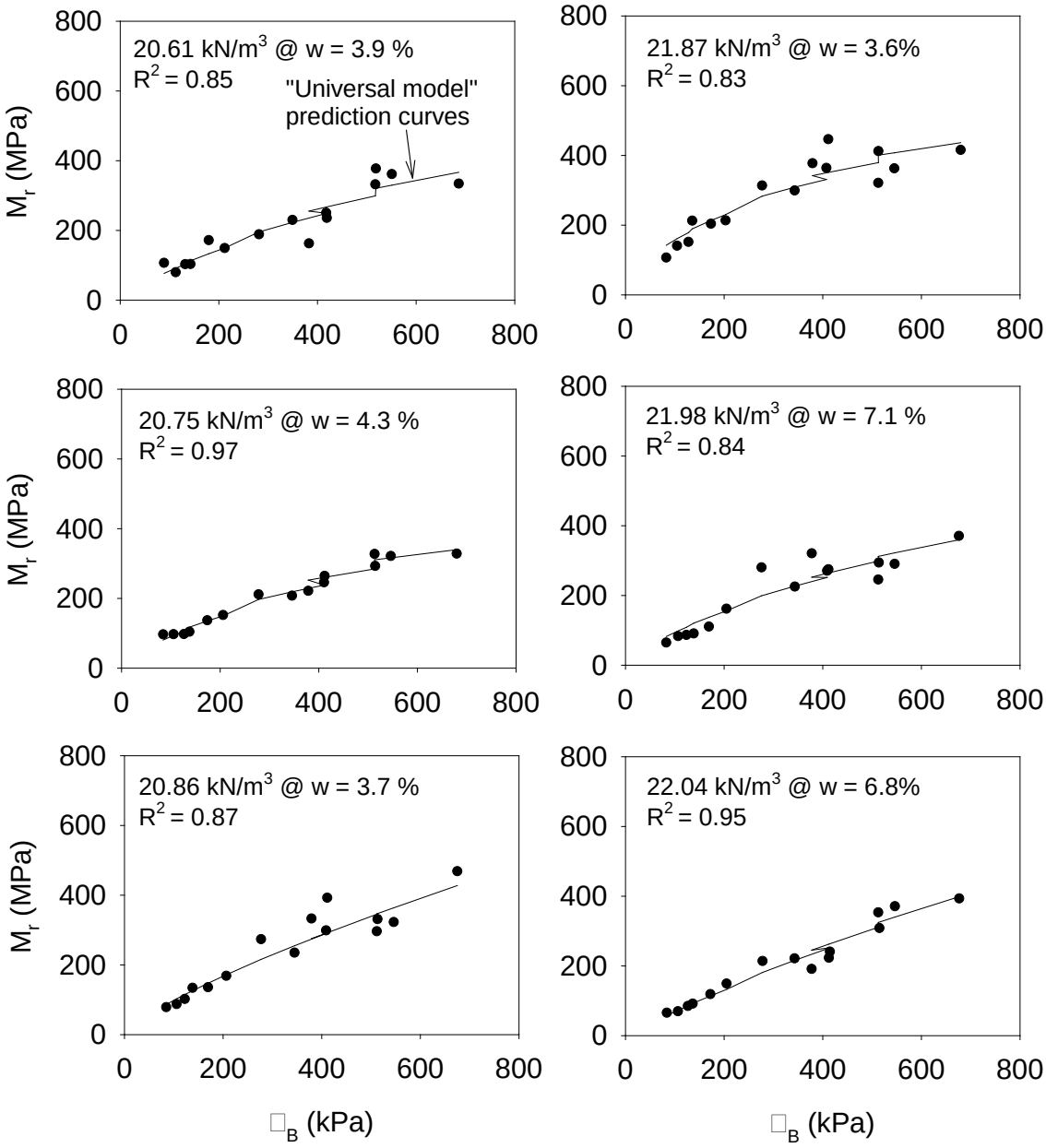

Figure 37. M_r test results for select sand special backfill samples

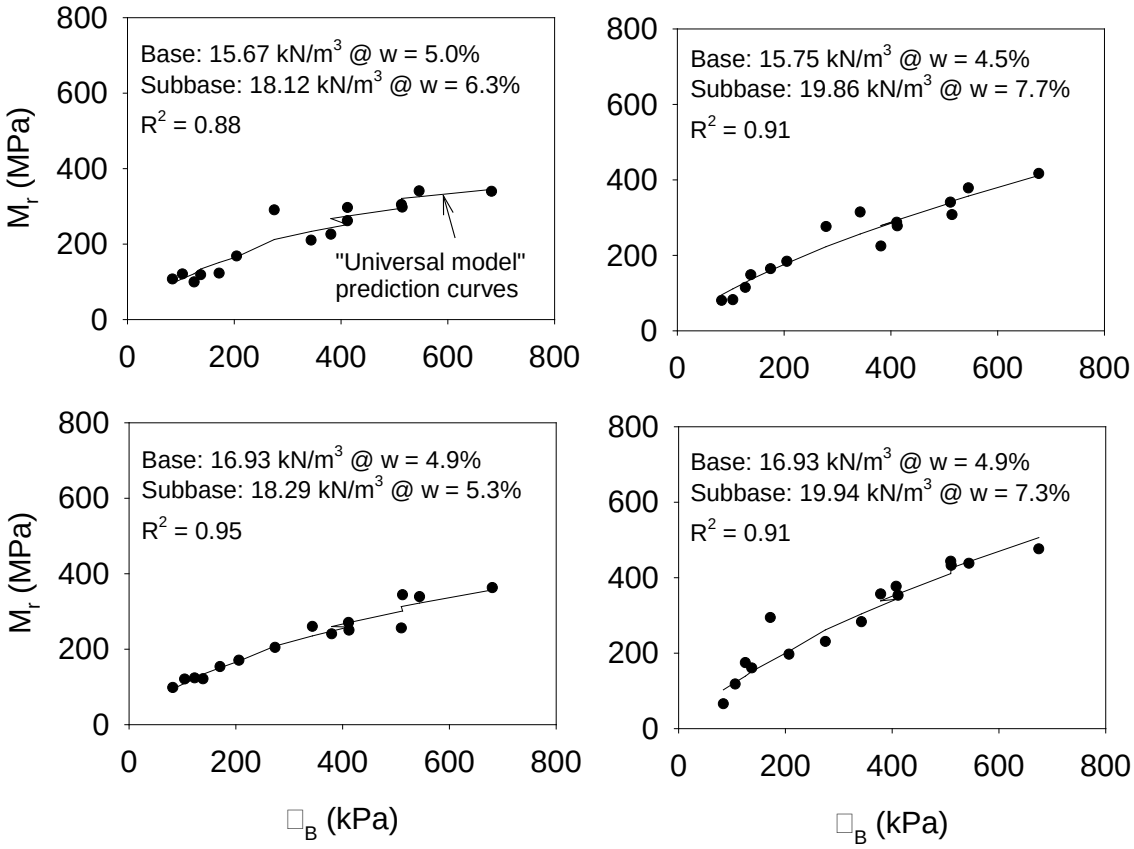

Figure 38. M_r test results for RPCC over recycled asphalt layered composite samples

Figure 39. Photos of the RPCC (16.93 kN/m^3 at *w* = 4.9%) over recycled asphalt (19.94 kN/m^3 at *w* = 7.3%) layered composite sample after UU testing with the membrane intact (left) and open (right)

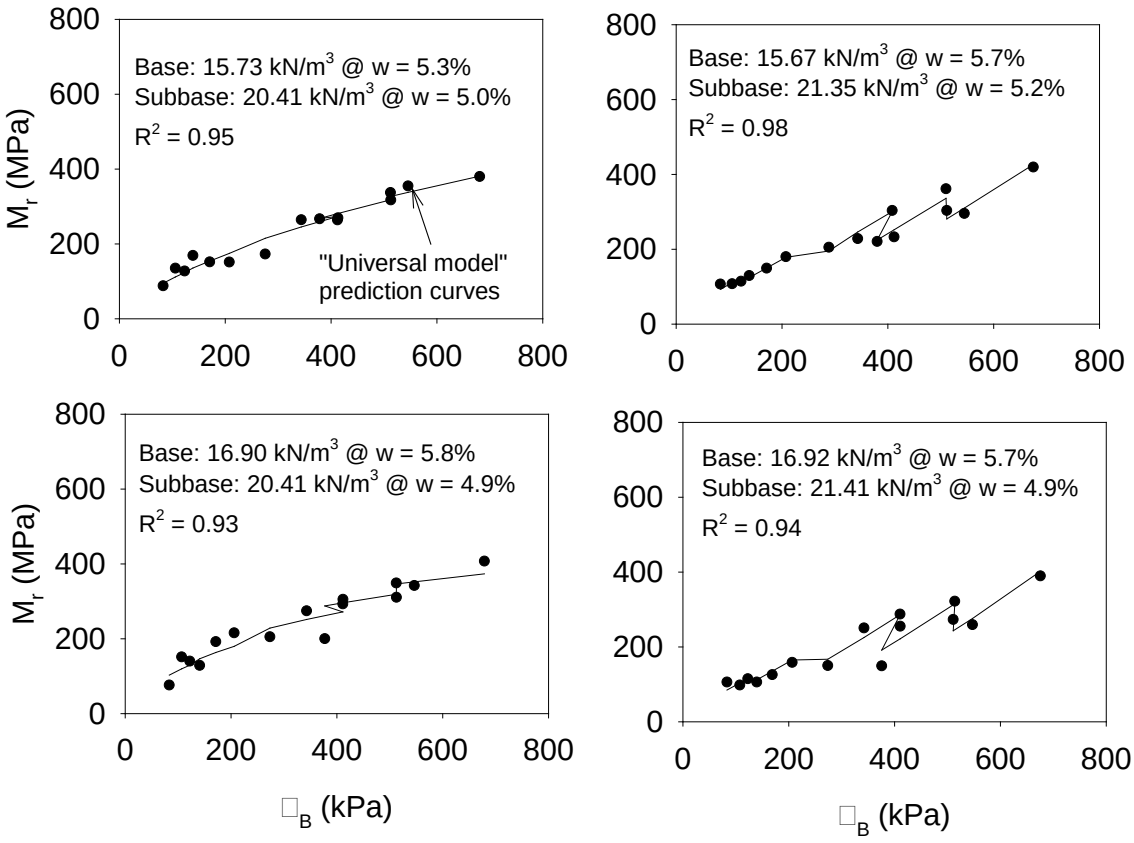

Figure 40. M_r test results for the RPCC over select sand layered composite samples

Figure 41. Photos of the RPCC (16.92 kN/m³ at *w* = 5.7%) over select sand (21.41 kN/m³ at *w* = 4.9%) layered composite sample after UU testing with the membrane intact (left) and open (right)

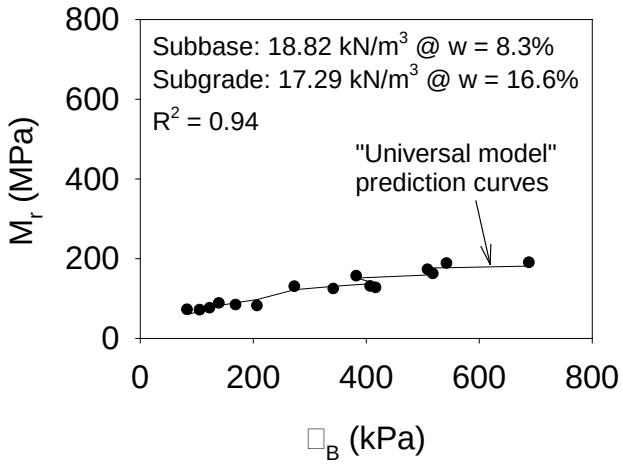

Figure 42. M_r test results for the recycled asphalt over subgrade layered composite samples

Figure 43. A photo of the recycled asphalt (18.82 kN/m^3 at *w* = 8.3%) over subgrade (17.29 kN/m^3 at *w* = 16.6%) layered composite sample after UU testing

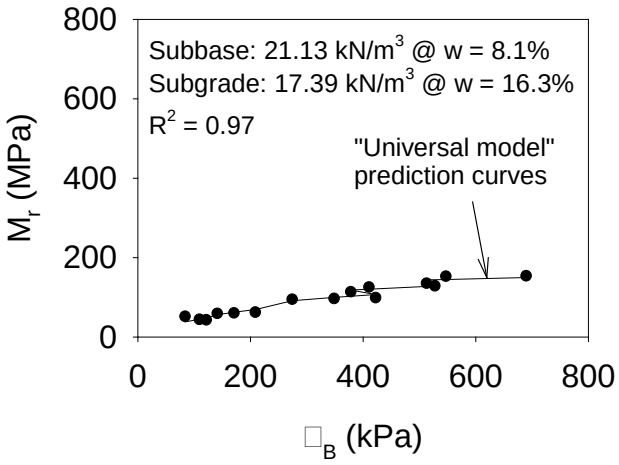

Figure 44. M_r test results for the select sand over subgrade layered composite sample

Figure 45. A photo of the select sand (21.13 kN/m^3 at *w* = 8.1%) over subgrade (17.39 kN/m^3 at *w* = 16.3%) layered composite sample after UU testing

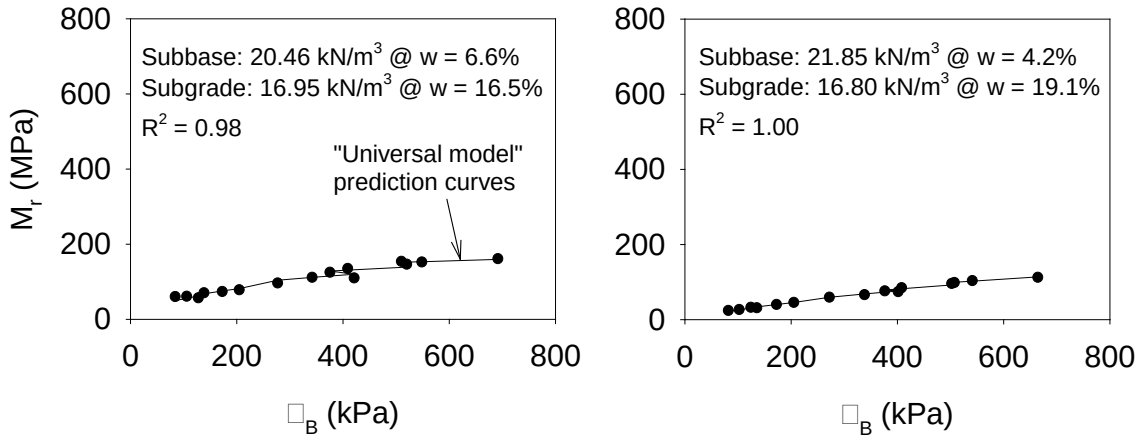

Figure 46. M_r test results for the existing sand subbase over subgrade layered composite samples

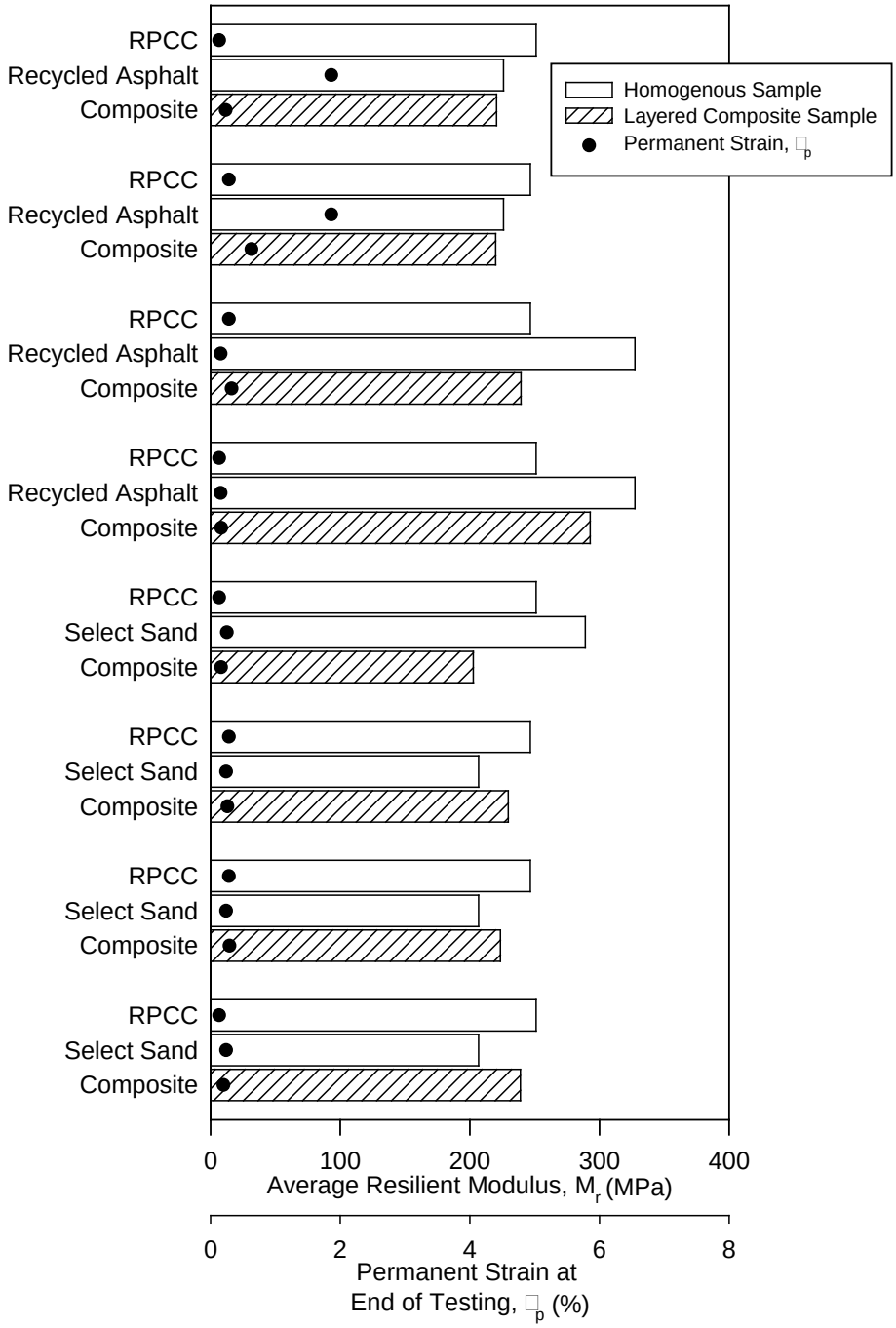

Figure 47. Average M_r and permanent strain values at the end of Mr testing for homogeneous samples and samples with subbase and special backfill layers

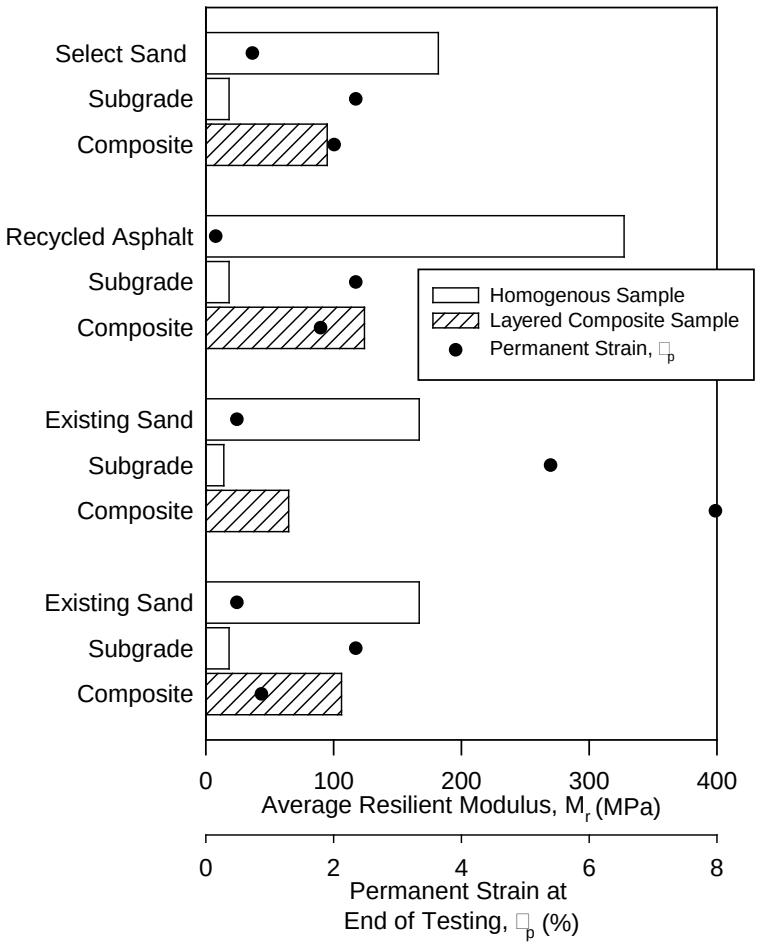

Figure 48. Average M_r values and permanent strain values at the end of M_r testing of homogenous and composite samples with subbase and subgrade layers

Frost Heave and Thaw Weakening Test Results

Frost-heave and thaw-weakening tests were conducted on four compacted subgrade samples. The samples were compacted to a target w = 17.8% and γ_d = 16.39 kN/m^3. The actual w of the samples varied between 17.9% and 18.4%, and the actual γ_d varied between 15.99 kN/m^3 and 16.28 kN/m^3, with a degree of saturation at about 76% to 78%. The CBR of the compacted sample before saturation was determined as 21.8%.

The frost-heave and temperature versus time results are shown in Figure 49. Results indicated that the heave rate was greater for the second freezing cycle than for the first freeze cycle, which indicates that the material is susceptible to increased heave with greater freeze-thaw cycles. The average heave rates for the 1st and 2nd freezing cycles are summarized in Table 8. Based on the frost-heave rate measurements, the soil is classified to have high potential to frost-heave according to ASTM D5918.

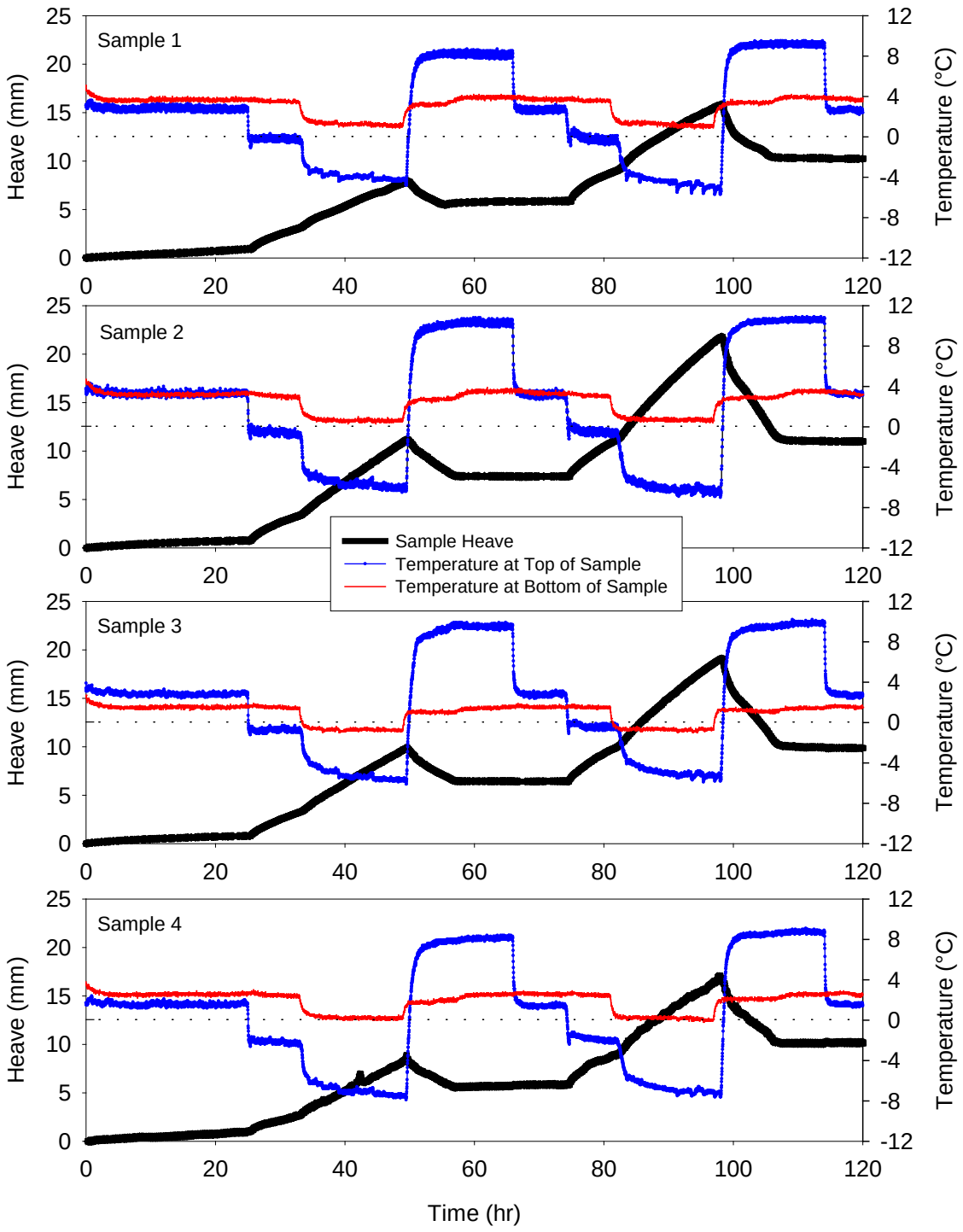

Figure 49. Frost heave and temperature versus time plots for the four lean clay subgrade samples

The height of the samples increased by about 25 to 38 mm (16% to 25%) after the two cycles and the mass of the sample increased by about 443 to 471 g (9% to 10%). This indicates that the moisture drawn into the sample during the freezing periods by capillary action did not drain from

the soil during the thawing periods. Moisture contents at six depths were determined for each sample immediately after F/T testing (Figure 50). The moisture content at 100% saturation (assuming the initial γ_d of each sample) and the initial moisture content of the sample during compaction are also shown on Figure 50 for reference. Results indicated that the moisture content was higher at all depths in the samples compared to the initial moisture content. Further, the moisture content at the top of the sample was higher than at the middle or bottom of the sample, which indicates that water was drawn to the top cold plate through capillary action caused by the temperature gradient in the samples.

CBR values of the post freeze-thaw samples decreased from 22 to an average CBR < 1.0 on the four samples (Table 8). Based on the thawed CBR values, the soil is classified to have very high potential to thaw-weakening according to ASTM D5918.

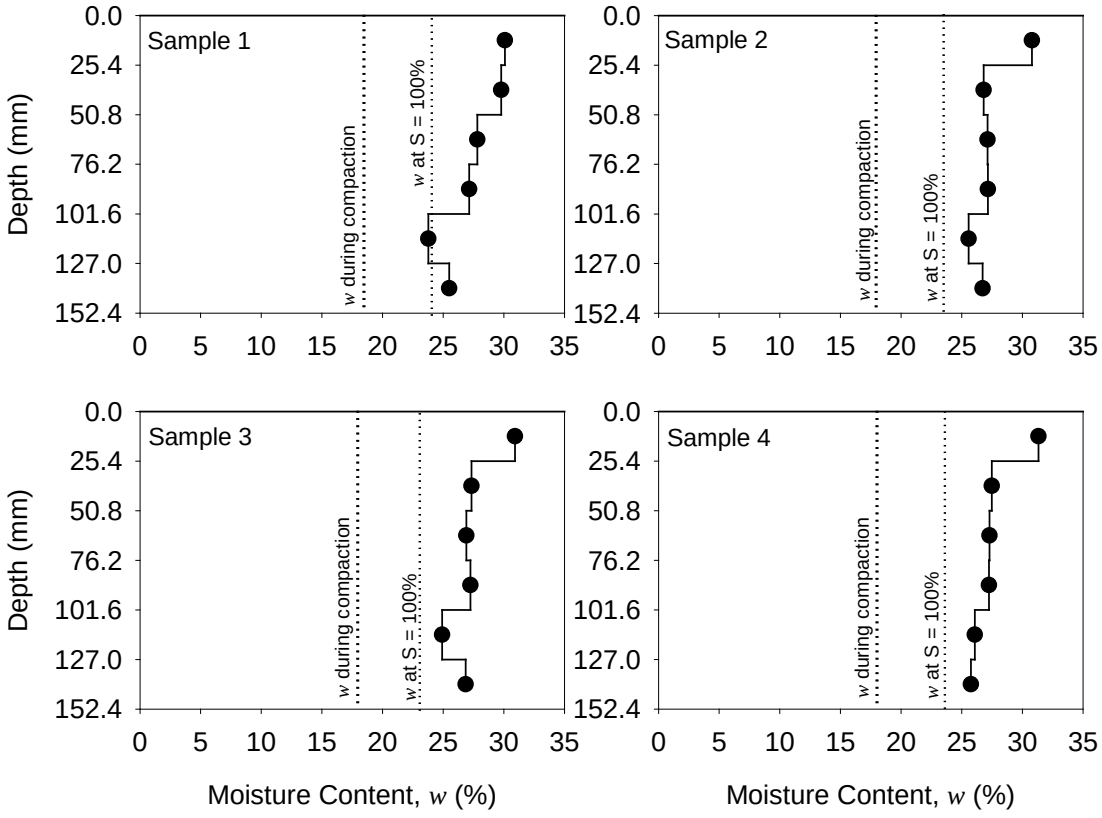

Figure 50. Moisture content profiles immediately after F/T testing on compacted subgrade samples

Table 8. Summary of frost-heave and thaw-weakening test results on subgrade samples

Parameter	μ	σ	COV (%)	Number of samples
CBR (%) (standard test)	21.8	—	—	1
CBR (%) (after frost-susceptibility test)	0.7	0.0	12.0	4
1st Frost-heave rate (mm/day)	8.4	1.4	16.8	
2nd Frost-heave rate (mm/day)	12.4	2.2	17.9	
1st Frost-heave susceptibility rating	High	—	—	
2nd Frost-heave susceptibility rating	High	—	—	
Thaw-weakening susceptibility rating	Very high	—	—	

CHAPTER 5: IN SITU TEST RESULTS

Description of Test Sections

A total of ten test sections were tested as part of this project. Of these, four test sections consisted of FWD and DCP testing on the existing CRCP, on test section (TS) consisted of FWD and DCP testing on the new JPCP, and the remaining five test sections consisted of RICM mapping and in situ testing (NG, DCP, LWD) of foundation layers directly during construction.

Table 9. Summary of test sections and in situ testing

TS	Date	Location	Material	In situ Tests	Comments
1	7/14/09	I-29 NB Left Lane Sta. 2755+00 to 2852+00	Existing CRCP surface	FWD, DCP	FWD tests every +50 station on pavement surface, and DCP tests every +100 station directly on foundation layers.
2		I-29 NB Left Lane Sta. 2800+00 to 2801+00	Existing CRCP surface	FWD	FWD tests about every +05 station on left and right wheel paths.
3	7/22 – 7/23/09	I-29 NB Left and Right Lanes Sta. 2890+00 to 2925+00	Existing CRCP surface	FWD, DCP	FWD tests every +50 station. DCP tests at selected locations on foundation layers by drilling a hole in the pavement
4	7/22/09	I-29 NB Left and Right Lanes Sta. 2892+00 to 2893+05	Existing CRCP surface	FWD	FWD tests every +02 to +05 station on left and right wheel paths on both lanes.
5	9/10/09	I-29 NB Sta. 2745+07 to 2780+07	New JPCP surface	FWD, DCP	FWD tests about every +100 station. DCP tests every +500 station on foundation layers by drilling a hole in the pavement
6	9/1/09	Near Sta. 2900	Subgrade	RICM	RICM maps in low and high amplitude settings followed by in situ point testing
7			Recycled asphalt subbase over subgrade	RICM, NG, DCP, LWD	
8	9/1/09	Near Sta. 2890	Recycled asphalt subbase	None	
9	9/2/09		RPCC base over Recycled asphalt subbase	RICM, NG, LWD	
10	9/10/09	I-29 NB just south of exit ramp to Hwy 175	Select sand subbase over subgrade	RICM, NG, LWD, and DCP	

Note: NG – nuclear gauge; DCP – dynamic cone penetrometer; LWD – light weight deflectometer; FWD – falling weight deflectometer; RICM – roller-integrated compaction monitoring using Volvo smooth drum roller.

In Situ Testing on Existing Pavement Constructed in the 1960s and on New Pavement Constructed in 2009

FWD and DCP tests were conducted on the existing CRCP (TS1, TS2, TS3, and TS4) and on the new JPCP (TS5) (see Figure 51 and Figure 52). All tests were conducted on the northbound (NB) lanes. On TS1 and TS3, FWD tests were conducted at about every +50 station, and DCP tests were conducted at about every +100 station along the center of the lanes (note that +100 station = 30 m). DCP tests on TS1 were conducted directly on the foundation layers after the CRCP layer was removed, and DCP tests on TS3 were conducted by drilling a hole through the pavement. On TS2 and TS4, FWD tests were conducted at about every +02 to +05 station on the left and right wheel paths over about a 30 m long section. On TS5, FWD tests were conducted at about every +100 station along the center of the right lane, and DCP tests were conducted at about every +500 station.

Results from FWD tests from each TS are presented in Figure 53 to Figure 57. FWD deflection basins on the existing CRCP and the new JPCP at similar test locations between Sta. 2755 and 2775 are presented in Figure 58. Figure 59 presents *k* values determined from DCP-CBR measurements (of treated subgrade and weak subgrade) on new JPCP. Histogram plots of FWD test measurements on the existing CRCP and new JPCP are presented in Figure 60 and Figure 61. DCP-CBR profiles on each TS are presented in Figure 62 to Figure 64. Figure 64 presents DCP-CBR profiles comparing foundation layers under the existing CRCP and the new JPCP at nearby locations between Sta. 2755 and Sta. 2770. Key findings from this testing are as follows:

- On average, D_0 at 40 kN applied load on the new JPCP was about 0.4 times the D_0 on the existing CRCP.
- The intercept values on the existing CRCP and new JPCP were low (< 0.04 mm) and did not indicate voids beneath the pavement.
- The *k* values determined from DCP-CBR measurements and FWD measurements indicated higher values on the new JPCP than on the existing CRCP.
- Based on tests conducted on the new JPCP sections, the composite *k* values determined using FWD ($k_{\text{FWD-Static-Corr-comp-PCA}}$) were similar to the values determined using CBR of the weak layers ($k_{\text{comp-PCA-Weak Subgrade}}$) and were about 17 times lower than the values determined using CBR of the treated subgrade ($k_{\text{comp-PCA}}$). This indicates that a weak layer within the top 450 mm of the subgrade contributed to low values observed in the FWD testing and that the use of high CBR values in the treated subgrade layers can result in unreasonably high *k* values.

Figure 51. FWD and DCP testing on existing CRCP

Figure 52. FWD and DCP testing on new JPCP

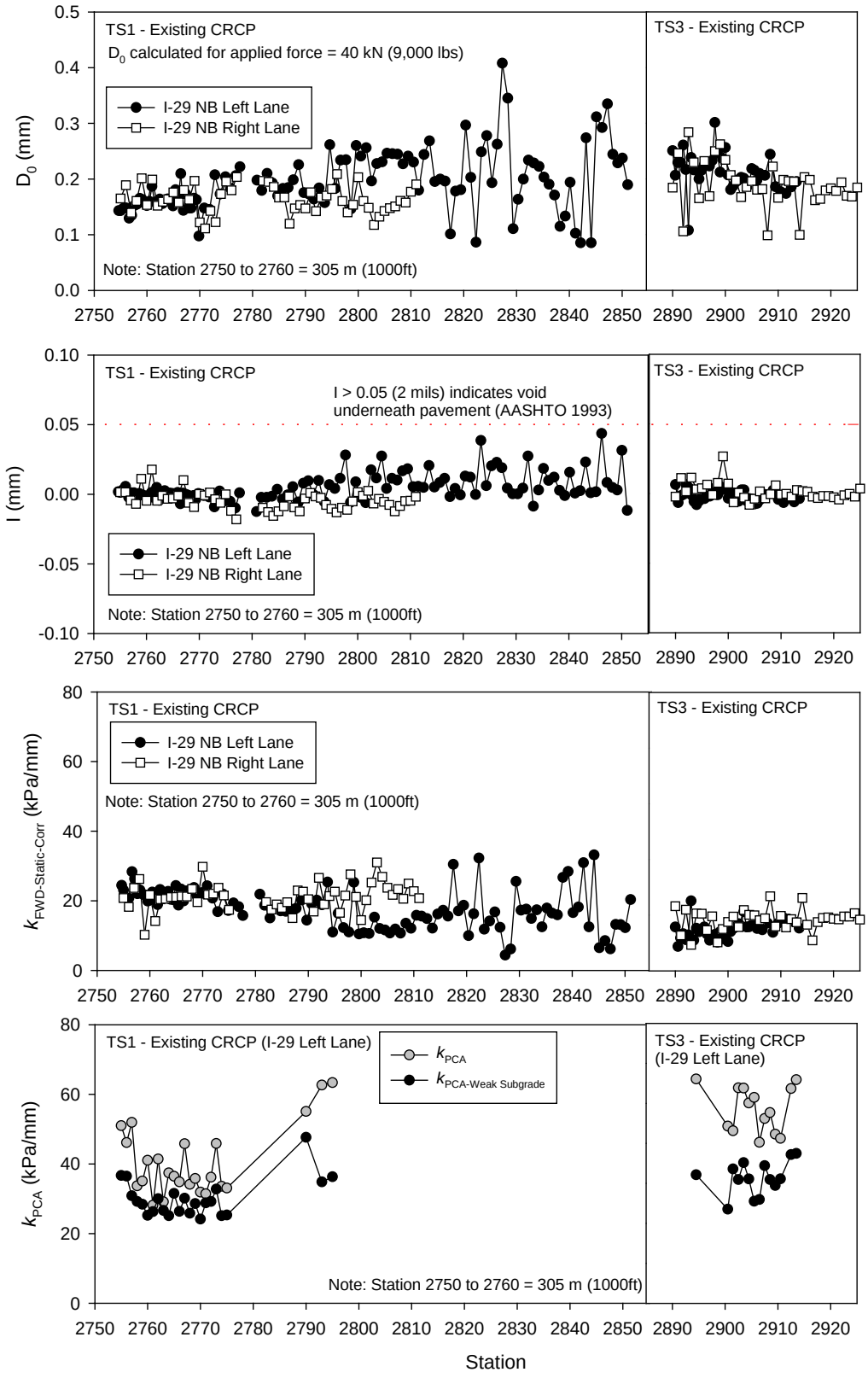

Figure 53. D_0, I, $k_{FWD\text{-}Static\text{-}Corr}$, k_{PCA}, and $k_{PCA\text{-}Weak\ Subgrade}$ on existing CRCP TS1 and TS3 on I-29 NB left and right lanes

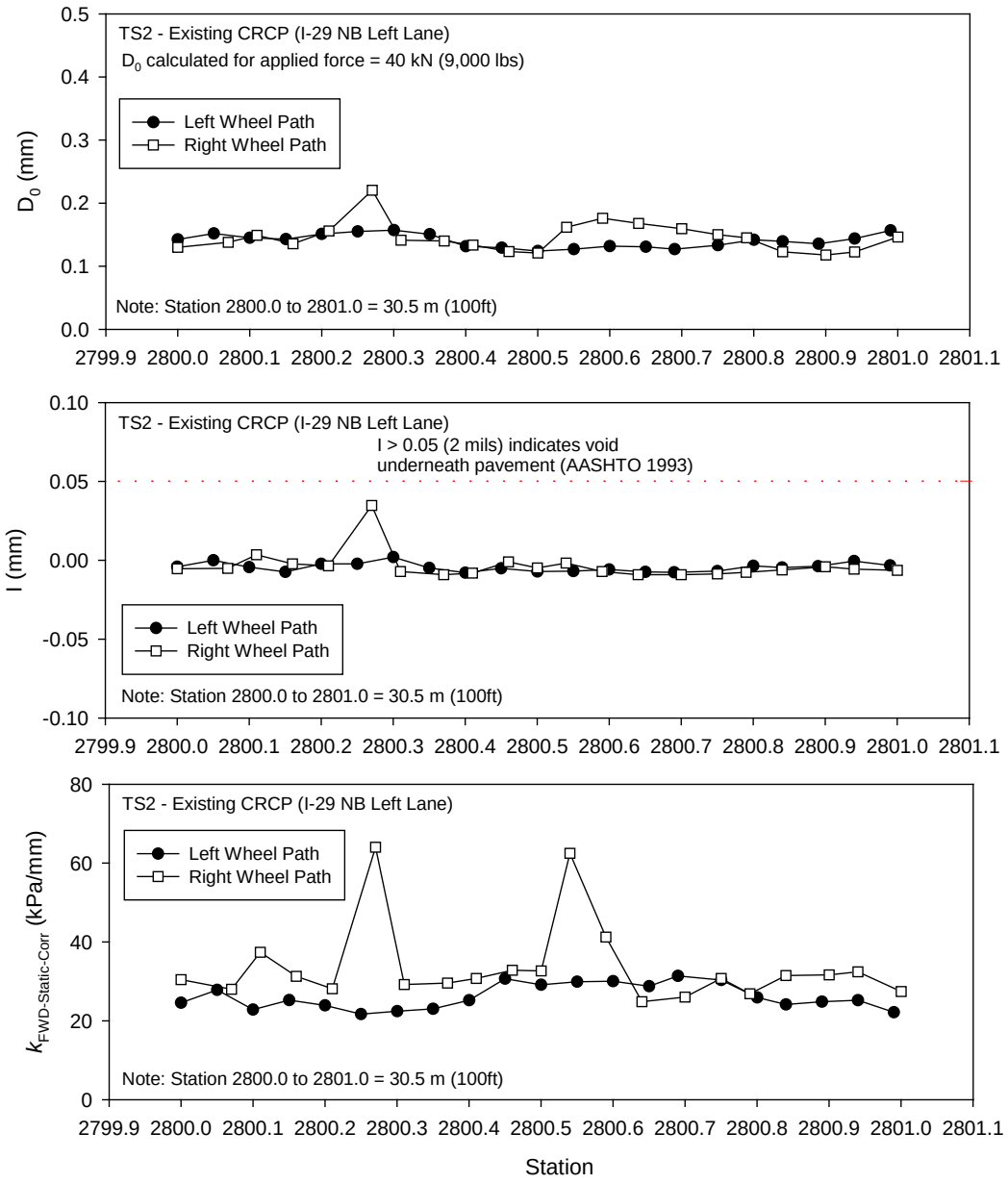

Figure 54. D_0, I, and $k_{FWD\text{-}Static\text{-}Corr}$ on existing CRCP TS2 on I-29 NB left lane along left and right wheel paths

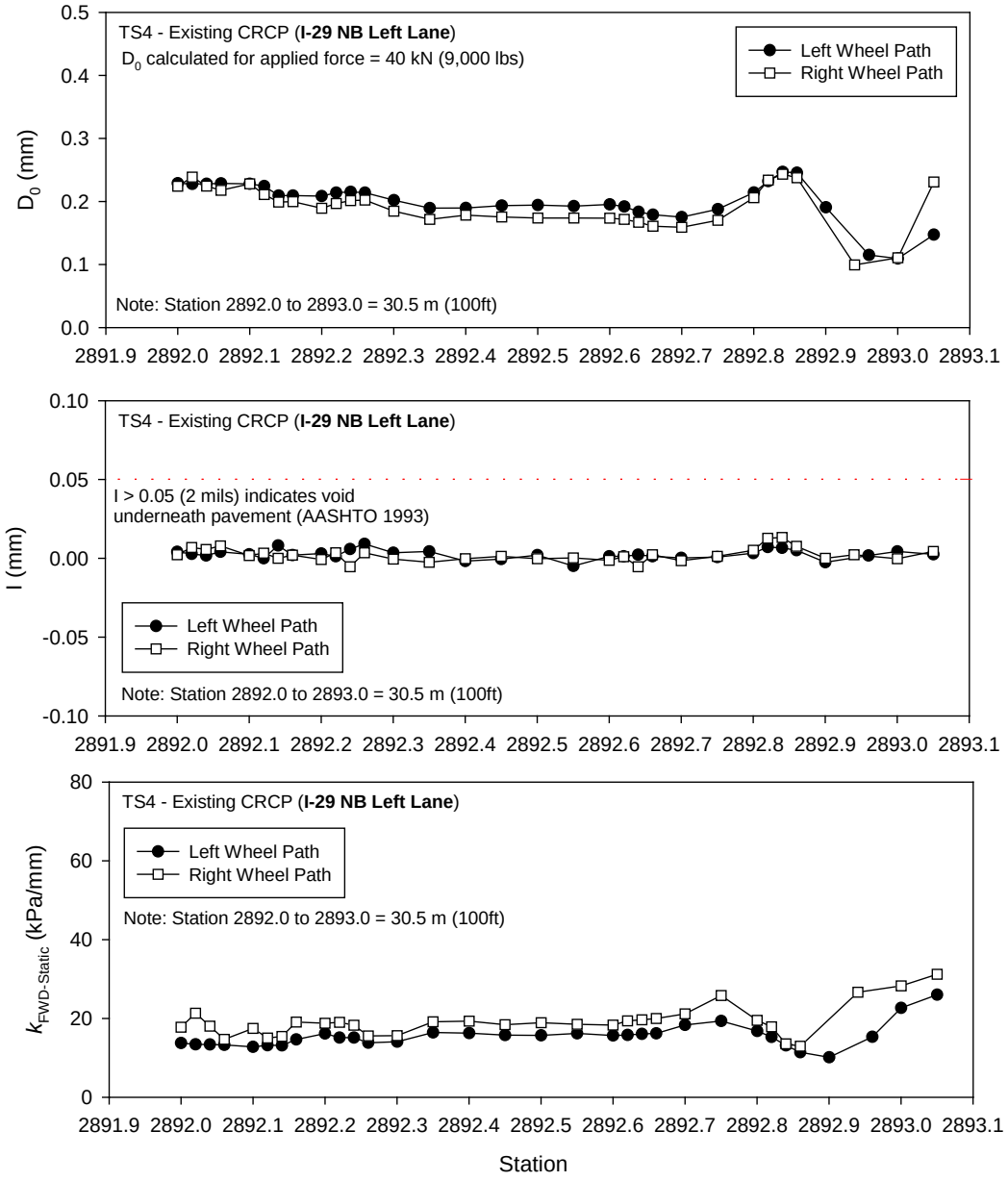

Figure 55. D_0, I, and $k_{FWD\text{-}Static}$ on existing CRCP TS4 on I-29 NB left lane along left and right wheel paths about every +02 station

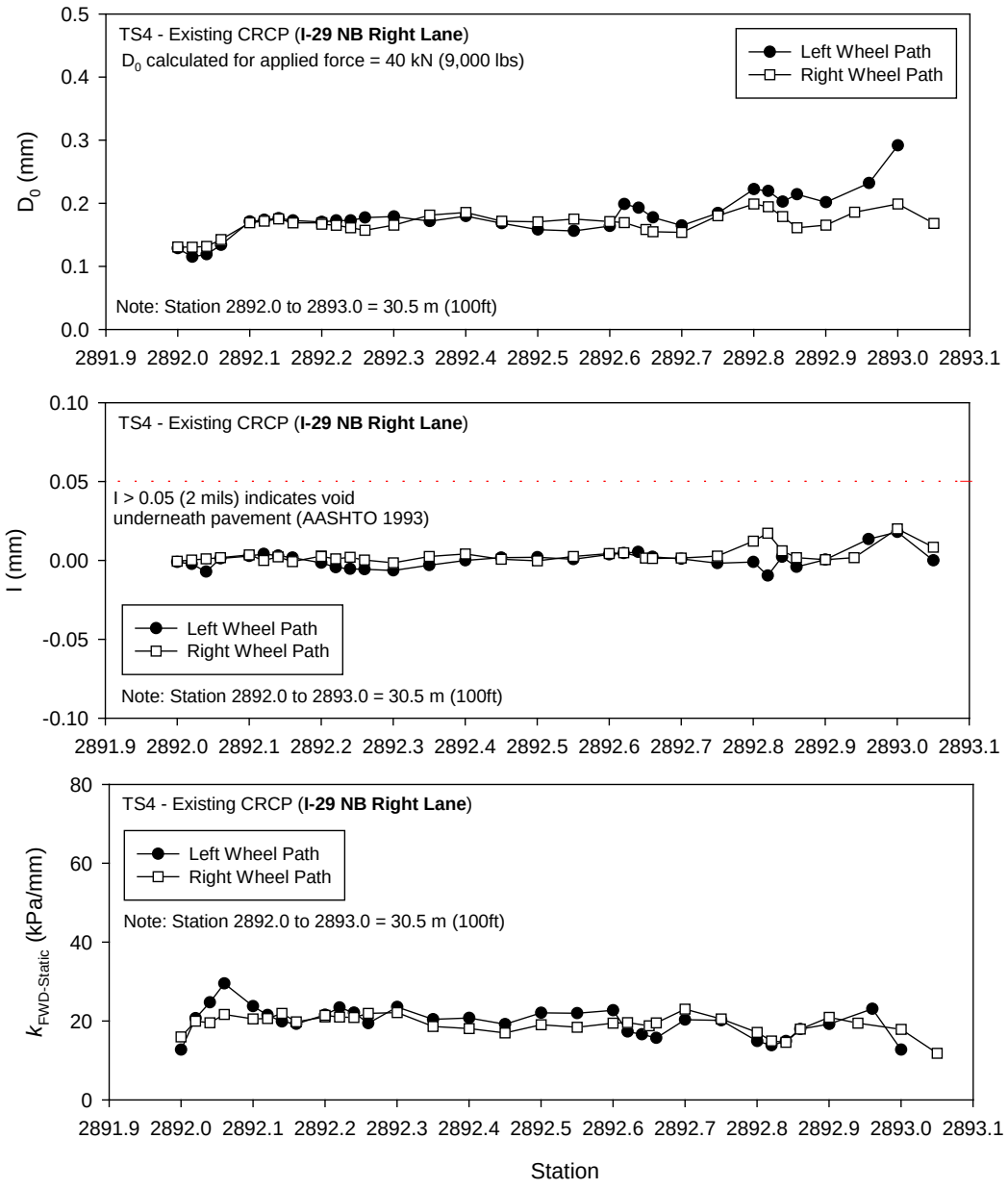

Figure 56. D_0, I, and $k_{FWD\text{-}Static}$ on existing CRCP TS4 on I-29 NB right lane along left and right wheel paths about every +02 station

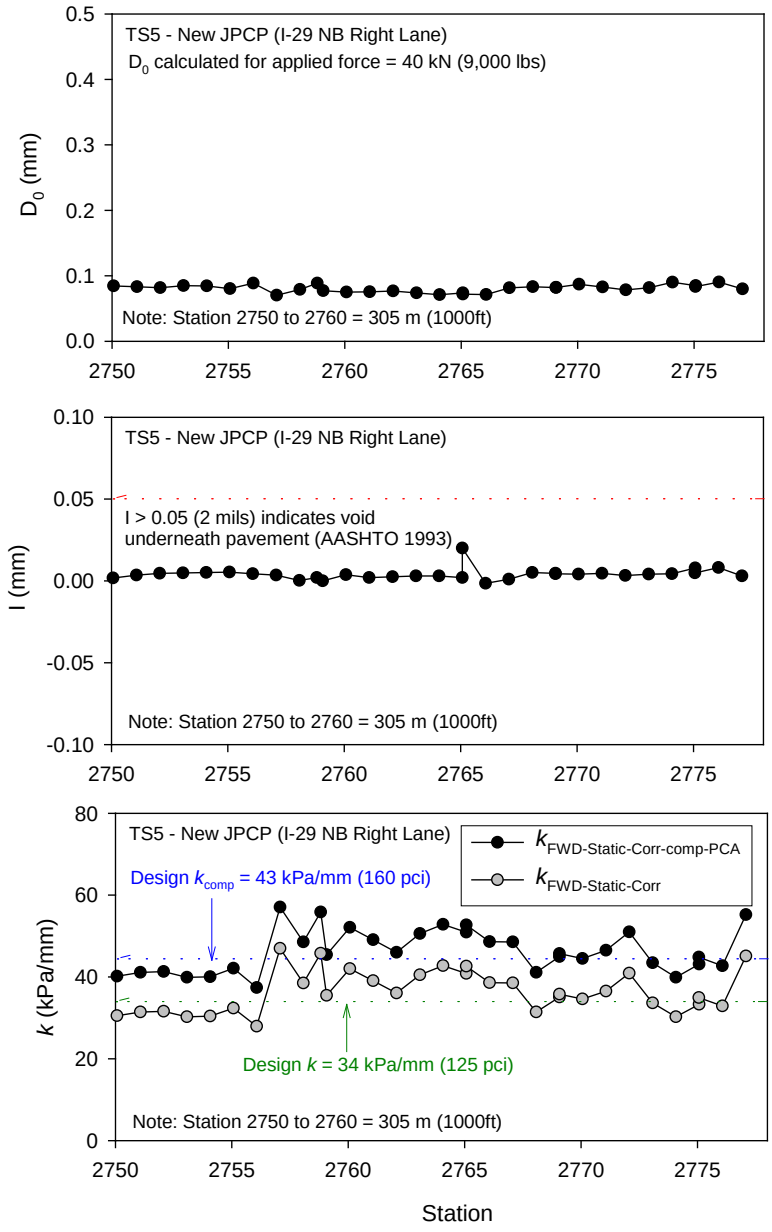

Figure 57. D_0, I, and *k* values from FWD tests on new JPCP TS5 I-29 NB right lane

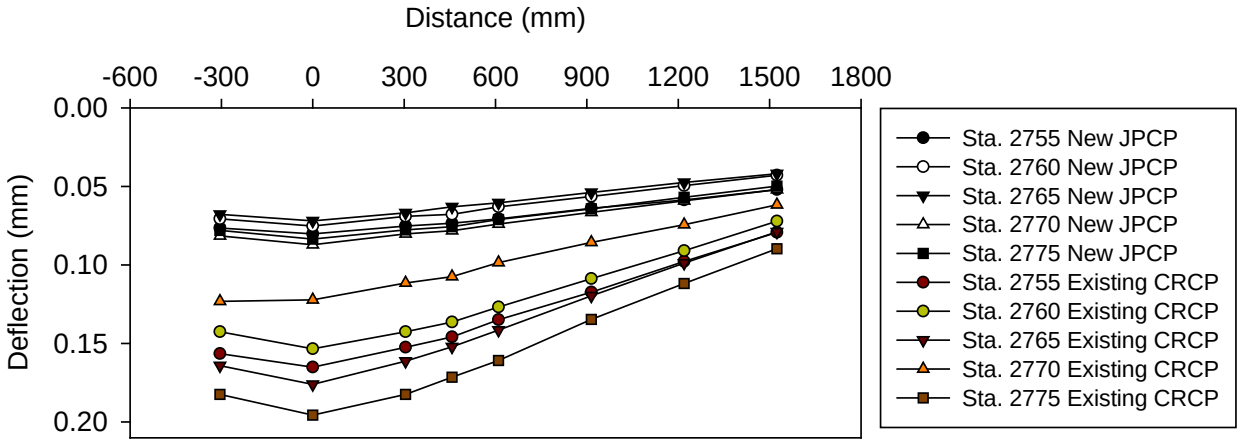

Figure 58. TS5: Comparison of FWD deflection basins on new JPCP and existing CRCP between Sta. 2755 and Sta. 2775

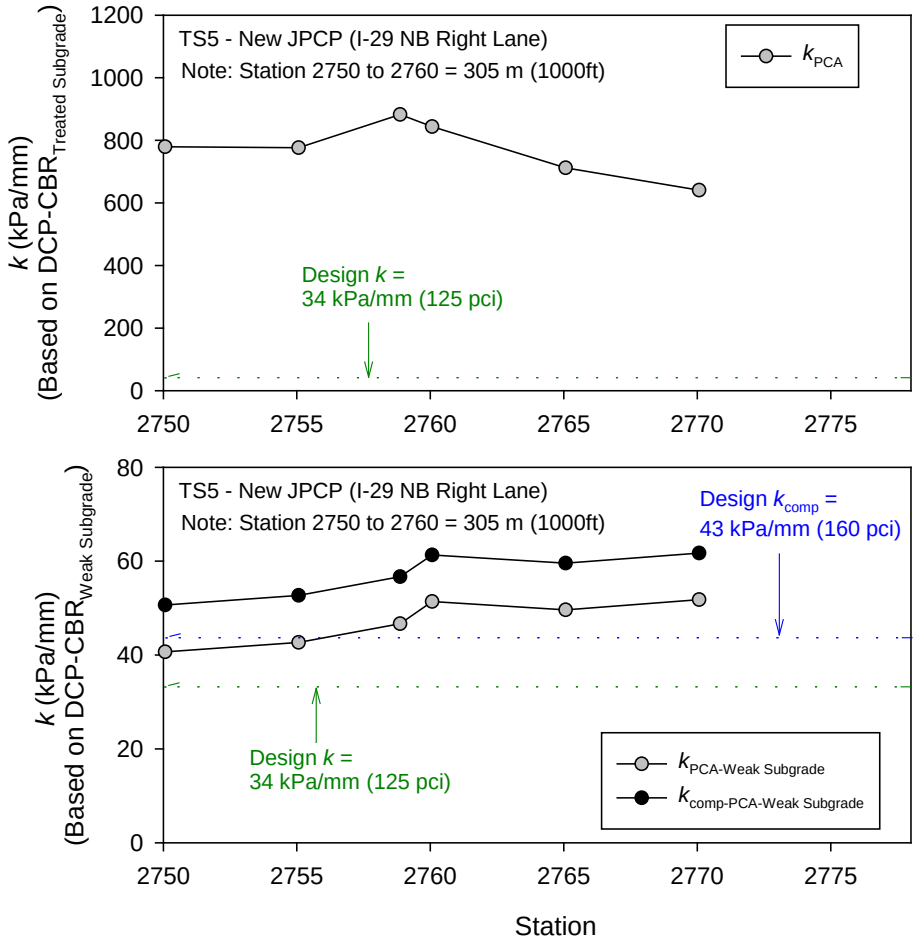

Figure 59. TS5 new JPCP I-29 NB right lane: *k* values from DCP-CBR tests

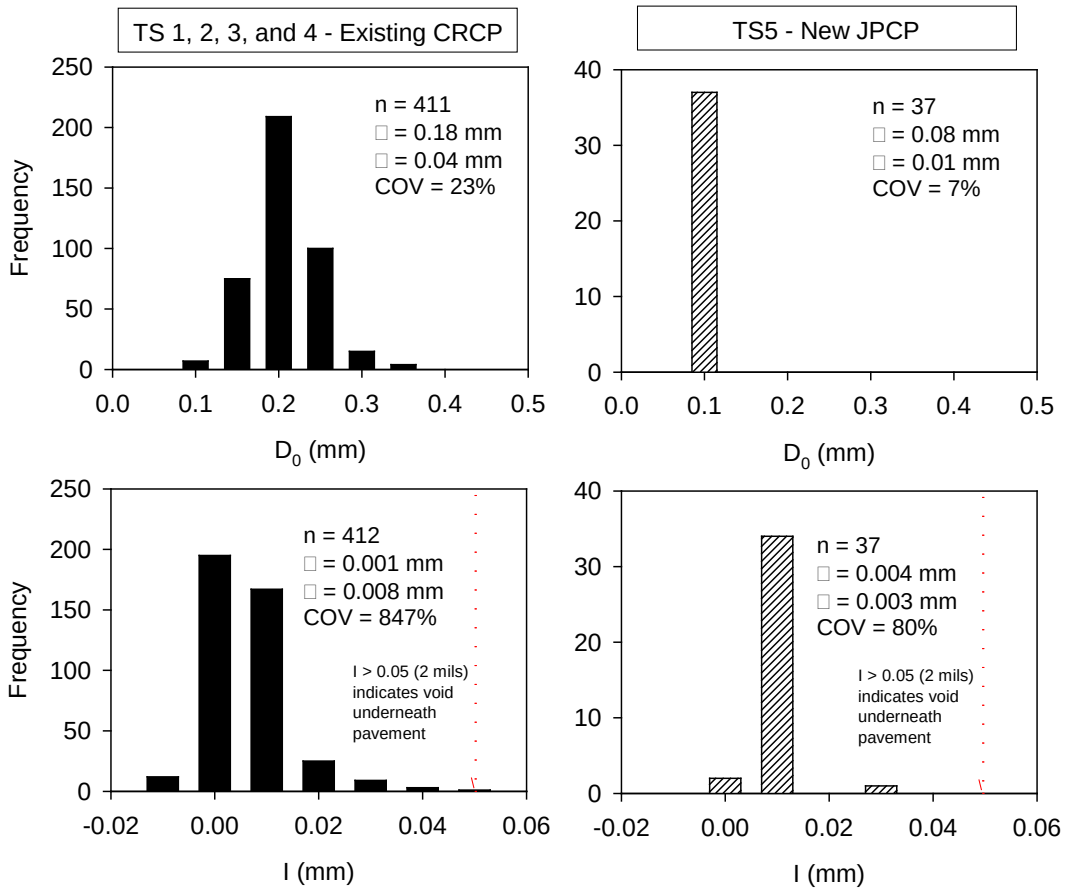

Figure 60. Histograms of FWD test measurements D_0 and I from tests on existing CRCP (TS1, TS2, TS3, and TS4) and new JPCP (TS5)

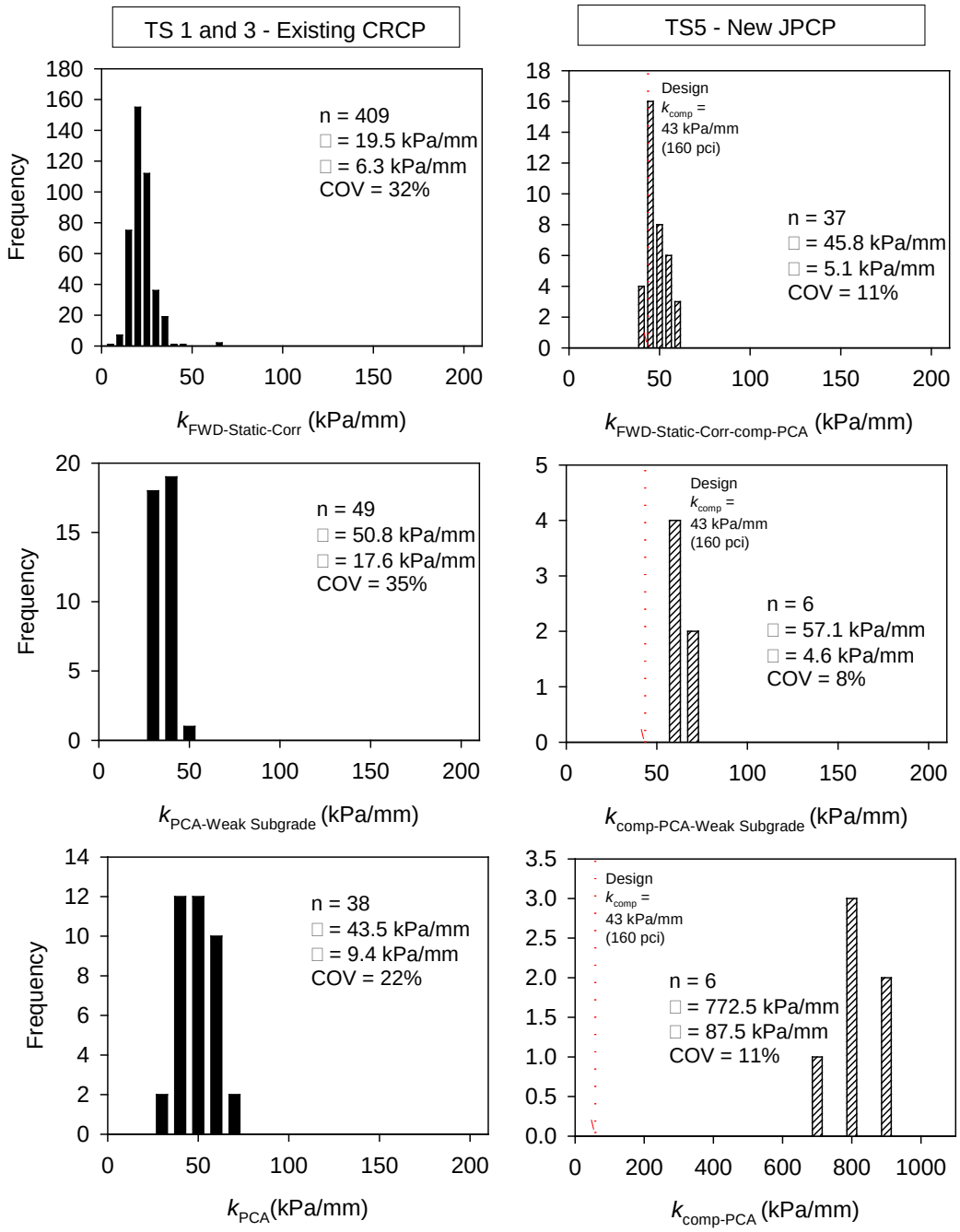

Figure 61. Histograms of *k* values on new on existing CRCP (TS1 and TS3) and new JPCP (TS5)

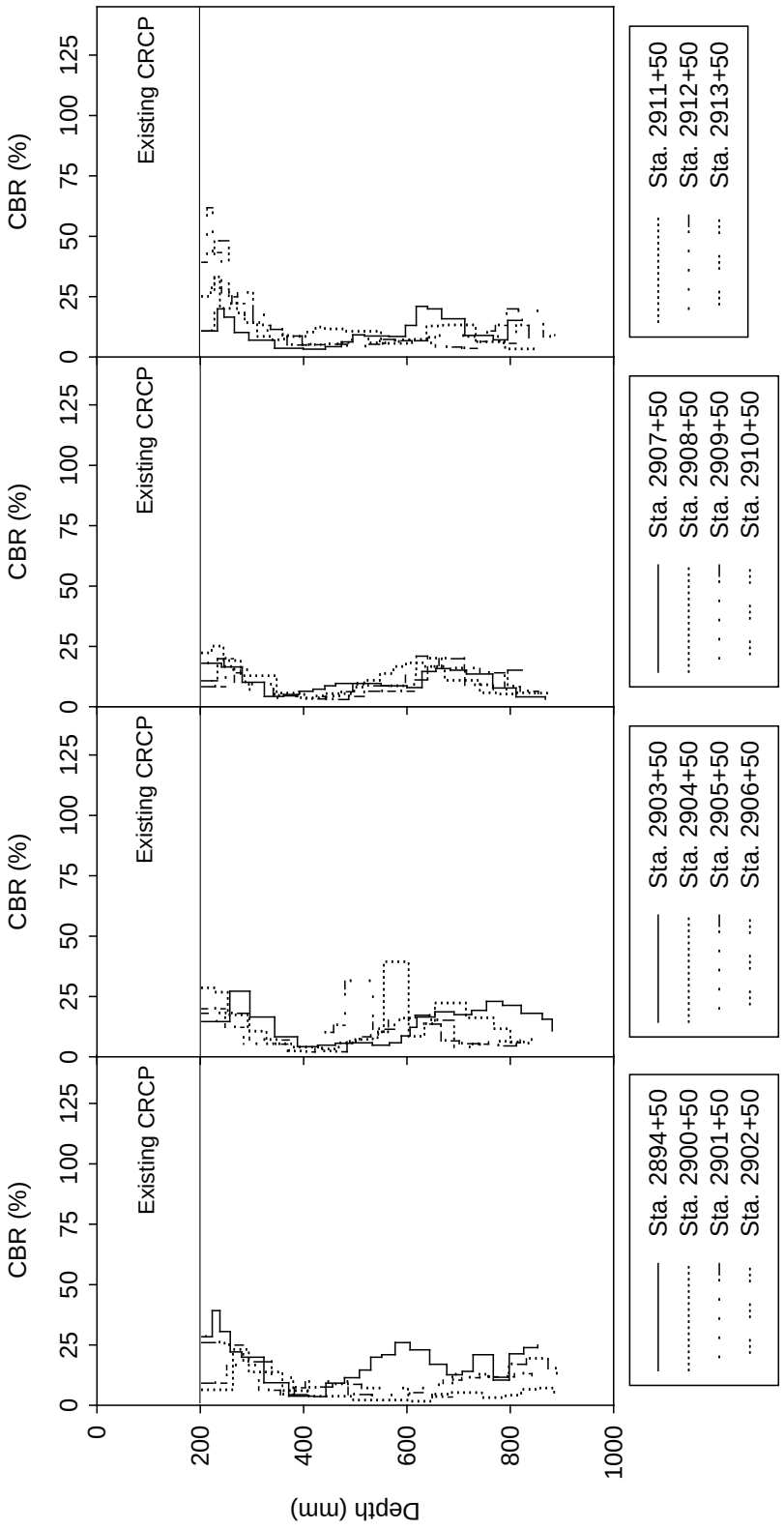

Figure 62. DCP-CBR profiles from TS3 FWD test locations in the foundation layers obtained by drilling a hole in the pavement

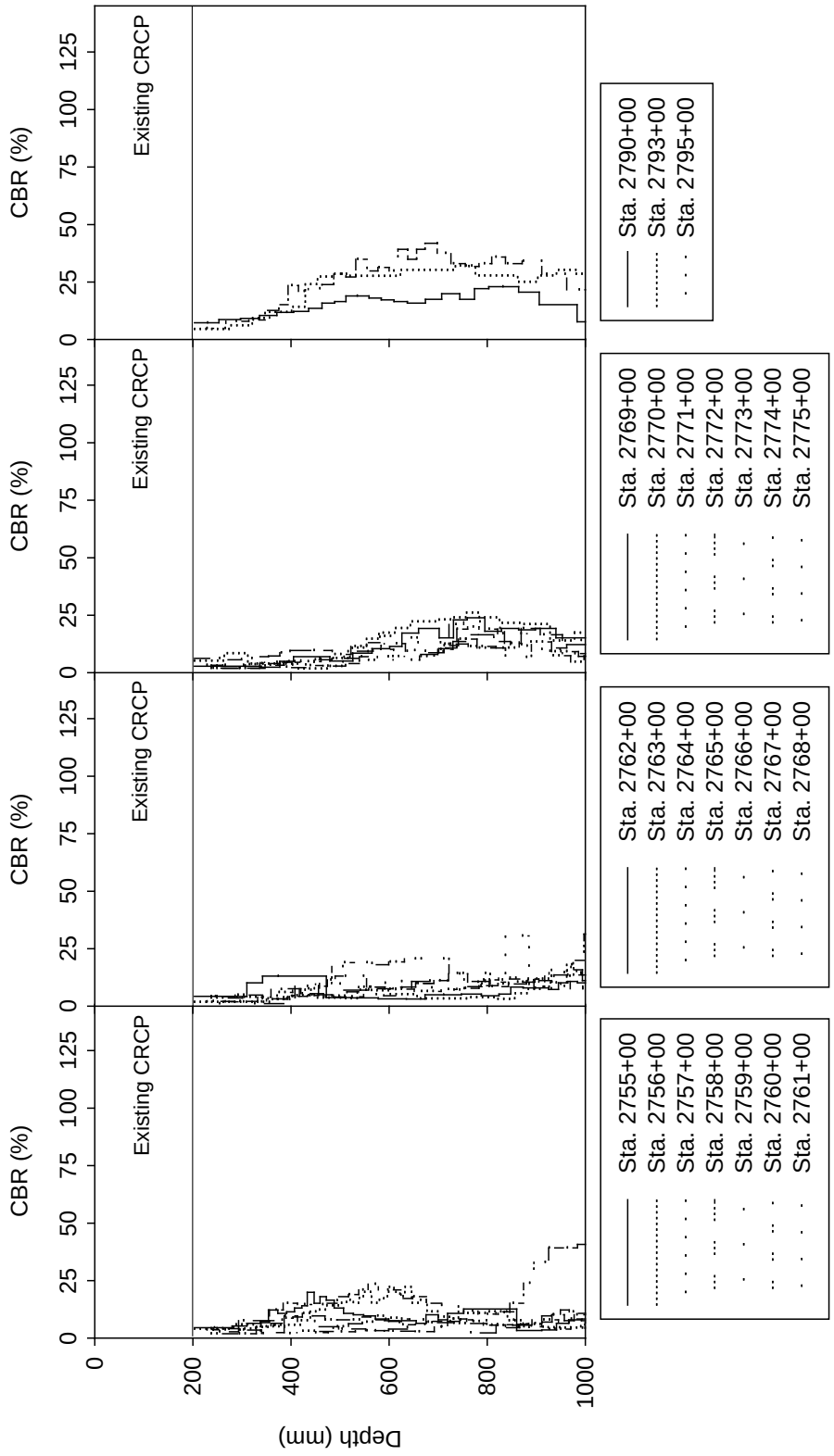

Figure 63. DCP-CBR profiles from TS1 FWD test locations directly on the foundation layers

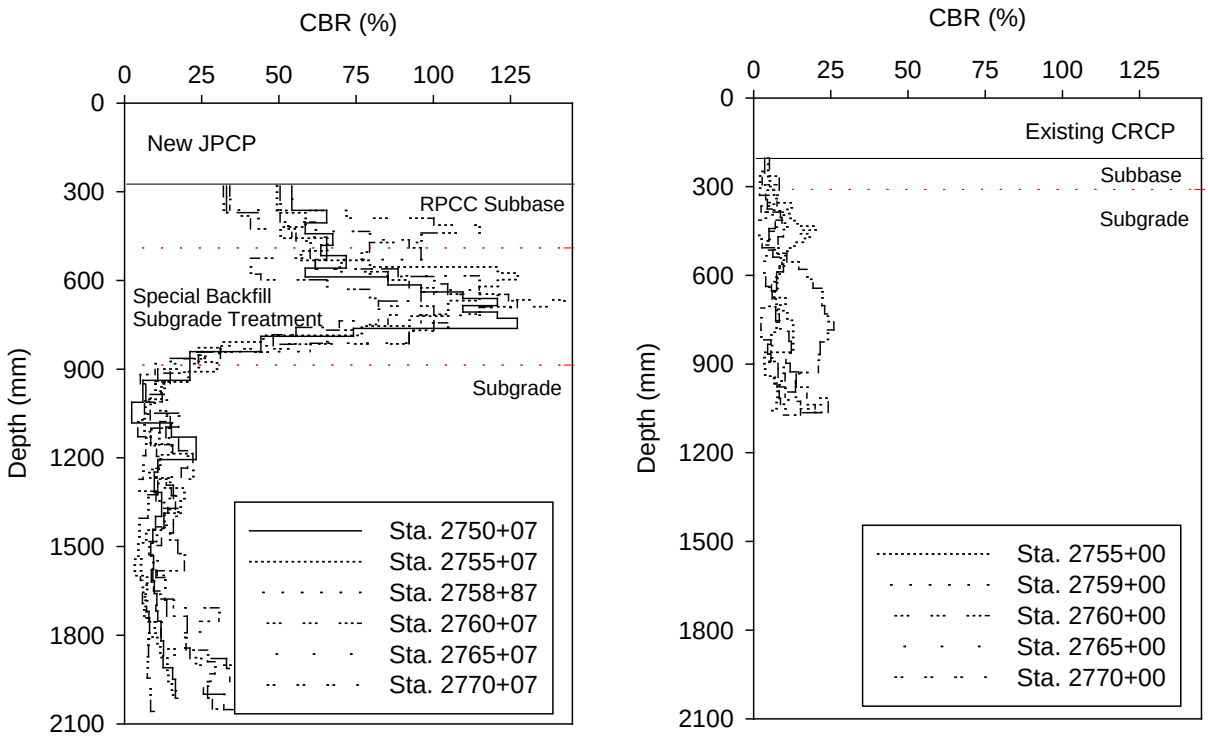

Figure 64. DCP-CBR profiles on new JPCP TS5 (left) and on existing CRCP TS1 (right) at FWD test locations between Sta. 2750 and Sta. 2775 (tests conducted in foundation layers by drilling a hole in the pavement)

In Situ Testing and Roller-Integrated Compaction Monitoring Results on Production Areas

A Volvo smooth drum roller equipped with an RICM system was used for the roller integrated compaction monitoring and mapping that was conducted on TS6, TS7, TS8, TS9, and TS10 after all of the compaction passes on subgrade, special backfill subbase, and base layers had been completed. All areas were mapped using low and high amplitude settings (i.e., a = 1.60 mm and 2.00 mm, respectively). TS6 and TS7 consisted of mapping the subgrade and recycled asphalt subbase layers, respectively over a plan area of about 9 m (32 ft) x 85 m (280 ft) on I-29 NB near station 2900. TS8 and TS9 consisted of mapping recycled asphalt subbase and RPCC base layers, respectively over a plan area of about 14 m (46 ft) x 250 m (820 ft) on I-29 NB near station 2850. TS10 consisted of mapping select sand subbase layer over a plan area of about 10 m (32 ft) x 170 m (558 ft) near the intersection of I-29 and Hwy 175. Following mapping passes, in situ point testing using LWD, DCP, and NG were conducted on TS6, TS7, TS9, and TS10. In situ test locations were selected based on CMV maps seen in the roller.

Kriged contour maps for CMV were generated using roller data obtained approximately every 0.2 m (0.65 ft). These maps are presented in Figure 65 to Figure 67 along with DCP-CBR profiles, $E_{LWD\text{-}Z3}$, w, and γ_d measurements. Comparing CMV maps with in situ test measurements generally indicates that relatively low, medium, and high CMV locations match with relatively

low, medium, and high E_{LWD-Z3} and CBR point measurements. CMV maps obtained on special backfill subbase and the overlaid RPCC base layers indicate that "hard" and "soft" zones in the subbase layer maps are reflected on the RPCC base layer maps as shown in Figure 66.

Maps obtained on TS10 (Figure 67) identify the location of a utility concrete culvert (photo in Figure 68). The CMV measurements directly over the top of the concrete culvert were higher compared to locations beyond the culvert. In situ point measurements (E_{LWD-Z3}, γ_d, *w*, and CBR) were obtained from directly above the culvert area (points 5 to 8) and along the edge of the culvert (points 1 to 4). E_{LWD-Z3}, CBR, and γ_d measurements obtained directly above the culvert area showed relatively high values compared to measurements along the edge of the culvert (average E_{LWD-Z3} = 25.2 MPa along the edge and 37.7 MPa above the culvert; CBR = 8.3 along the edge and 16.1 above the culvert; γ_d = 21.00 kN/m^3 along the edge and 21.46 kN/m^3 above the culvert). Relatively low CMV and in situ point measurements along the edge of culverts are commonly encountered because it is difficult to compact material along the edges of concrete walls.

CMV maps in different amplitude settings indicate that the CMV measurements are influenced by vibration amplitude. CMV measurements on the subgrade were on average about 1.1 to 1.3 times greater in high amplitude setting (i.e., a = 2.00 mm) than in low amplitude setting (i.e., a = 1.50 mm). Similarly, CMV measurements on the subbase and base layers were on average about 1.2 to 1.5 times greater in high amplitude setting than in low amplitude setting. This is likely due to potential differences in the magnitude of stresses applied on the materials by the roller drum under different amplitude settings (Vennapusa et al. 2010).

In addition to the CMV measurements obtained from TS6, TS7, TS8, TS9, and TS10, CMV measurements were obtained from several other calibration and production areas on this site as part of an Iowa DOT research project. Results from all of those areas are presented in detail in White et al. (2010). Correlations between CMV obtained in low and high amplitude settings and in situ point measurements of all of the test sections are presented in Figure 69 and Figure 70, respectively. Non-linear exponential relationships showed the best fit for CMV vs. E_{LWD-Z3} with R^2 = 0.66 to 0.86. Relatively weak regression relationships with R^2 = 0.12 to 0.18 were observed for CMV vs. CBR. No statistically significant relationships were found for CMV vs. γ_d.

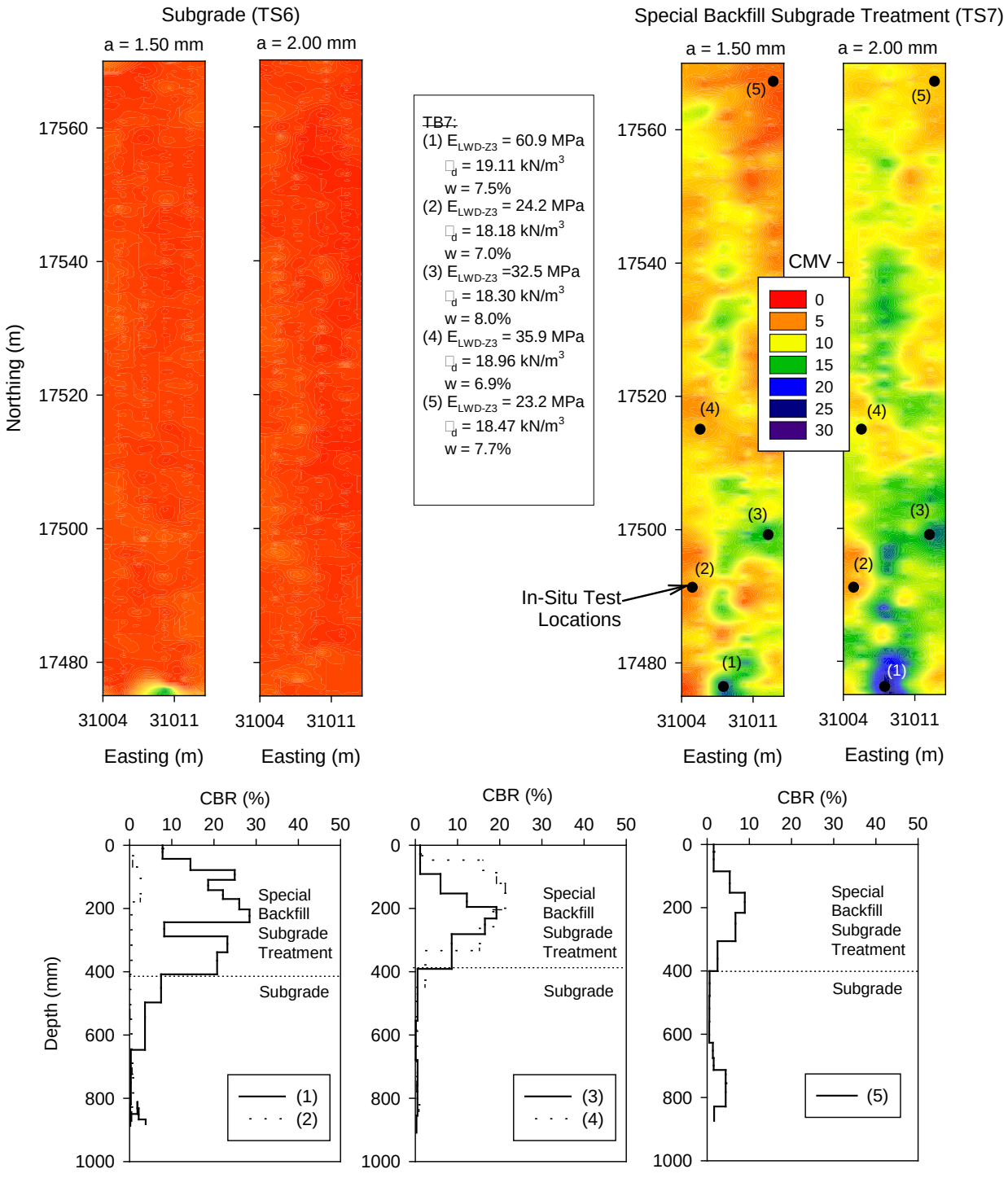

Figure 65. CMV spatial maps of TS6 (subgrade layer) and TS7 (special backfill subgrade treatment layer) and DCP-CBR profiles at five in situ test locations

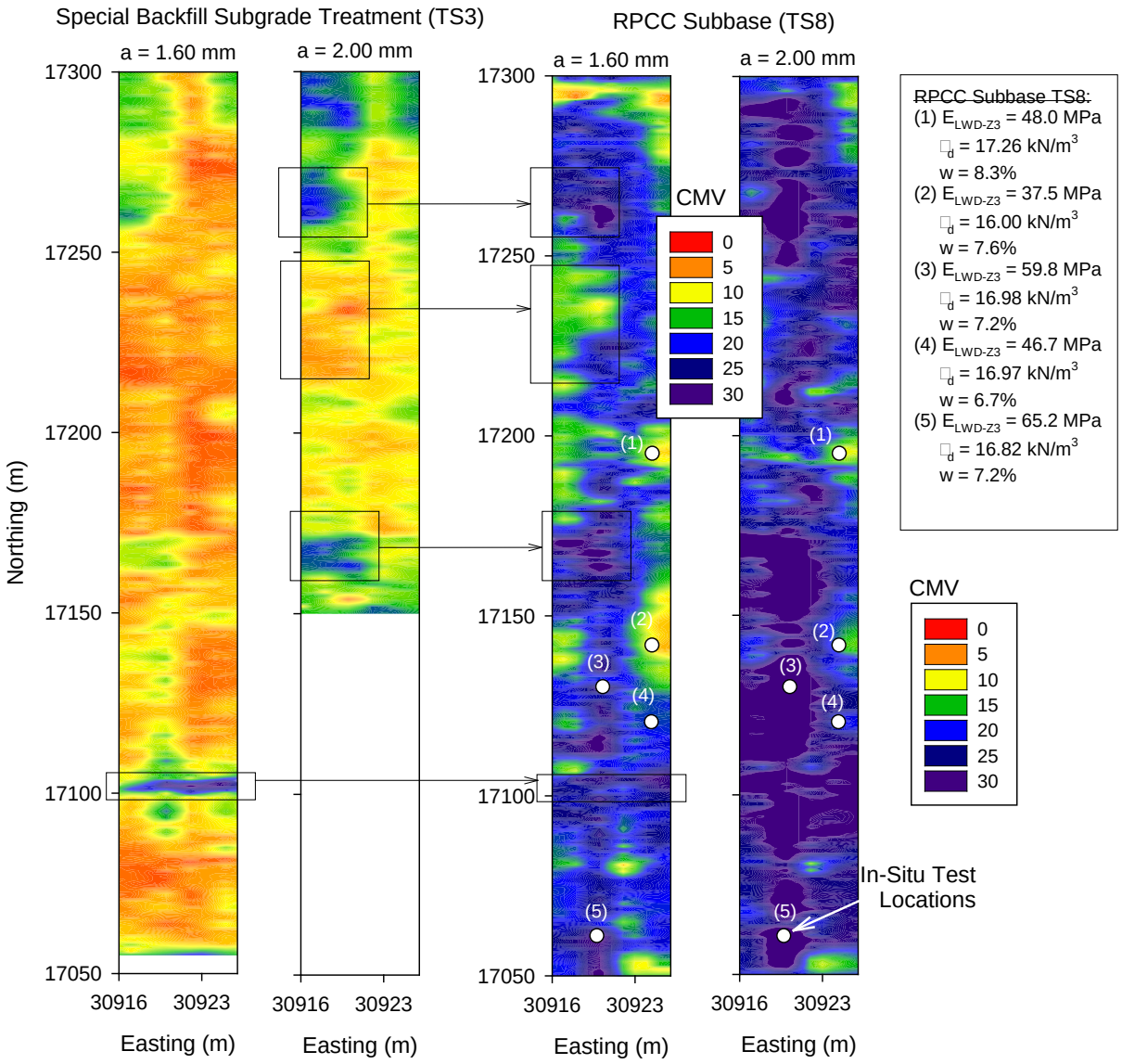

Figure 66. CMV spatial maps of TS8 (special backfill subbase layer) and TS9 (RPCC base layer) and $E_{LWD\text{-}Z3}$, γ_d, and *w* at five in situ test locations

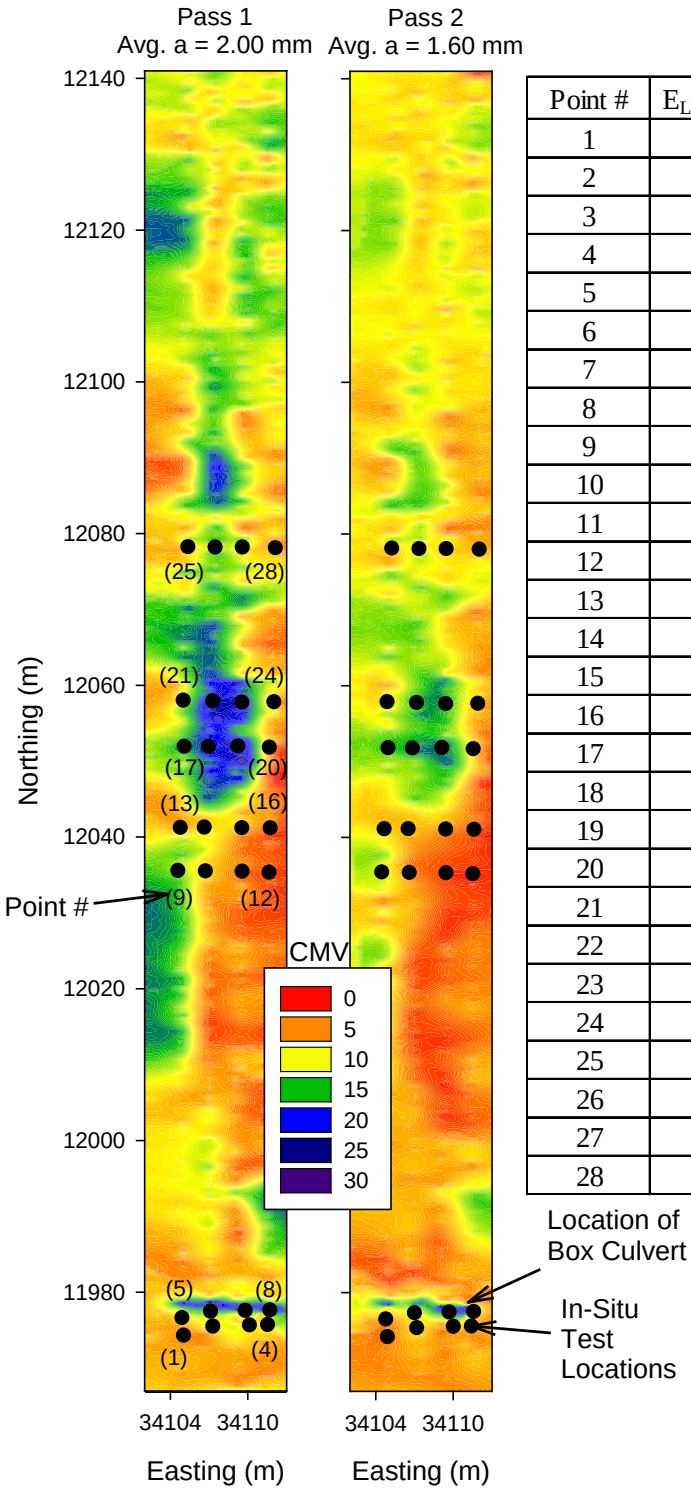

Point #	E_{LWD-Z3} (MPa)	γ_d (kN/m^3)	w (%)	CBR (%)
1	28.7	21.47	4.2	6.7
2	31.9	21.43	7.1	15.5
3	20.1	20.69	5.9	7.1
4	20.1	20.23	6.8	4.2
5	35.9	21.18	5	12.5
6	35.5	21.13	6.3	16.5
7	36.7	21.60	4.8	18.3
8	42.6	21.91	5.4	16.9
9	36.7	20.86	5.2	--
10	36.7	21.05	5.4	--
11	22.1	21.02	4.6	--
12	22.1	21.27	4.6	--
13	35.2	20.89	5.5	--
14	28.4	20.74	5.6	--
15	29.1	21.14	4.3	--
16	20.5	20.53	5.4	--
17	48.7	21.24	4.4	--
18	52.5	20.81	5.6	--
19	48.7	21.27	4.7	--
20	40.6	20.94	5.1	--
21	42.6	20.80	4.8	--
22	47.4	21.11	5.2	--
23	46.7	20.85	6.4	--
24	36.7	20.67	5.5	--
25	32.8	20.89	4.6	--
26	33.8	21.18	5.4	--
27	24.2	20.58	6.9	--
28	28.4	20.26	6.1	--

Figure 67. CMV spatial maps of TS10 (select sand subgrade treatment layer) using high and low amplitude settings and a table showing in situ test results from 28 locations

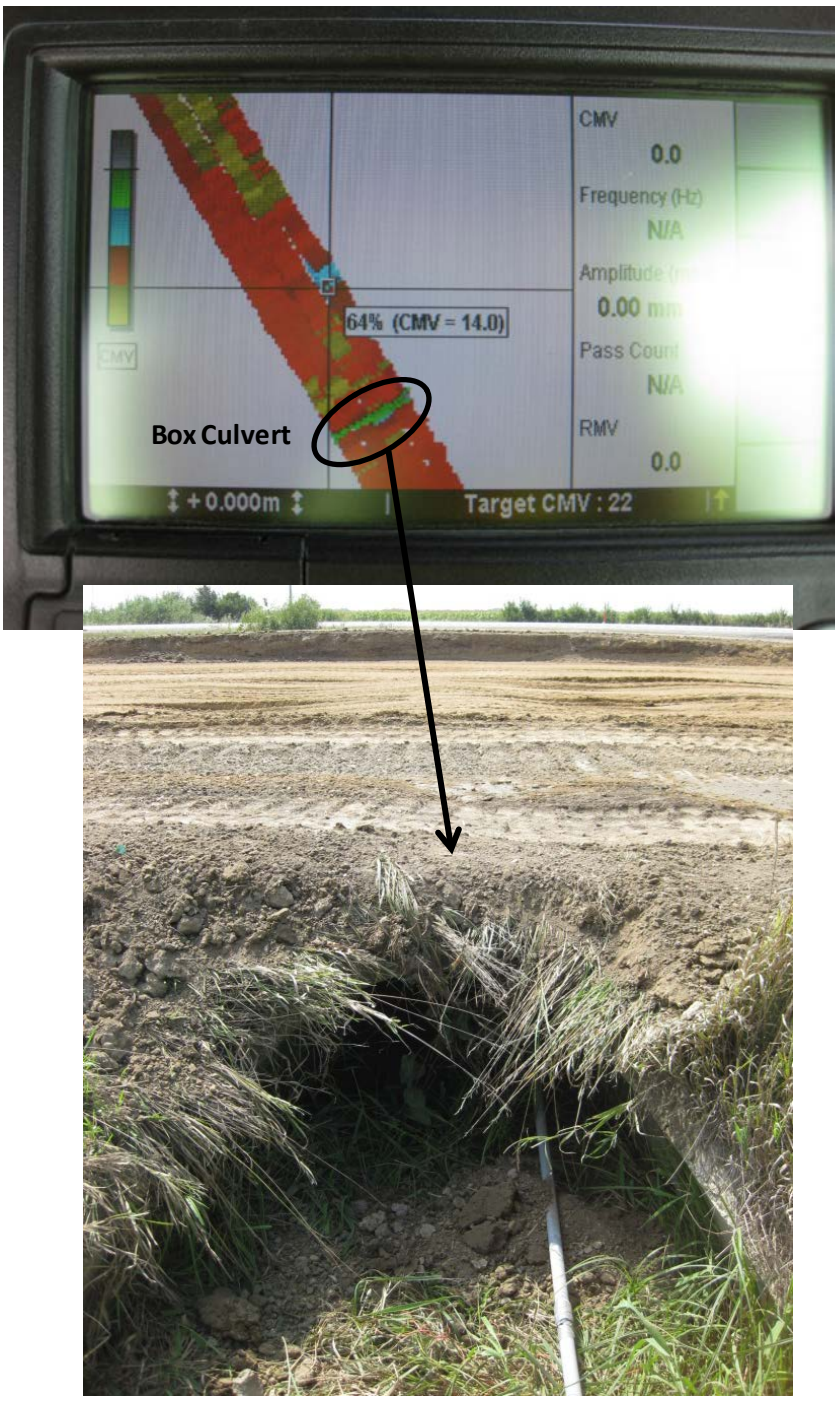

Figure 68. Box culvert location in TS10 highlighted on AccuGrade CMV map display (top) and photograph of the culvert (bottom)

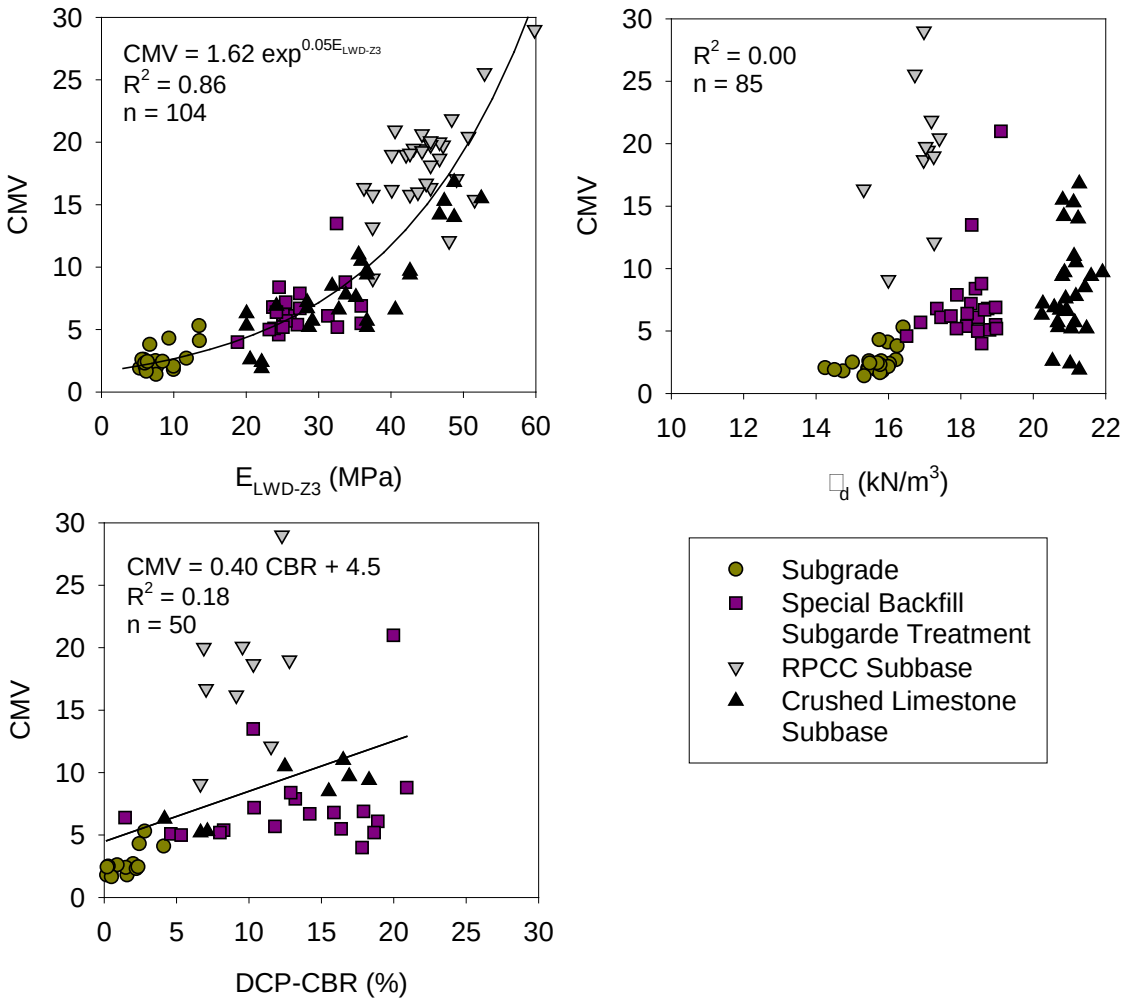

Figure 69. Empirical correlations between CMV and in situ point measurements (a = 1.60 mm)

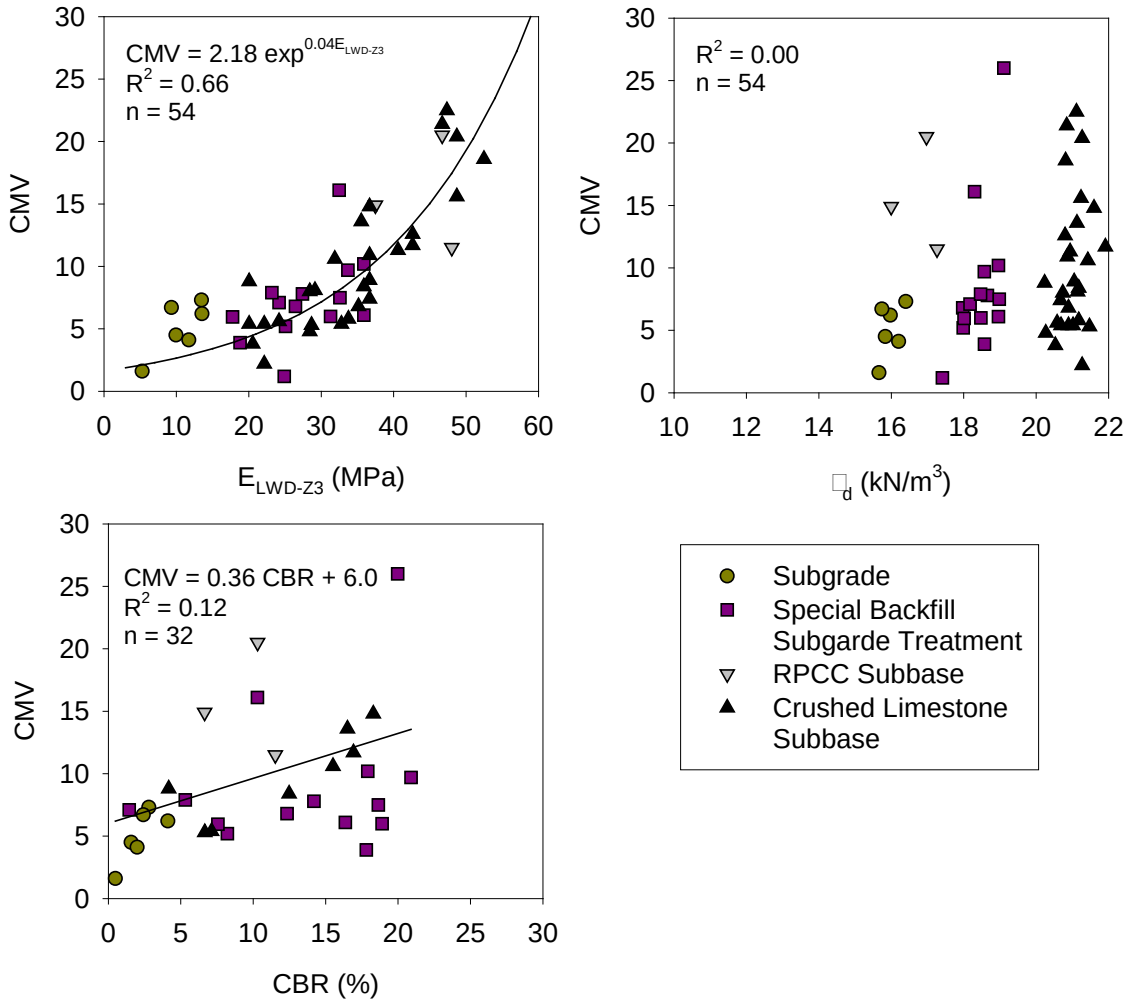

Figure 70. Empirical correlations between CMV and in situ point measurements (*a* = 2.00 mm)

Comparing Design Values, In situ Measurements, and Laboratory Measurements

A summary of in situ measurement statistics from tests on TS5 new JPCP foundation layers is provided in Table 10Table 10. Summary statistics of in situ test results on TS5 new JPCP. The summary table shows *k* values and k_{comp} values determined from FWD and DCP tests. Design parameters and the measured/estimated parameters based on in situ and laboratory measurements are provided in Table 11. *k* values were determined from FWD and DCP field measurements, and laboratory CBR measurements obtained from pre- and post-F/T testing. Details of the procedures followed in estimating these parameters are provided in the Table 11 notes.

Table 10. Summary statistics of in situ test results on TS5 new JPCP

Measurement	n	μ	σ	COV (%)
$k_{FWD\text{-}Static\text{-}Corr}$ (kPa/mm)	37	36.0	4.7	13
k_{PCA} (kPa/mm)	6	772.5	87.5	11
$k_{PCA\text{-}Weak\ Subgrade}$ (kPa/mm)	6	47.1	4.7	10
$k_{FWD\text{-}Static\text{-}Corr\text{-}comp\text{-}PCA}$ (kPa/mm)	37	45.8	5.1	11
$k_{comp\text{-}PCA}$ (kPa/mm)	6	772.5	87.5	11
$k_{comp\text{-}PCA\text{-}Weak\ Subgrade}$ (kPa/mm)	6	57.1	4.6	8

Table 11. Summary of design, in situ, and laboratory values

PCA Design Parameter	Design Value	In situ Measurements (Average)*	Laboratory Measurements (Average)
Subgrade *k*	34 kPa/mm (125 pci)	$k_{PCA\text{-}Treated\ Subgrade}$ = 773 kPa/mm (2,830 pci)[1] $k_{PCA\text{-}Weak\ Subgrade}$ = 47.1 kPa/mm (172 pci)[2] $k_{FWD\text{-}Static\text{-}Corr}$ = 36.0 kPa/mm (132 pci)[3]	$k_{subgrade}$ = 75 kPa/mm (276 pci) [as-compacted][8] $k_{subgrade}$ = 12 kPa/mm (43 pci) [thawed][9]
Subbase layer thickness	Min. = 150 mm Avg. = 200 mm	Avg. = 150 mm[4]	N/A
k_{comp}	43 kPa/mm (160 pci)	$k_{comp\text{-}PCA}$ = 772.5 kPa/mm (319 pci)[5] $k_{comp\text{-}PCA\text{-}Weak\ Subgrade}$ = 57.1 kPa/mm (209 pci)[6] $k_{FWD\text{-}Static\text{-}Corr\text{-}comp\text{-}PCA}$ = 45.8 kPa/mm (168 pci)[7]	$k_{comp\text{-}PCA}$ = 109.8 kPa/mm (404 pci) [as-compacted][10] $k_{comp\text{-}PCA}$ = 30.1 kPa/mm (110 pci) [thawed][10]

*Average of all measurements obtained from TS5; [1]Empricially estimated from DCP-$CBR_{Treated\text{-}Subgrade}$ following PCA (1984); [2]Empirically estimated from DCP-$CBR_{Weak\ Subgrade}$ following PCA (1984); [3]Obtained from FWD test using the AREA method and corrected for slab size; [4]Obtained from DCP measurements; [5]The k_{PCA} values calculated were significantly higher than the values provided in PCA (1984) in estimating $k_{comp\text{-}PCA}$ values, therefore k_{PCA} was assumed to be the same as the composite values; [6]Empirically estimated from DCP-$CBR_{Weak\ Subgrade}$ and $H_{Subbase}$ = 150 mm following PCA (1984); [7]Calculated using $k_{FWD\text{-}Static\text{-}Corr}$ and $H_{Subbase}$ = 150 mm following PCA (1984); [8]Empirically estimated from CBR-*k* relationships in PCA (1984) with CBR obtained on a sample compacted to a target w = 17.8% and γ_d = 16.39 kN/m^3 during frost-heave and thaw-weakening susceptibility testing; [9]Empirically estimated from CBR-*k* relationships in PCA (1984) with CBR obtained on a sample compacted to a target w = 17.8% and γ_d = 16.39 kN/m^3 and thawed during frost-heave and thaw-weakening susceptibility testing; [10]Estimated using subgrade *k* and $H_{Subbase}$ = 300 mm following PCA (1984).

Comparisons of the target design parameters and the measured or estimated parameters from laboratory and in situ testing reveal some important aspects that are summarized as follows:

- The subgrade *k* values estimated from laboratory CBR measurements from post freeze-thaw testing were about 2.8 times lower than the design value

- The average treated subgrade *k* value ($k_{PCA\text{-}Treated\ Subgrade}$) estimated from DCP-CBR measurements was about 23 times higher than the design value, while the untreated weak subgrade *k* value ($k_{PCA\text{-}Weak\ Subgrade}$) estimated from DCP-CBR was about 1.4 times higher than the design value. The average *k* value determined from FWD tests ($k_{FWD\text{-}Static\text{-}Corr}$), however, was about the same as the design value.

CHAPTER 6: SUMMARY AND CONCLUSIONS

This report presents results and analysis of field and laboratory tests from a field study conducted on the I-29 interstate highway reconstruction project in Monona and Harrison Counties, Iowa. The project involved removal of the existing CRCP; reconstruction of the pavement foundation layers (base, subbase, and subgrade); and placement of a new JPCP on the north and south bound lanes of I-29, between just south of County road F-20 to just north of I-75.

In situ FWD tests and DCP tests were conducted on the existing CRCP and the exposed foundation layers shortly after the old pavement was removed and on the new JPCP shortly after it was placed. The FWD and DCP tests were conducted to compare the foundation layer strength/stiffness profiles of the old and new foundation layers and to obtain mechanistic properties of the new foundation layers (i.e., modulus of subgrade reaction *k*) to compare with the design *k* values. Some key findings from this testing and data analysis are as follows:

- On average, the plate deflection under a 40 kN applied load on the new JPCP was about 0.4 times the deflection on the existing CRCP.
- The FWD intercept values on the existing CRCP and new JPCP were low (< 0.04 mm) which do not indicate voids beneath the pavement.
- The average static *k* value determined from the FWD on the new JPCP was on average about 1.6 times higher than on the existing CRCP. This indicates that there was improvement in the foundation layer stiffness values under the new pavement compared to the old pavement.
- The *k* values determined from both DCP-CBR measurements and FWD measurements indicated higher values on the new JPCP than on the existing CRCP.
- Based on tests conducted on the new JPCP sections, the *k* values determined using FWD were similar to the values determined using CBR of the weak layer within the top 450 mm of the subgrade, but were about 17 times lower than the values determined using CBR of the treated subgrade. This indicates that a weak layer within the top 450 mm of the subgrade contributes to low values observed in the FWD testing and that the use of high CBR values in the treated subgrade layers can result in unreasonably high *k* values.
- The subgrade *k* values estimated from laboratory CBR measurements in thawed state were about 2.8 times lower than the design value. The average treated subgrade *k* value estimated from DCP-CBR measurements was about 23 times higher than the design value, while the untreated weak subgrade *k* value estimated from DCP-CBR was about 1.4 times higher than the design value. The average *k* value determined from FWD testing, however, was about the same as the design value.

Five foundation layer production areas on the project were mapped during construction using a Volvo vibratory smooth drum roller equipped with Trimble's roller integrated compaction monitoring (RICM) system. The RICM system used on this project measured compaction meter value (CMV). In situ nuclear gauge density, moisture content, light weight

deflectometer (LWD) and DCP tests were conducted for correlation with CMV measurements. Some key findings from this testing are as follows:

- CMV maps with virtually 100% coverage of the compacted foundation layers revealed "soft" and "stiff" areas that were verified with in situ DCP and LWD measurements.
- CMV measurements were influenced by amplitude settings. CMV measurements were on average about 1.1 to 1.5 times greater in high amplitude setting than in low amplitude setting. This is likely due to potential differences in the magnitude of stresses applied on the materials by the roller drum under different amplitude settings.
- Results obtained from another study (White et al. 2010) were combined with the results obtained from this project to obtain correlations over a wide measurement range between LWD modulus, DCP-CBR, and nuclear gauge dry unit weight measurements and CMV. Results showed non-linear exponential relationships for CMV vs. LWD modulus with $R^2 = 0.66$ to 0.86. Relatively weak regression relationships with $R^2 = 0.12$ to 0.18 were observed for CMV vs. CBR, and no statistically significant relationships were found for CMV vs. dry unit weight. This was expected as CMV provides a measure of composite layer ground stiffness and not necessarily the dry unit weight of a single layer.

Laboratory testing was conducted on foundation layer materials obtained from field to determine index properties, moisture-dry unit weight relationships from compaction tests, resilient modulus (M_r) values, and frost-heave and thaw-weakening susceptibility ratings. The M_r tests were conducted on homogenous samples as well as on layered composite samples (i.e., RPCC base over subbase and subbase over subgrade) to assess the influence of composite soil layer configurations on M_r values. The frost-heave tests were conducted on subgrade samples by exposing the samples to two freeze-thaw cycles. Thaw-weakening susceptibility ratings were determined by conducting CBR tests on compacted samples before and after two thawing cycles. Some key findings from laboratory M_r and frost-heave/thaw-weakening susceptibility rating tests are as follows:

- Comparing the M_r values of the homogenous samples and the layered composite samples indicated that the average M_r of the composite sample was either similar to the layer with a lower M_r value or about average of the two layer's M_r values.
- Frost-heave test results on subgrade samples indicated that the heave rate was greater for the second freezing cycle than for the first freezing cycle, which indicates that the material is susceptible to increased heave with greater freeze-thaw cycles. Based on the frost-heave rate measurements, the subgrade soil is classified to have high potential to frost-heave according to ASTM D5918.
- A moisture content profile of each sample was obtained after the two freeze-thaw cycles by taking samples at different depths. Results showed that the moisture content was higher at all depths in the samples compared to the initial moisture content, as expected. The moisture content at the top of the sample was higher than at the middle or bottom of the sample, which indicates that water was drawn to the top cold plate through capillary action caused by the temperature gradient in the samples during testing.

- The average CBR of the four post freeze-thaw test samples decreased to CBR < 1.0 from the pre freeze-thaw sample with about CBR = 22. Based on the post freeze-thaw CBR values, the soil is classified to have very high potential to thaw-weakening according to ASTM D5918.

REFERENCES

AASHTO T-307. (1999). "Standard method of test for determining the resilient modulus of soils and aggregate materials" American Association of State Highway and Transportation Officials (AASHTO), Washington, DC.

AASHTO. (1993). *AASHTO design guide for design of pavement structures*. American Association of State Highway and Transportation Officials, Washington DC.

Andrei, D., Witczak, M. W., Schwartz, C. W., and Uzan, J. (2004). "Harmonized resilient modulus test method for unbound pavement materials." *Transportation Research Record: Journal of the Transportation Research Board.* No. 1874, Transportation Research Board of the National Academies, Washington, DC, 29-37.

ASTM C136-06. (2010). "Standard test method for sieve analysis of fine and coarse aggregates." American Standards for Testing Methods (ASTM), West Conshohocken, PA.

ASTM D422-63. (2010). "Standard Test Method for Particle-Size Analysis of Soils." American Standards for Testing Methods (ASTM), West Conshohocken, PA.

ASTM D698-07e1. (2010). "Standard test method for laboratory compaction characteristics of soil using standard effort (12,400 ft-lbf/ft^3 (600 kN-m/m^3))." American Standards for Testing Methods (ASTM), West Conshohocken, PA.

ASTM D854-10 (2010). "Standard test methods for specific gravity of soil solids by water pycnometer". American Standards for Testing Methods (ASTM), West Conshohocken, PA.

ASTM D1557-09. (2010). "Standard test method for laboratory compaction characteristics of soil using modified effort (56,000 ft-lbf/ft^3 (2,700 kN-m/m^3))." American Standards for Testing Methods (ASTM), West Conshohocken, PA.

ASTM D1883-07e2 (2010). "Standard test method for CBR (California Bearing Ratio) of laboratory compacted soils." American Standards for Testing Methods (ASTM), West Conshohocken, PA.

ASTM D2487-10 (2010). "Standard test method for classification of soil for engineering purposes (unified soil classification system)." American Standards for Testing Methods (ASTM), West Conshohocken, PA.

ASTM D3282-09 (2010). "Standard test method for classification of soils and soil-aggregate mixtures for highway construction purposes." American Standards for Testing Methods (ASTM), West Conshohocken, PA.

ASTM D4253-00. (2010). "Standard test methods for maximum index density and unit weight of soils using a vibratory table." American Standards for Testing Methods (ASTM), West Conshohocken, PA.

ASTM D4254-00. (2010). "Standard test methods for minimum index density and unit weight of soils and calculation of relative density." American Standards for Testing Methods (ASTM), West Conshohocken, PA.

ASTM D4318-10. (2010). "Standard test methods for liquid limit, plastic limit, and plasticity index of soils." American Standards for Testing Methods (ASTM), West Conshohocken, PA.

ASTM D4694-09. (2009). "Standard Test Method for Deflections with a Falling-Weight-Type Impulse Load Device." American Standards for Testing Methods (ASTM), West Conshohocken, PA.

ASTM D5918-06 (2010). “Standard test methods for frost heave and thaw weakening susceptibility of soils.” American Standards for Testing Methods (ASTM), West Conshohocken, PA.

ASTM D6951-03 (2010). “Standard test method for use of the dynamic cone penetrometer in shallow pavement applications.” American Standards for Testing Methods (ASTM), West Conshohocken, PA.

ASTM D6938-10 (2010). “Standard test method for in-place density and water content of soil and soil-aggregate by nuclear methods (shallow depth).” American Standards for Testing Methods (ASTM), West Conshohocken, PA.

Brandl, H., and D. Adam. (1997). “Sophisticated continuous compaction control of soils and granular materials.” Proceedings of the 14th International Conference of Soil Mechanics and Foundation Engineering. Hamburg, Germany, 1-6.

Barbenberg, E. J., and Petros, K. A. (1991). *Evaluation of Concrete Pavements Using NDT Results,* Illinois Highway Research Project IHR-512, University of Illinois and Illinois Department of Transportation, Report No. UILU-ENG-91-2006, IL.

Crovetti, J. A. (1994). “Evaluation of jointed concrete pavement systems incorporating open-graded bases.” Ph.D. Dissertation, University of Illinois at Urbana-Champaign, IL.

Darter, M. I., Hall, K. T., and Kuo, C-M. (1995). *Support under Portland Cement Concrete Pavements,* NCHRP Report 372, Transportation Research Board, Washington, D.C.

ERES Consultants Inc. (1982). *Techniques for Pavement Rehabilitation: A Training Course*. U.S. Department of Transportation, FHWA, Washington, D.C.

Floss, R., G. Bräu, M. Gahbauer, N. Gruber, and J. Obermayer. (1991). Dynamische Verdichtungsprüfung bei Erd-und Straßenbauten. *Prüfamt fur Grundbau, Boden-und Felsmechanik Technische Universität München*, Heft 612, München, Germany (in German).

Foxworthy, P. T. (1985). “Concepts for the Development of a Nondestructive Testing and Evaluation System for Rigid Airfield Pavements.” Ph.D. Thesis, University of Illinois at Urbana-Champaign, IL.

Hoffman, M. S., and Thompson, M. R. (1981). *Mechanistic Interpretation of Nondestructive Pavement Testing Deflections.* Transportation Engineering Series No. 32, Illinois cooperative Highway and Transportation Research Series No. 190, University of Illinois at Urbana-Champaign, Champaign, IL.

Ioannides, A. M. (1990). “Dimensional analysis in NDT rigid pavement evaluation”, *Transportation Engineering Journal*, ASCE, Vol. 116, No. TE1.

Jannsen, D., and Snyder, M. (2000). Temperature-Moment Concept for Evaluating Pavement Temperature Data. *Journal of Infrastructure Systems*, *6*(2), 81–83.

PCA. (1984). *Thickness design for concrete highway and street pavements,* Portland Cement Association, Skokie, IL.

Quintus, V. H. L., and A. L. Simpson. (2002). *Backcalculation of Layer Parameters for LTPP Test Sections, Volume II: Layered Elastic Analysis for Flexible and Rigid Pavements, Research Report, Long-Term Pavement Performance Program,* Report No. FHWA-RD-01-113, Federal Highway Administration, Washington, DC, October 2002.

Samaras, A. A., R. Lamm, and J. Treiterer. (1991). “Application of continuous dynamic compaction control for earthworks in railroad construction.” *Transportation Research Record: Journal of the Transportation Research Board.* No. 1309, Transportation Research Board of the National Academies, Washington, D.C., 42–46.

Sandström, Å. (1994). *Numerical simulation of a vibratory roller on cohesionless soil*. Internal Report, Geodynamik, Stockholm, Sweden.

Sandström Å., and C. B. Pettersson. (2004). Intelligent systems for QA/QC in soil compaction, *Proceedings of the TRB 2004 Annual Meeting* (CD-ROM), Transportation Research Board, Washington, D.C.

Schmalzer, P. (2006). *LTPP Manual for Falling Weight Deflectometer Measurements–Version 4.1* (Report No. FHWA-HRT-06-132). Washington, D.C.: Federal Highway Administration.

Smith, K. D., Wade, M. J., Bruinsma, J. E., Chatti, K., Vandenbossche, J. M., Yu, H. T., Hoerner, T. E., Tayabji, S. D. (2007). *Using Falling Weight Deflectometer Data with Mechanistic-Empirical Design and Analysis*, Draft Interim Report, DTFH61-06-C-0046, Federal Highway Administration, Washington, D.C.

Substad, R. N., Jiang, Y. J., and Lukanen, E. O. (2006). *Guidelines for Review and Evaluation of Backcalculation Results*, FHWA-RD-05-152, Federal Highway Administration, Washington, D.C.

Thompson, M., and D. White. (2008). "Estimating compaction of cohesive soils from machine drive power." *Journal of Geotechnical and Geoenvironmental Engineering*, ASCE, 134(12), 1771-1777.

Vandenbossche, J. M. (2005). "Effects of slab temperature profiles on the use of falling weight deflectometer data to monitor joint performance and detect voids." *Transportation Research Record: Journal of the Transportation Research Board.* No. 2005, Transportation Research Board of the National Academies, Washington, DC, pp. 75-85.

Van Til, C. J., B. F. McCullough, B. A. Vallerga, and R. G. Hicks. (1972). *Evaluation of AASHO Interim Guides for Design of Pavement Structures*. NCHRP 128, Highway Research Board.

Vennapusa, P., and D. J. White. (2009). "Comparison of light weight deflectometer measurements for pavement foundation materials." *Geotechnical Testing Journal*, ASTM, 32(3), 239–251.

White, D. J., and M. Thompson. (2008). "Relationships between in situ and roller-integrated compaction measurements for granular soils." *Journal of Geotechnical and Geoenvironmental Engineering*, ASCE, 134(2), 1763–1770.

White, D. J., Vennapusa, P., Gieselman, H. (2010). *Iowa DOT Intelligent Compaction Research and Implementation - Phase I*, Report No. ER10-06, Iowa State University, Report submitted to the Iowa Department of Transportation, November.

Witczak, M. W., and J. Uzan. (1988). *The universal airport design system – Report I of IV: Granular material characterization*. Department of Civil Engineering, University of Maryland, College Park. MD.

Zorn, G. (2003). *Operating manual: Light drop-weight tester ZFG2000*, Zorn Stendal, Germany.

APPENDIX: AASHTO (1993) AND PCA (1984) DESIGN CHARTS

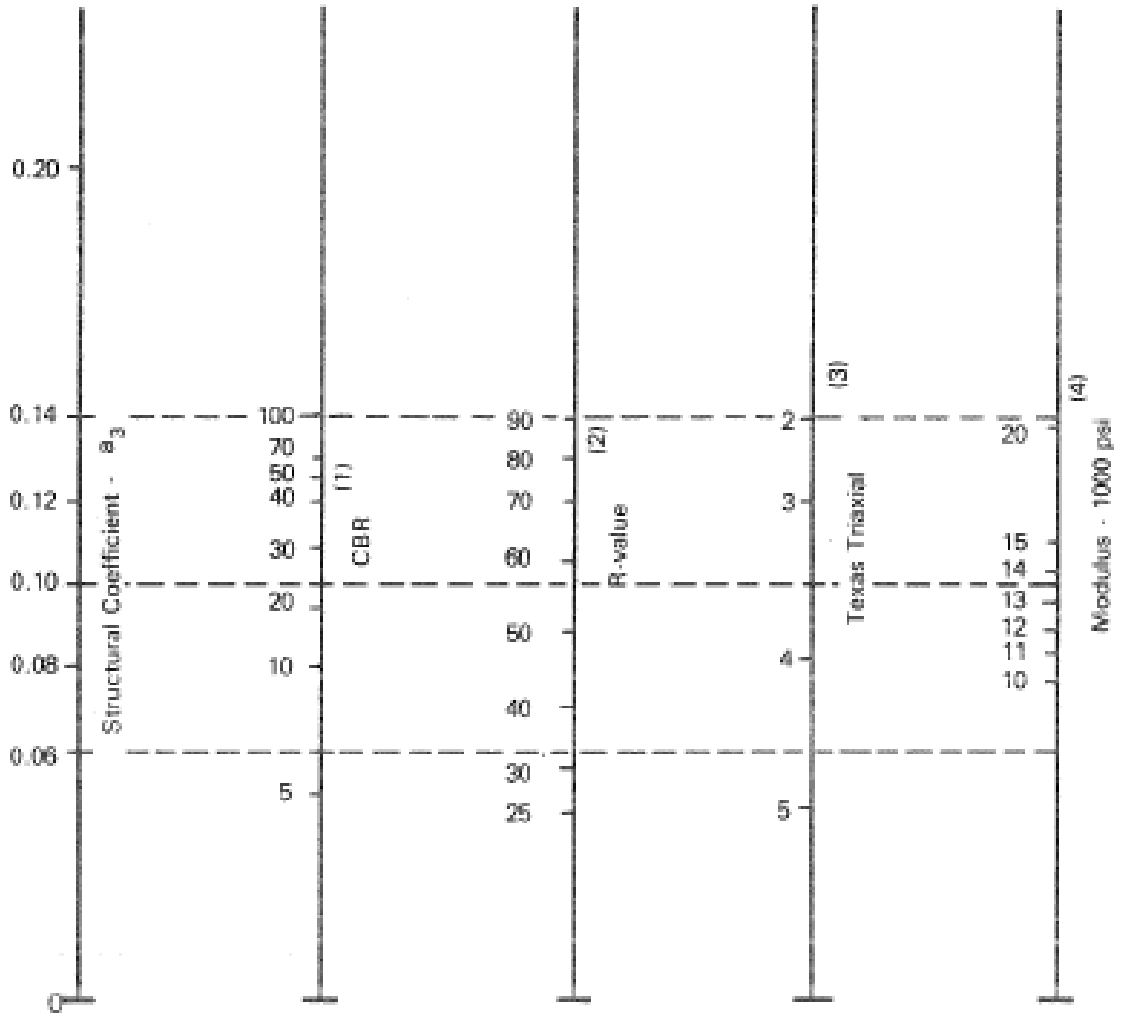

(1) Scale derived from correlations from Illinois.

(2) Scale derived from correlations obtained from The Asphalt Institute, California, New Mexico and Wyoming.

(3) Scale derived from correlations obtained from Texas.

(4) Scale derived on NCHRP project *(3)*.

Figure 71. Chart for estimating modulus of subbase layer (E_{SB}) from CBR (from AASHTO 1993 based on results from Til et al. 1972)

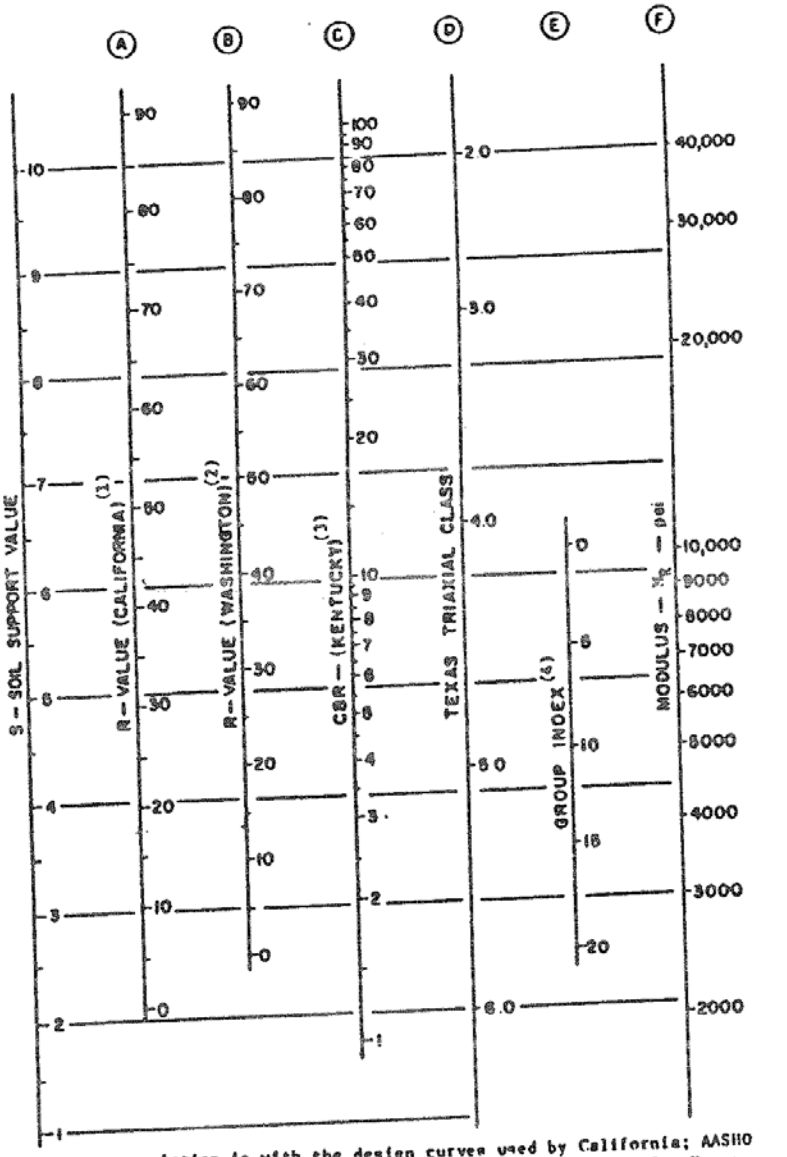

(1) The correlation is with the design curves used by California; AASHO designation is T-173-60, and exudation pressure is 240 psi. See Hveem, F.N., and Carmany, R.M., "The Factors Underlying the Rational Design of Pavements." Proc. HRB, Vol. 28 (1948) pp. 101-136.
(2) The correlation is with the design curves used by Washington Dept. of Highways; exudation pressure is 300 psi. See "Flexible Pavement Design Correlation Study." HRB Bull. 133 (1956).
(3) The correlation is with the CBR design curves developed by Kentucky. See Drake, W.B., and Havens, J.H., "Re-Evaluation of Kentucky Flexible Pavement Design Criterion." HRB Bull. 233 (1959) pp. 33-56. The following conditions apply to the laboratory-modified CBR: specimen is to be molded at or near the optimum moisture content as determined by AASHO T-99; dynamic compaction is to be used with a hammer weight of 10 lb dropped from a height of 18 in.; specimen is to be compacted in five equal layers with each layer receiving 10 blows; specimen is to be soaked for 4 days.
(4) This scale has been developed by comparison between the California R-value and the Group Index determined by the procedure in Proc. HRB Vol. 25 (1945) pp. 376-392.

Figure 72. Chart for estimating resilient modulus (M_r) of subgrade from CBR (from AASHTO 1993 Appendix FF based on results from Til et al. 1972)

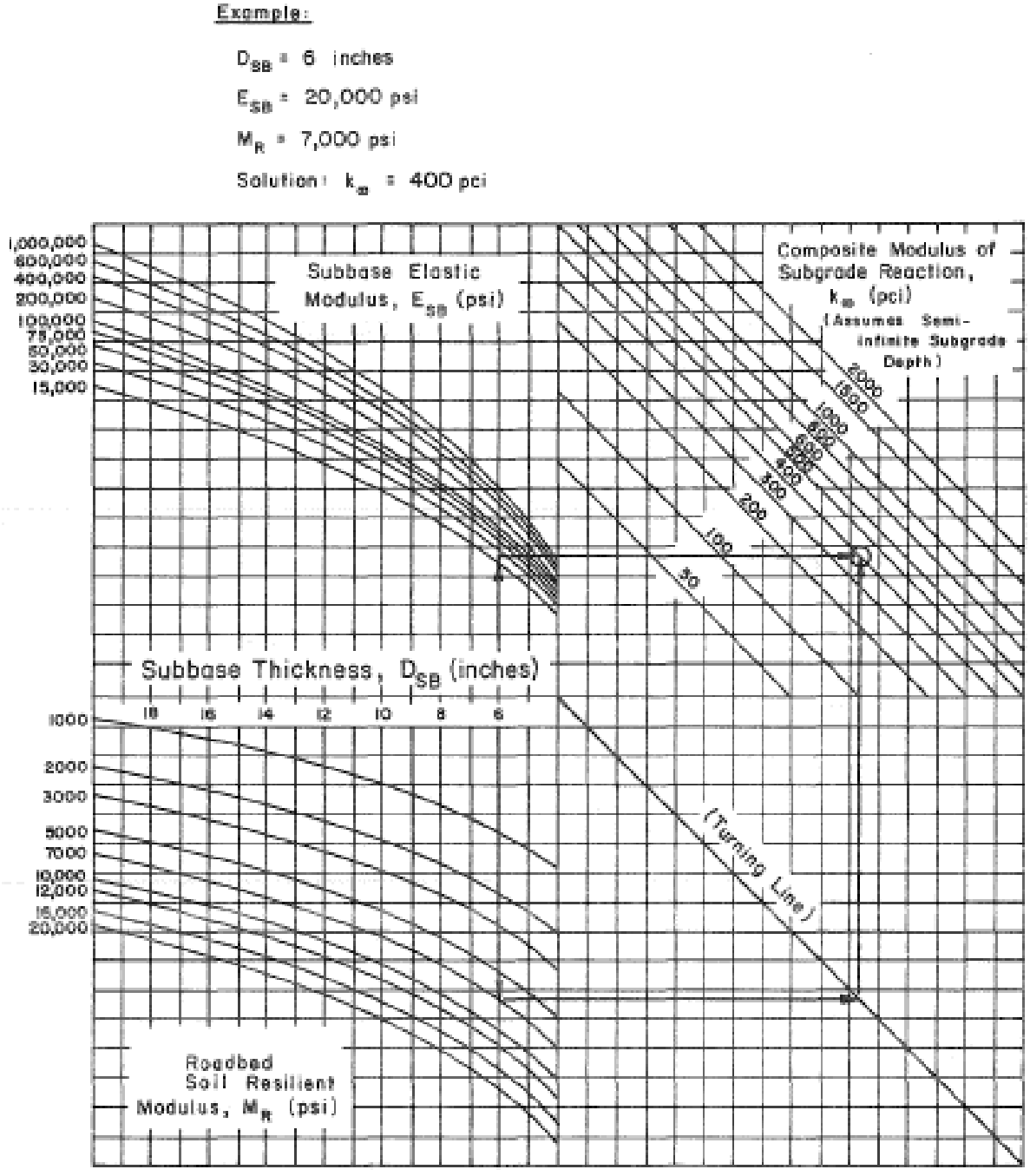

Figure 3.3. Chart for Estimating Composite Modulus of Subgrade Reaction, k_∞, Assuming a Semi-Infinite Subgrade Depth. (For practical purposes, a semi-infinite depth is considered to be greater than 10 feet below the surface of the subgrade.)

Figure 73. Chart for estimating composite modulus of subgrade reaction (k_{comp}) assuming a semi-infinite subgrade depth (from AASHTO 1993)

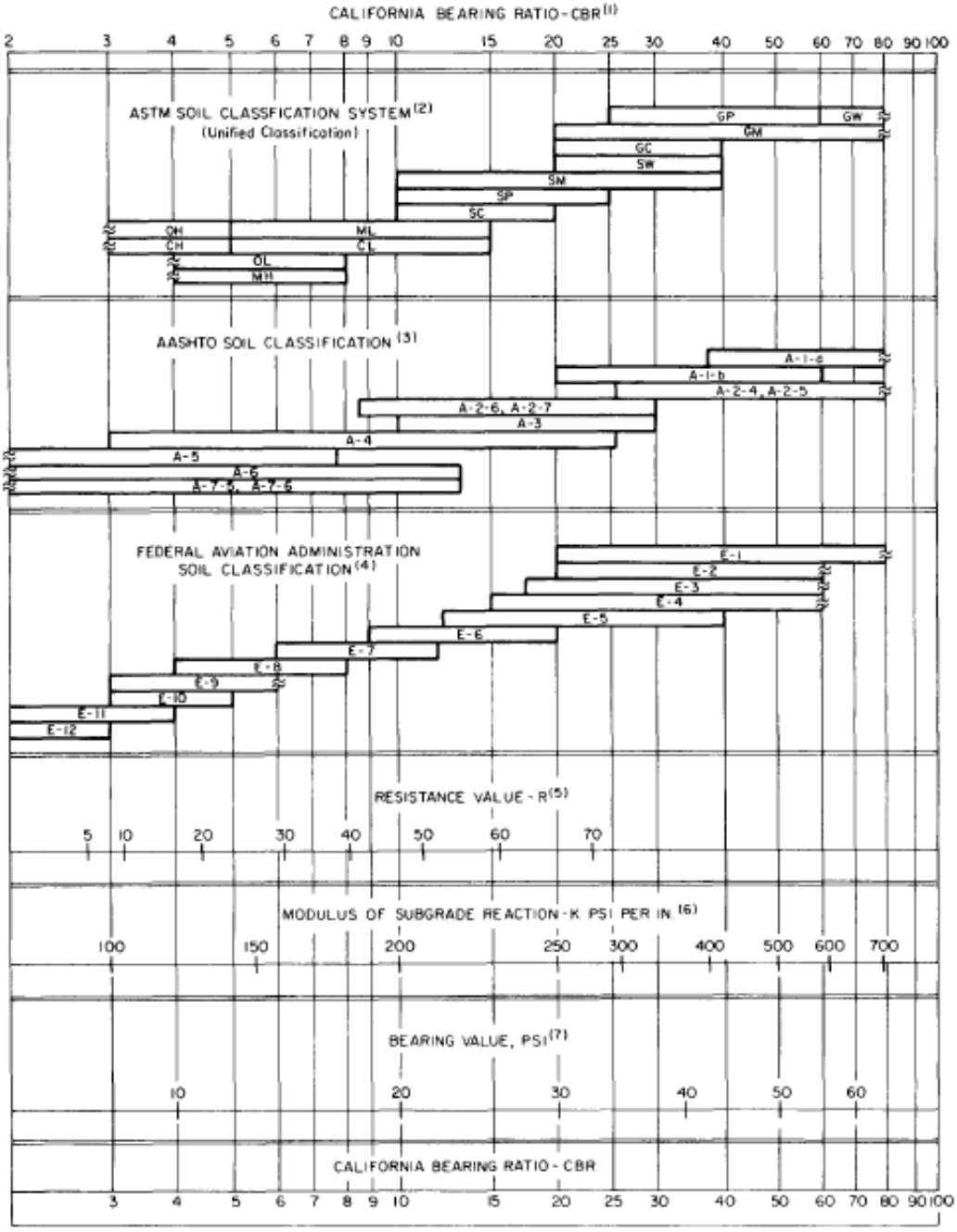

(1) For the basic idea, see O. J. Porter, "Foundations for Flexible Pavements," Highway Research Board *Proceedings of the Twenty-second Annual Meeting*, 1942, Vol. 22, pages 100-136.
(2) ASTM Designation D2487.
(3) "Classification of Highway Subgrade Materials," Highway Research Board *Proceedings of the Twenty-fifth Annual Meeting*, 1945, Vol. 25, pages 376-392.
(4) *Airport Paving*, U.S. Department of Commerce, Federal Aviation Agency, May 1948, pages 11-16. Estimated using values given in FAA *Design Manual for Airport Pavements*. (Formerly used FAA Classification; Unified Classification now used.)
(5) C. E. Warnes, "Correlation Between *R* Value and *k* Value," unpublished report, Portland Cement Association, Rocky Mountain-Northwest Region, October 1971 (best-fit correlation with correction for saturation).
(6) See T. A. Middlebrooks and G. E. Bertram, "Soil Tests for Design of Runway Pavements," Highway Research Board *Proceedings of the Twenty-second Annual Meeting*, 1942, Vol. 22, page 152.
(7) See item (6), page 184.

Figure 74. Chart for estimating modulus of subgrade reaction (*k*) from CBR (from PCA 1984)